University of Alberta
Department of Civil Engineering

Structural Engineering Report No. 163

AN ANALYSIS OF THE PERFORMANCE OF WELDED WIDE FLANGE COLUMNS

by

DIANA E. CHERNENKO

and

D. J. LAURIE KENNEDY

DECEMBER, 1988

Structural Engineering Report 163

An Analysis of the Performance of Welded Wide Flange Columns

by

Diana E. Chernenko

and

D.J. Laurie Kennedy

Department of Civil Engineering

University of Alberta

Edmonton, Alberta

December 1988

ABSTRACT

Currently CSA Standard CAN3-S16.1-M84 "Steel Structures for Buildings - Limit States Design" assigns welded wide flange (WWF) columns to the column curve for rolled H-shape sections. This approach appears to be conservative because of differences in the production of WWF sections and rolled H-shapes. The residual stress pattern for welded wide flange sections, stipulated to have edges of the flanges flame cut and thus inducing favourable tensile residual stresses, results in a delayed loss of stiffness as weak axis inelastic buckling occurs. This means that the weak axis and strong axis buckling curves lie closer together for WWF shapes than is the case for rolled H-shapes. Close tolerances on out-of-straightness are obtained with the automatic cutting and welding processes. As well, the statistical variations in the geometric properties are favourable.

A detailed statistical analysis of data collected from mill records and on-site measurements was made to obtain measured/nominal ratios and coefficients of variation of relevant geometric and material properties. A finite element program, modelling inelastic behaviour, residual strain patterns, out-of-straightness and material properties has been used with the test results of others to establish test/predicted ratios of column strengths. Parametric studies using the finite element program provide an assessment of the effect of varying residual strain patterns and column out-of-straightness. This information formed the basis for determining the factored compressive

resistance of WWF sections for three different slenderness ratios. Further experimental confirmation will be required.

Acknowledgements

This report is based on an MSc. Thesis of the same title submitted by Diana E. Chernenko to the Faculty of Graduate Studies and Research at the University of Alberta in the Winter of 1988-89. Dr. D.J. Laurie Kennedy supervised the preparation of the thesis.

Thanks is given to Dr. D. W. Murray, professor of Civil Engineering at the University of Alberta, for his time and direction toward valuable information on finite-element analyses and column, beam-column theory. Considerable help was provided by Kurt Ratzlaff, Anita Brattland, Garry Mah, and Robert Shelby during the coupon tests.

Financial support for this study was provided by the Canadian Steel Construction Council under project number 8503. The authors greatly appreciate the assistance of Algoma Steel Corporation in providing field data. Special thanks are given to Algoma personnel Joe Troje, Erminio Cerilli, and Murray MacLean for their time and effort in assisting in the collection of field data.

LIST OF SYMBOLS

Note: symbols appearing in the text with and without a bar, e.g., $\bar{A}$ and A, denote the measured and nominal values, respectively.

A	area
b	width of cross section
C_{NISA}	column strength predicted by NISA
$C_{S16.1}$	column strength predicted by S16.1
C_y	nominal compressive resistance of a stub column = $A \cdot \sigma_y$
Cr	factored compressive resistance of a column
d	depth of cross section
E	modulus of elasticity
E_T	tangent modulus of elasticity
$f(\lambda)$	equation in S16.1 describing variation in column strength as a function of λ
F	quantity which is a function of the yield strength and $f(\lambda)$, [2.20]
F_y	specified minimum yield strength (nominal)
$\{F\}$	matrix of nodal forces
$\{\Delta F\}$	matrix of incremental nodal forces
g	size of fillet weld
G	subscript indicating geometric property
h	height of cross-section
I	moment of inertia
k	empirical factor
K	effective length ratio

$[K_g]$	geometric stiffness matrix
$[K_s]$	elastic flexural stiffness matrix
L	column length
M	subscript indicating material property
n	sample size
P	column strength; subscript indicating professional factor
$P_{1,2,3}$	participation factors
P_E	Euler load (elastic buckling load)
P_{max}	maximum column load
$P_{T_{cr}}$	tangent modulus critical buckling load
P_y	nominal compressive resistance of a stub column = $A\sigma_y$
r	radius of gyration
R	resistance of a member
S	effect of loads
t	plate thickness; flange plate thickness
{U}	matrix of nodal displacements
$\{U_i\}$	matrix of initial geometric imperfections
$\{\Delta U\}$	matrix of incremental nodal displacements
V	coefficient of variation with subscripts A, Cr, E, F, F_y, G, I, M, P, r, R, S
V_e	coefficient of variation due to error in measurements
V_{ex}	coefficient of variation of the experimental factor
V_n	coefficient of variation of the normalized professional factor
V_s	coefficient of variation of the test specimen

V_t coefficient of variation due to uncertainties in the test loads

$V_{\Delta/L}$ coefficient of variation of the simulated professional factor as related to out-of-straightness

V_{σ_r} coefficient of variation of the simulated professional factor as related to residual stresses

w web plate thickness

x subscript indicating major principal axis

y subscript indicating minor principal axis

α separation factor with subscripts R, S, when associated with these quantities

α' load factor for effective loads

β safety or reliability index

δ mid-height deflection

Δ/L initial out-of-straightness (mid-height)

ϵ_a applied strain

$\epsilon_{t(max)}$ maximum tensile residual strain

ϵ_y yield strain

λ slenderness parameter $= \frac{KL}{r}\left(\frac{F_y}{\pi^2 \cdot E}\right)^{1/2}$

μ mean

ϕ resistance factor

ρ measured-to-nominal ratio with subscripts A, Cr, E, f(λ), F, F_y, G, I, M, P, r, R, S, λ

ρ_{ex} ratio of test (experimental) strength to that predicted by S16.1

ρ_n normalized professional factor

ρ_{NISA} column strength predicted by computer simulation (NISA) divided by P_y

ρ_s simulated professional factor

ρ_s' simulated professional factor evaluated at the mean out-of straightness

$\rho_{\bar{s}}$ simulated professional factor evaluated at the mean out-of-straightness and mean value of the average compressive residual stress

$\rho_{s_{eq}}$ simulated professional ratio calculated from best-fit equation

$\rho_{S16.1}$ column strength predicted by S16.1 divided by P_y

σ standard deviation with subscripts E, F, F_y, r.

σ_r residual stress

σ_{rc} average compressive residual stress

σ_u ultimate tensile load

σ_y specified minimum yield strength (nominal)

Table of Contents

List of Tables

List of Figures

Chapter 1

Introduction

CSA standard CAN3-S16.1-M84 - "Steel Structures for Building - Limit States Design" (Canadian Standards Association 1984) gives two curves for the design of columns. Each curve, used for specific types of columns, is intended to reflect the differences in behaviour as a result of different manufacturing processes. In the 1974 edition of S16.1 (Canadian Standards Association 1974) only a single column curve, that given in clause 13.3.1 of S16.1-M84, was given. However, the favourable residual stress pattern and the relatively small magnitude of out-of-straightness of class H hollow structural sections (Kennedy and Gad Aly 1980) suggested that a higher curve than clause 13.3.1 was appropriate for them. This formed the basis for assigning these sections to the second (higher) curve (clause 13.3.2) in the 1978 edition (Canadian Standards Association 1978). Examination of the residual stresses and out-of-straightness, both of which affect column strength, suggests that Canadian WWF column sections may also be unnecessarily penalized with their current classification in the first (lower) S16.1 column curve along with rolled W sections.

The WWF sections have a unique residual stress pattern characteristic of the manufacturing process. CSA standard S16.1 stipulates that "welded H-shapes should have flange edges flame cut". The flame-cutting produces relatively high, but favourable, tensile residual stresses at the flange tips. These tensile residual stresses delay the deterioration in minor axis stiffness, as compared to rolled W sections, where yielding begins at the tips and progresses inwardly. This delay in minor axis buckling is of great significance as it generally governs the buckling of H-shapes. It also means that the weak axis and strong axis buckling curves lie closer together than is the case for rolled H-shapes.

Out-of-straightness, more specifically called camber or sweep depending about which axis, major or minor, respectively, the out-of-straightness occurs, is also of major consequence. Currently, the S16.1 column curve for H-shapes is based on the maximum allowable out-of-straightness of 1/1000 for both axes (Bjorhovde 1972). It is more appropriate to base any design equation, including column curves, on statistical quantities, that is, on mean values and associated coefficients of variation.

In addition, examination of the differences in the manufacturing processes of WWF sections and rolled W sections reveals that the geometric variations of the former are smaller because of smaller variations in the plates used to manufacture WWF sections than the geometric variations of rolled W sections. This tight control on geometric variations will also have a positive effect on the prediction of

column strength.

The differences between WWF sections and rolled W sections affect column strengths over the entire range of column lengths and suggest that different column curves should be used for the two types of sections. Geometric variations affect columns irrespective of their lengths. The effect of residual stresses and out-of-straightness are length dependent. By definition, long columns fail by elastic instability and, therefore, residual stresses have no effect in this range while out-of-straightness may. For sufficiently short columns neither residual stresses nor out-of-straightness have a significant effect. The most notable effects of both residual stresses and out-of-straightness are observed in the intermediate range of column lengths where they both reduce the strength of columns.

1.1. Objectives and scope

The objective of this study was to investigate statistically the resistance of WWF columns produced in Canada by evaluating resistance factors appropriate for use with existing column curves. Recommendations for design equations and resistance factors are given. A detailed statistical analysis of the variations in the geometric and material properties of the plates used to produce WWF sections and the sections themselves was carried out. A finite element program, NISA (Stegmüller *et al.* 1983), was used to assess quantitatively the effects of variations in the characteristic residual stress pattern, the effects of out-of-straightness, and their combined effect. Out-of-straightness was

restricted to a cubic deflected shape with the maximum out-of-straightness at mid-height. The study was limited to centrally loaded, pin-ended columns, buckling about the major or minor axis and laterally supported about the other axis when required. Local buckling, buckling about both axes simultaneously, and lateral torsional buckling were not considered. Resistance factors were evaluated for values of the slenderness parameter, λ, of 0.336, 0.672, and 1.007

Chapter 2

Literature Review

2.1. Historical development of theories on column behaviour, strength, and design

Although columns have been used since man began constructing structures, scientific approaches for solving the column behaviour and strength problem appears to have begun as late as the eighteenth century. Tall (1964a) identifies the first paper concerned with column strength as one published in 1729 by van Musschenbroek (Salmon 1921) who presented an empirical column curve, developed on the basis of experimental work, for rectangular sections:

$$[2.1] \quad P = k \frac{bd^2}{L^2}$$

The development of calculus in the seventeenth century provided a most powerful tool enabling Leonard Euler (1759) to identify elastic buckling in which column failure occurs because of geometric instability with no fibre exceeding its elastic limit. The elastic buckling or Euler load for centrally loaded, perfectly straight, pin-ended columns is

$$[2.2] \quad P_E = \frac{\pi^2 EI}{L^2}$$

Although fault could not be found in Euler's logic, reluctance prevailed in accepting his work because of it's failure to predict the strength of short columns. In 1845, Lamarle recognized that if the extreme fibres of a column are stressed beyond their limit of elasticity then inelastic behaviour occurs and thus established "the elastic limit" to which Euler's column formula applies (Bleich 1952). Lamarle recognized inelastic column behaviour but could not explain it.

Considère in France and Engesser in Germany independently developed the concept of adjusting the modulus of elasticity to take inelastic behaviour into account. In 1889, Engesser (1889) presented the tangent modulus theory, modifying Euler's equation by substituting the tangent modulus of elasticity, E_T, for the modulus of elasticity, E. Thus for a non-linear stress-strain curve the tangent modulus critical buckling load is

$$[2.3] \quad P_{T_{cr}} = \frac{\pi^2 E_T I}{L^2}$$

Considère (1889), who presented a similar concept, remarked that as one side of the column is loading and stressed beyond the elastic limit, the other side would begin to unload elastically as bending progressed. This comment and those of Jasinsky (1895) led Engesser (1895) to present the double (reduced) modulus theory. This theory was later supported by experimental work by von Kármán (1910).

During this time a second group of researchers concentrated their efforts on establishing column curves taking into account the effects of imperfections such as initial out-of-straightness and eccentric axial loads. This work led to the secant curve, semi-empirical column curves such as the Rankine-Gordon and Perry-Robertson formulas as well as empirical column curves such as the Johnson parabola and simplified straight-line approximations (Salmon 1921; Tall 1964a; Bleich 1952). Each formula was to cover the inelastic range with the Euler formula to be used for the elastic range. These semi-empirical and empirical formulas were the most widely used for many years and some are still in use today (Narayanan 1982). Their popularity may largely be attributed to their simplicity and ease of use for the design engineer. Any curve, whatever its basis in theory or experiment, is ultimately only of practical use to the design engineer if it compares well with experimental results. Apart from von Kármán's verification, researchers observed experimental results which agreed more closely with the tangent modulus theory rather than the double modulus theory. This created considerable confusion about Engesser's work and may also have been, in part, responsible for the popularity of the semi-empirical and empirical formulas.

In 1947, Shanley (1949) clarified this confusion establishing Engesser's tangent modulus theory as a lower bound solution and the double modulus theory as an upper bound solution. Shanley also showed that an initially perfect column buckles at the tangent modulus load, as stated by Engesser, but bends only a limited amount. The

column then attains higher loads while bending further until the ultimate load is reached at which point further bending occurs at reduced loads. This concept of column behaviour, adopted in association with Engesser's tangent modulus theory, is known as the Engesser-Shanley model.

Although the presence of residual stresses were well know and attempts were made to establish whether they affect the load-carrying capacity of steel columns (Wilson and Brown 1935), it was not until 1951 that Osgood (1951) presented the first viable theory on residual stresses while applying the Engesser-Shanley theory. Together with the work of Yang *et al.* (1952), this brought attention of the research community to examine the impact residual stresses have on column strength. Considerable work at Lehigh University provided extensive analytical and experimental verification that residual stresses are responsible for reducing column strength for short and intermediate length columns (Huber and Beedle 1954 ; Ketter *et al.* 1955 ; Huber and Ketter 1958; Beedle and Tall 1962) with several dissertations dedicated to this topic (Huber 1956; Fujita 1956; Tall 1961; Estuar 1965). The reduction in strength is greatest at L/r ratios of 70 to 90, with recorded reductions of 25% (Beedle and Tall 1960).

The development of residual stresses resulting from welding was established as early as 1936 by Boulton and Lance Martin (1936). Their analytical work, verified with experimental results, showed that after a weld cools plastic deformations arise creating residual stresses. Work

was extended at Lehigh University to determine the effect of residual stresses on column strength of welded plates and built-up sections (Nagaraja Rao and Tall 1961; Estuar and Tall 1963; Tall 1964b; and Nagaraja Rao *et al.* 1964). In all studies, it was found that the performance of welded shapes, fabricated from universal mill plates, was inferior to their rolled equivalents because of the higher compressive residual stresses at the flange tips. McFalls and Tall (1969), Alpsten and Tall (1970), Alpsten (1972a), Bjorhorde *et al.* (1972), and Alpsten (1972b) investigated the strength of welded shapes made from plates with flame-cut edges. The flame-cutting process was discovered to improve the strength of welded columns significantly.

Early in the work involving residual stresses it became apparent that to predict column strengths accurately it was necessary to incorporate both out-of-straightness and residual stresses in the analysis. Although the Engesser-Shanley theory could account for non-linear stress-strain relationships and residual stresses, it could not take into account geometric imperfections such as out-of-straightness and eccentric loading conditions.

As early as 1921, it was known that out-of-straightness affects column strength immensely (Salmon 1921), as confirmed subsequently by many such as Lin (1950) and Wilder *et al.* (1953). The complexity of including both out-of-straightness and residual stresses prevented significant progress until the advent of computer technology.

While work continued on the tangent modulus approach (Johnston 1961), the Lehigh group, in particular, Fugita (1956), Nitta (1960), and Tall (1961), were among the first to apply the ultimate strength theory to inelastic columns. In the ultimate strength theory the relationship between the load and mid-height deflection are determined by calculating the equilibrium between external and internal forces and moments at the mid-height cross-section using incremental load steps. Out-of-straightness and residual stresses are accounted for simultaneously. Even so, the tangent modulus theory was not easily replaced by the ultimate strength theory. The tangent modulus theory was thought to compare well with the ultimate strength theory because the ultimate strength is reduced slightly due to the initial out-of-straightness (McFalls and Tall 1969). Ultimate strength theories are now used in conjunction with progressively advancing numerical analysis techniques such as finite element simulations.

Fig. 2.1 illustrates the load-deflection curves for various inelastic column theories. The reduced modulus and tangent modulus curves form upper and lower bounds, respectively, for initially straight columns with the Engesser-Shanley tangent modulus curve located between them. Below these curves lies the ultimate strength curve for initially curved columns, as lateral deflections proceed immediately with the onset of loading. The bifurcation phenomenon exhibited by the tangent modulus theories for initially perfectly straight columns is replaced by a strength phenomenon.

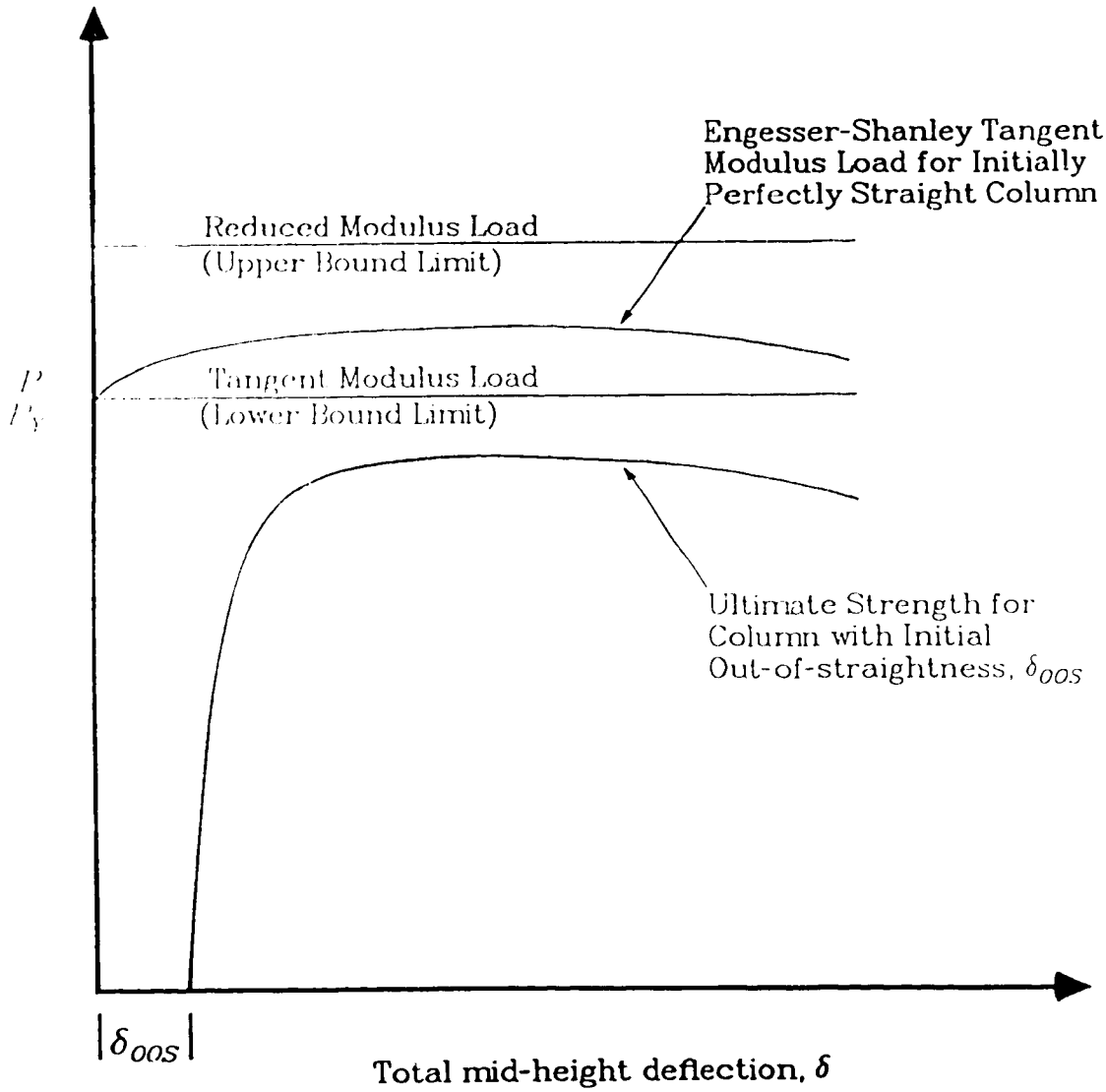

Fig. 2.1 Load deflection curves of various inelastic column theories

Bjorhovde (1972) integrated probability theory into the analysis of centrally loaded, initially curved, prismatic steel columns with residual stresses. He recognized that all parameters influencing column strength demonstrate inherent variability. In addition, he proposed a set of three column curves to reflect the different strengths of columns produced in industry. The Structural Stability Research Council (1976) adopted the concept of multiple column curves. Two of these curves are currently in use in CSA standard CAN3-S16.1-M84 - "Steel Structures for Building - Limit States Design" (Canadian Standards Association 1984).

2.2. Residual stresses

2.2.1. General

Residual stresses exist in every steel member (unless deliberately relieved) prior to the application of external loads due to the manufacturing process. Residual stresses are classified as cold working residual stresses and thermal residual stresses.

Cold-working operations such as gagging and rotorizing, used to straighten initially curved members or to induce a desired curvature or camber into a member, create residual stresses. Gagging, an outdated but still used operation, involves the application of concentrated loads, bending and local yielding of the member at specific intervals with the net effect of altering the curvature of the member as a whole. Rotorizing is the preferred practice for straightening and cambering a

member. It involves passing a member through a series of rollers offset from a straight line. This process deforms the member evenly along the length unlike gagging which results in localized and heavily concentrated yielding. These cold-working procedures introduce new residual stresses which override the thermal residual stresses (Lay 1982). However, not all steel members are subjected to these forces. In fact, less than 2% of WWF columns, in particular, require straightening. When straightening is required, welding torches are used to heat the member at several intervals rather than using a cold-working process. For these reasons, thermal residual stresses are of chief significance for WWF members.

Thermal residual stresses are created as a result of uneven cooling during rolling, welding and flame-cutting operations. For rolled sections, cooling begins at the flange tips and progresses inwardly towards the web-flange junction. As the steel cools, its stiffness increases and the material shrinks. While the cooler and stiffer flange tips shrink, the hotter web-flange junction is subjected to compressive forces and because of its lower material stiffness, yields easily, deforming plastically. When the web-flange junction eventually cools, it too develops shrinkage forces while increasing in stiffness. However, it is prevented from shrinking by the already stiff and set, cold flange tips. Thus the restrained web-flange junction goes into tension and the flange tips go into compression. The same principle applies to welding and flame-cutting operations. The hotter areas are the last to cool developing tensile residual stresses while the remaining portions of the section are

induced into compression. Fig. 2.2 shows models of residual stress patterns characteristic of various manufacturing procedures for structural steel H-shaped members. The residual stress pattern is, in a sense, a blue-print revealing the stress history of the member.

Residual stress or strain patterns tend to be symmetrical about the major and minor axes of a cross-section. Fig. 2.3, giving the results of detailed experimental work by McFalls and Tall (1969) on residual stress distributions for two welded shapes, exemplifies this symmetry. Although small deviations are observed, equilibrium is never compromised. Ultimately, a free member with no external forces must be in equilibrium. Thus, the sum of internal axial forces, bending moments about both the major and minor axes, and torsional moments must all be zero. Residual stresses are more or less constant throughout the length of the member except for a distance equivalent to the largest dimension of the cross section (Alpsten and Tall 1970).

2.2.2. The effect of residual stresses on column strength

Compressive residual stresses reduce the strength of intermediate length columns, that is, those that fail by inelastic buckling. The column yields at a load level equal to the yield stress minus the maximum residual stress. For example, those portions of the section with a maximum compressive residual stress of 25% of the yield stress will yield at a load of 75% of the yield stress. The yielded portions have reduced stiffness.

However, in a stub column test flexural stiffness is not of concern as the column is short. Premature yielding due to compressive residual

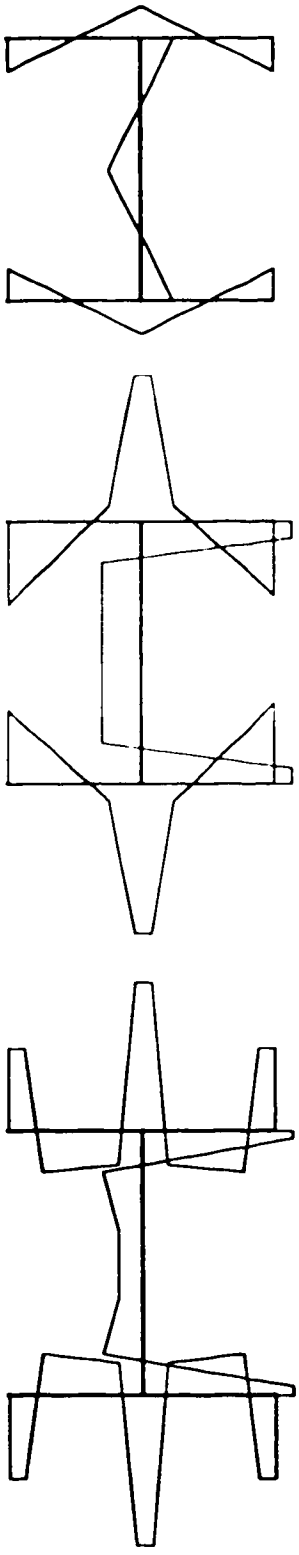

Fig. 2.2 **Models of typical residual stress distributions for various manufacturing procedures.**

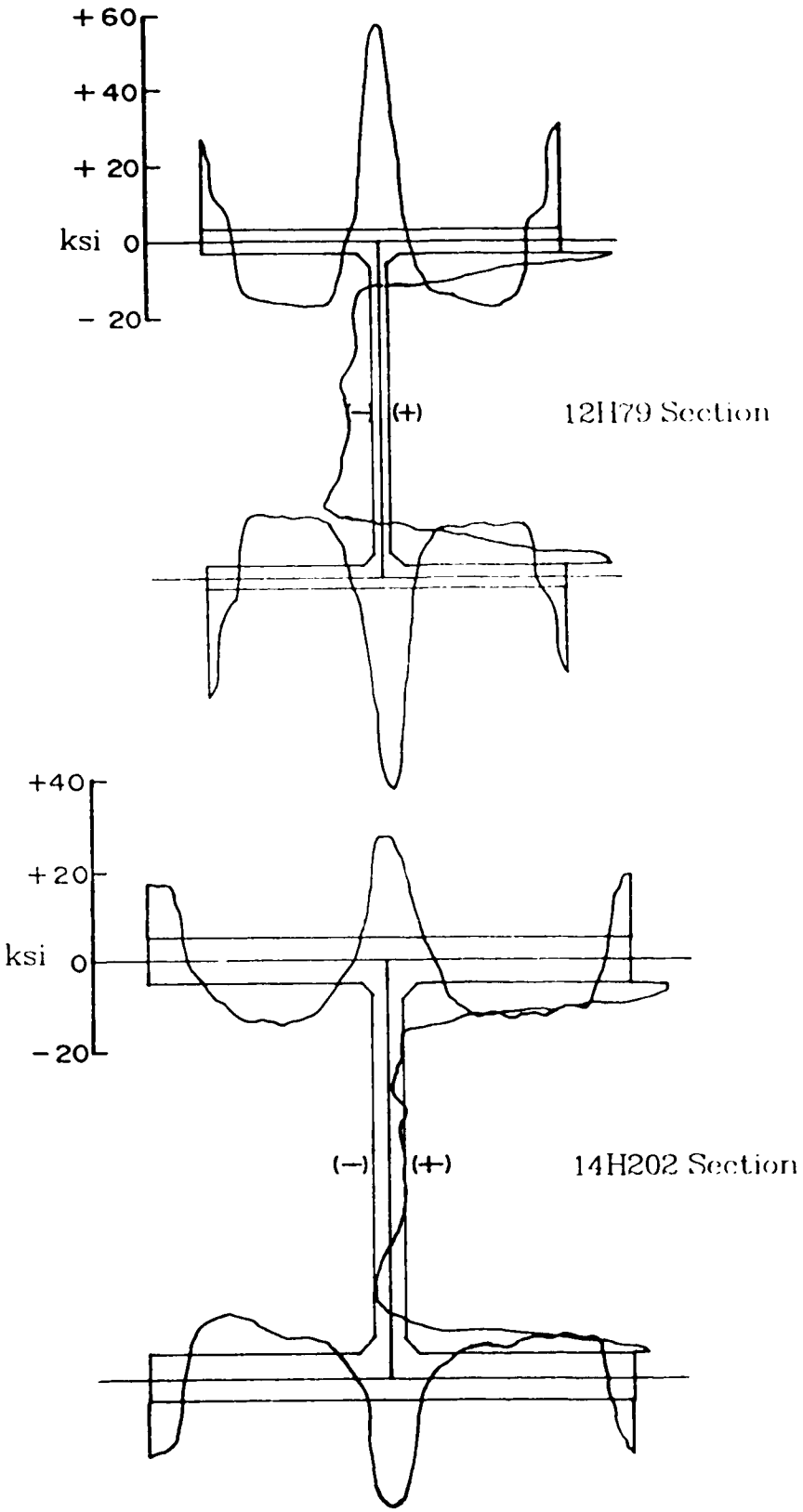

Fig. 2.3 Typical residual stress distributions for 12H79 and 14H202 Sections (McFalls and Tall 1969)

stresses is compensated for by those portions of the section with tensile residual stresses which prolong the column's ability to attain further load. The last portion of the cross-section, that with the maximum tensile residual stress, yields when the applied strain, ϵ_a, is equal to

$$\epsilon_a = \epsilon_y + \epsilon_{t(max)} \quad [2.4]$$

There is no net effect of residual stresses on the stub column strength although the load-deflection (stress-strain) curve is rounded because of the early yielding. Once the section is fully yielded, strain-hardening may allow the column to attain further load. This increase in capacity is not considered in design standards as local buckling generally ensues shortly thereafter.

The magnitude of compressive residual stresses for rolled sections, are typically in the order of 70 to 100 MPa (Adams *et al.* 1981), corresponding to 23 to 30% of the yield strength of 300W steel. Thus, such columns begin to yield at 70 to 77% of the yield strength with accompanying loss in stiffness and capacity.

Welded members fabricated from universal mill plates have a similar distribution but greater magnitude of residual stresses, in the order of 75 to 175 MPa (Lay 1982). These correspond to 25 to 58% of the yield stress of 300W steel and extend over as much as 67% (Alpsten and Tall 1970) of the flanges as compared to 50% for rolled sections. Therefore, welded shapes made from universal-mill plates will not perform as well as equivalent rolled shapes as has been verified experimentally by

Beedle and Tall (1960), and Nagaraja Rao and Tall (1961).

Welded members fabricated from flame cut plates exhibit higher compressive residual stresses than rolled sections as well. They are in the order of 80 to 110 MPa (McFalls and Tall, 1969), corresponding to 27 to 37% of the yield strength of 300W steel. About 50 to 60% of the flange area is subjected to the compressive residual stresses. Although these compressive residual stresses are relatively high and extend over a large portion of the flange area, they are compensated for by the high tensile residual stresses at the flange tips induced by the flame cutting operation. These vary from 125 to 210 MPa (McFalls and Tall 1969) corresponding to 42 to 70% of the yield strength of grade 300W steel.

The distribution of compressive residual stresses over the cross-section greatly affects the performance of columns that buckle inelastically as stiffness is first lost where the compressive residual stresses are maximum. For rolled sections, this occurs at the flange tips resulting in the rapid loss of weak axis stiffness which is accelerated by the progressive reduction in the moment arms of the unyielded portions of the cross-section. For strong axis buckling the effect is less severe because areas with tensile residual stresses, which therefore exhibit delayed yielding, are as far from the neutral axis as those with compressive residual stresses. The tensile residual stresses at the flange tips of WWF members delay the rapid loss in cross-sectional stiffness observed in rolled and universal-mill welded shapes. Thus, the strong and weak axis buckling strengths are virtually the same for a

WWF member of a given slenderness ratio with approximately equal cross-sectional width and depth. Rolled columns exhibit a significant difference in the buckling curves about the two axes and WWF columns made from universal mill plate exhibit even a greater difference. When columns are designed on the basis of a single curve for both weak and strong axes buckling, the lower curve for weak axis buckling must be used. Thus, the objective of maintaining relatively uniform safety for all structural members is not met for rolled and welded universal-mill columns as it is for oxygen-cut WWF members.

The magnitude of residual stresses depends on the size of the plate elements and therefore the performance of both light and heavy sections needs to be examined. McFalls and Tall (1969) reported that the magnitudes of residual stresses due to flame cutting and welding in heavy flame-cut welded columns were less than in light sections. The heavier sections cooled more uniformly. The residual stress patterns in heavier sections were also less peaked than in lighter sections as shown in Fig. 2.3. Therefore, it would be expected, other things aside, that heavy columns would perform better than lighter columns.

The concern and complications that residual stresses bring forth can be alleviated by post-heating or annealing the members, a process where the cooling rate is controlled to give sufficient time for the internal stresses to be relieved. The test results of Huber and Beedle (1954) and Brozzetti *et al.* (1971) confirm that the performance of members in which residual stresses have been removed by annealing, is much supe-

rior to that of members containing residual stresses. However, the cost of the process generally renders it impractical for structural steel construction.

2.3. Limit states design

The designing of steel structures using the limit states design method was first introduced into Canada with CSA (1974) Standard CAN3-S16.1-1974, "Steel Structures to Building - Limit States Design". Limit states design provides a system of design of relatively uniform reliability (constant level of safety) and economy (Galambos and Ravindra 1977). Of prime concern in this study is the ultimate limit state associated with the strength of columns.

The basic criterion for an ultimate limit state is satisfied when the factored resistance is greater than or equal to the factored load effect, such that,

[2.5] $\phi R \geq \alpha' S$

Fig. 2.4a gives schematic distribution curves for the resistance, R, and the effect of loads, S.

The factors α' and ϕ are set such that the probability of failure is acceptably small, consistent with economic restraints. The analysis to determine these factors is simplified by combining the two curves in Fig. 2.4a to produce a risk distribution curve (Fig. 2.4b) of $\ln \frac{R}{S}$ (Galambos and Ravindra 1973a). The evaluation and implications of different risk models are given in Gad Aly (1978).

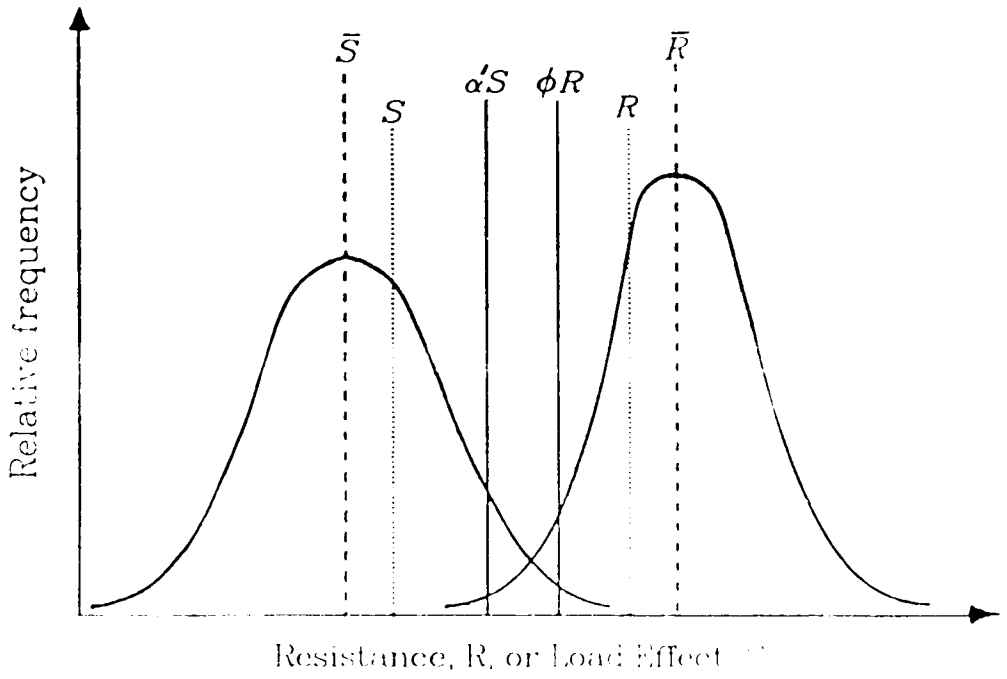

Fig. 2.4a Frequency distribution for the resistance and load effect

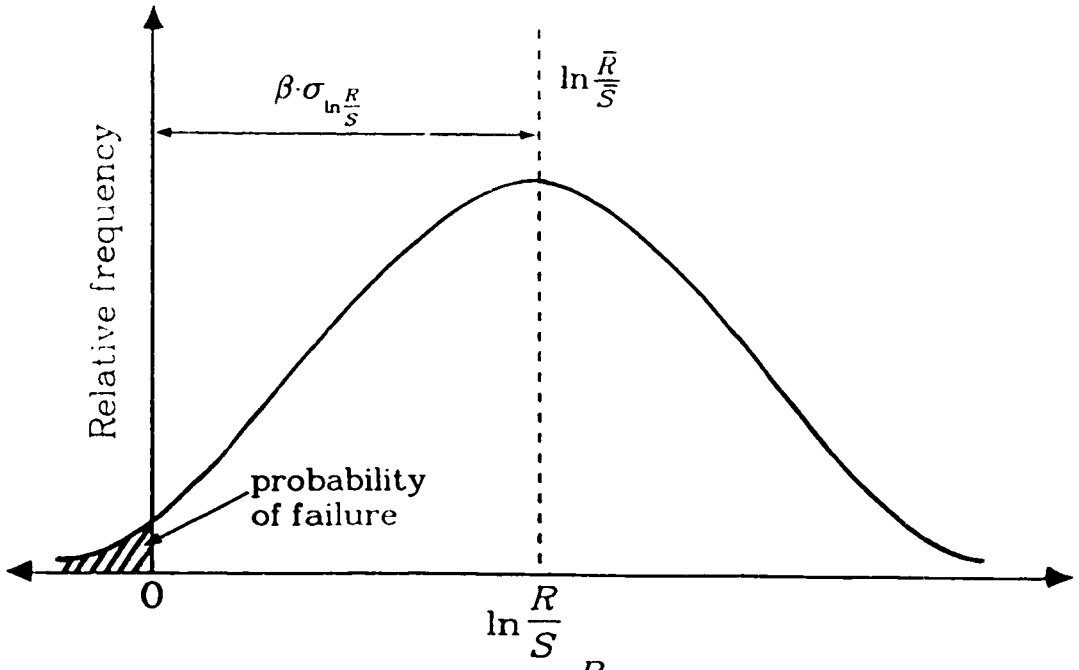

Fig. 2.4b Risk distribution curve for $\ln \frac{R}{S}$

The shaded area, when $\ln\frac{R}{S} < 0$, represents the probability of failure which can be set at any desired level by selecting a value of β. β is the number of standard deviations that the mean lies to the right of zero. The factor, β, the safety or reliability index is (Allen 1975)

$$[2.6] \qquad \beta = \frac{\ln\left[\frac{\bar{R}}{\bar{S}}\left(\frac{1+V_S^2}{1+V_R^2}\right)^{1/2}\right]}{\ln\left[(1+V_S^2)(1+V_R^2)\right]^2}$$

The target value of β adopted for building structures in the National Building Code of Canada is 3.0 (Allen 1975). Galambos and Ravindra (1973b) use a different approach to arrive at the same results.

Galambos and Ravindra (1973a) proposed a first order simplification of [2.6] to give

$$[2.7] \qquad \beta = \frac{\ln\frac{\bar{R}}{\bar{S}}}{\left[V_R^2+V_S^2\right]^{1/2}}$$

Galambos and Ravindra (1973b) further simplified [2.7] based on Lind's (1971) proposal of an approximate separation factor, α, such that:

$$[2.8] \qquad [V_R^2+V_S^2]^{1/2} = \alpha_R V_R + \alpha_S V_S = \alpha\left[V_R+V_S\right]$$

Galambos and Ravindra (1973b, 1977) used an error minimization process to obtain a value of 0.55 for α which results in a 10% probability of a total unconservative error of less than 2% in magnitude. Therefore, [2.7] becomes

$$[2.9] \quad \beta = \frac{\ln \frac{\bar{R}}{\bar{S}}}{\alpha(V_R+V_S)}$$

which can be rewritten to take the form

$$[2.10] \quad \bar{S} \cdot e^{\alpha\beta V_s} = \bar{R} \cdot e^{-\alpha\beta V_R}$$

Introducing the ratio of the measured-to-nominal value, such that

$$[2.11] \quad \rho_S = \frac{\bar{S}}{S}$$

and

$$[2.12] \quad \rho_R = \frac{\bar{R}}{R}$$

gives

$$[2.13] \quad \rho_S \cdot S \cdot e^{\alpha\beta V_s} = \rho_R \cdot R \cdot e^{-\alpha\beta V_R}$$

which, when compared with [2.5], defines the resistance factor, ϕ, as:

$$[2.14] \quad \phi = \rho_R \cdot e^{-\alpha\beta V_R}$$

and the load effect factor, α', as:

$$[2.15] \quad \alpha' = \rho_S \cdot e^{\alpha\beta V_S}$$

The measured-to-nominal ratio, ρ_R, and its associated coefficient of variation, V_R, for the resistance of a structural member depends on the equation to determine the resistance of the member which includes the variations of geometric and material properties and on how well the design equation fits the experimental test results, that is,

[2.16] $\rho_R = \rho_G \cdot \rho_M \cdot \rho_P$

For columns, the current CSA standard S16.1-M84 "Steel Structures for Buildings - Limit States Design" (1984) uses an equation of the form

[2.17] $Cr = \phi \cdot A \cdot F_y \cdot f(\lambda)$

where $f(\lambda)$ is an expression defining column strength as a function of the slenderness parameter λ, and

[2.18] $$\lambda = \frac{KL}{r}\left[\frac{F_y}{\pi^2 E}\right]^{1/2}$$

Therefore, the measured-to-nominal ratio, ρ_R, becomes

[2.19] $\rho_R = \rho_A \cdot \rho_{F_y} \cdot \rho_{f(\lambda)} \cdot \rho_P$

The slenderness parameter, λ, is a function of the yield strength, F_y, thus grouping the two terms F_y and $f(\lambda)$ such that

[2.20] $F = F_y \cdot f(\lambda)$

and

[2.21] $\bar{F} = \bar{F}_y \cdot f(\lambda)$

results in

[2.22] $\rho_F = \rho_{F_y} \cdot \rho_{f(\lambda)}$

The quantity F is therefore a function of the yield strength, radius of gyration of the section and the modulus of elasticity. The measured-to-nominal ratio for the professional factor, ρ_p, is the ratio of the test strength of a column to that predicted by the design equation. Therefore, [2.19] becomes

[2.23] $\rho_R = \rho_A \cdot \rho_F \cdot \rho_P$

The values for the measured-to-nominal ratios and coefficients of variation for the area and the professional factor are found by using simple statistical analyses. The derivations presented here for V_F follow Kennedy and Gad Aly (1980).

From CSA standard S16.1-M84, clause 13.3.1, for H shapes and class C hollow structural steel sections, $f(\lambda)$ is defined as:

[2.24] (a) $f(\lambda) = 1.0$, for $0 \leq \lambda \leq 0.15$

(b) $f(\lambda) = 1.035 - 0.202\lambda - 0.222\lambda^2$, for $0.15 < \lambda \leq 1.0$

(c) $f(\lambda) = -0.111 + 0.636\lambda^{-1} + 0.087\lambda^{-2}$, for $1.0 < \lambda \leq 2.0$

(d) $f(\lambda) = -0.009 + 0.877\lambda^{-2}$, for $2.0 < \lambda \leq 3.6$

(e) $f(\lambda) = \lambda^{-2}$, for $3.6 < \lambda$

Therefore, the mean of $f(\lambda)$ is:

[2.25] (a) $f(\bar{\lambda}) = 1.0$, for $0 \leq \bar{\lambda} \leq 0.15$

(b) $f(\bar{\lambda}) = 1.035 - 0.202\bar{\lambda} - 0.222\bar{\lambda}^2$, for $0.15 < \bar{\lambda} \leq 1.0$

(c) $f(\bar{\lambda}) = -0.111 + 0.636\bar{\lambda}^{-1} + 0.087\bar{\lambda}^{-2}$, for $1.0 < \bar{\lambda} \leq 2.0$

(d) $f(\bar{\lambda}) = -0.009 + 0.877\bar{\lambda}^{-2}$, for $2.0 < \bar{\lambda} \leq 3.6$

(e) $f(\bar{\lambda}) = \bar{\lambda}^{-2}$, for $3.6 < \bar{\lambda}$

Applying the definition of ρ, that is, the measured-to-nominal ratio, gives

[2.26] $\rho_\lambda = \dfrac{\bar{\lambda}}{\lambda}$

which reduces to

$$[2.27]\quad \rho_\lambda = \left[\frac{\rho_{F_y}}{\rho_r^2 \cdot \rho_E}\right]^{1/2}$$

Combining [2.21], [2.25], and [2.26] gives

$$[2.28]\ (a)\quad \bar{F} = \bar{F}_y \qquad \text{, for } 0 \le \bar{\lambda} \le 0.15$$

$$(b)\quad \bar{F} = \bar{F}_y(1.035 - 0.202\lambda\rho_\lambda - 0.222\lambda^2\rho_\lambda^2) \qquad \text{, for } 0.15 < \bar{\lambda} < 1.0$$

$$(c)\quad \bar{F} = \bar{F}_y(-0.111 + 0.636\lambda^{-1}\rho_\lambda^{-1} + 0.087\lambda^{-2}\rho_\lambda^{-2}) \qquad \text{, for } 1.0 < \bar{\lambda} \le 2.0$$

$$(d)\quad \bar{F} = \bar{F}_y(-0.009 + 0.877\lambda^{-2}\rho_\lambda^{-2}) \qquad \text{, for } 2.0 < \bar{\lambda} < 3.6$$

$$(e)\quad \bar{F} = \bar{F}_y(\lambda^{-2}\cdot\rho_\lambda^{-2}) \qquad \text{, for } 3.6 < \bar{\lambda}$$

The associated coefficient of variation, V_F, is calculated from fundamental equations of statistics for the standard deviation (Kennedy and Neville 1976) assuming that the variables affecting F, that is, F_y, r, and E are independent, such that

$$[2.29]\quad V_F = \frac{\sigma_F}{\bar{F}}$$

and

$$[2.30]\quad \sigma_F = \left[\left(\frac{\partial\bar{F}}{\partial F_y}\right)^2 \cdot \sigma_{F_y}^2 + \left(\frac{\partial\bar{F}}{\partial r}\right)^2 \cdot \sigma_r^2 + \left(\frac{\partial\bar{F}}{\partial E}\right)^2 \cdot \sigma_E^2\right]^{1/2}$$

From each term in [2.30] the participation of each of the variables affecting F is obtained. Using [2.28](b) as an example, the terms in [2.30] become:

$$[2.31]\ (a)\quad \left(\frac{\partial\bar{F}}{\partial F_y}\right)^2 \cdot \sigma_{F_y}^2 = (1.035 - 0.303\lambda - 0.444\lambda^2)^2 \cdot \frac{\bar{F}_y^2}{\bar{F}_y^2}\,\sigma_{F_y}^2$$

$$= (1.035 - 0.303\lambda - 0.444\lambda^2)^2 \cdot \bar{F}_y^2 \cdot V_{F_y}^2$$

$$= P_1^2 \cdot \bar{F}_y^2 \cdot V_{F_y}^2$$

(b) $$\left(\frac{\partial \bar{F}}{\partial r}\right)^2 \cdot \sigma_r^2 = (0.202\lambda + 0.444\lambda^2)^2 \cdot \frac{F_y^2}{\bar{F}^2} \cdot \sigma_r^2$$

$$= (0.202\lambda + 0.444\lambda^2)^2 \cdot \bar{F}_y^2 \cdot V_r^2$$

$$= P_2^2 \cdot \bar{F}_y^2 \cdot V_r^2$$

(c) $$\left(\frac{\partial \bar{F}}{\partial E}\right)^2 \cdot \sigma_E^2 = (0.101\lambda + 0.222\lambda^2)^2 \frac{\bar{F}_y^2}{\bar{E}^2} \cdot \sigma_E^2$$

$$= (0.101\lambda + 0.222\lambda^2)^2 \bar{F}_y^2 \cdot V_E^2$$

$$= P_3^2 \cdot \bar{F}_y^2 \cdot V_E^2$$

where P_1, P_2, and P_3 are the participation factors which represent that portion of the equation which is a function of λ. Therefore, [2.30] can be simplified to

[2.32] $$\sigma_F = \bar{F}_y \left[P_1^2 \cdot V_{F_y}^2 + P_2^2 \cdot V_r^2 + P_3^2 \cdot V_E^2 \right]^{1/2}$$

and thus [2.29], in general form, becomes

[2.33] $$V_F = \frac{\sigma_F}{\bar{F}} = \frac{\bar{F}_y \left[P_1^2 \cdot V_{F_y}^2 + P_2^2 \cdot V_r^2 + P_3^2 \cdot V_E^2 \right]^{1/2}}{\bar{F}_y \cdot f(\lambda)}$$

$$= \frac{\left[P_1^2 \cdot V_{F_y}^2 + P_2^2 \cdot V_r^2 + P_3^2 \cdot V_E^2 \right]^{1/2}}{f(\lambda)}$$

In summary, the statistical quantities ρ_{Cr} and V_{Cr} are:

[2.34] In accordance to clause 13.3.1:

I: For Short Columns: $0 \leq \lambda \leq 0.15$

$$\rho_{Cr} = \rho_A \cdot \rho_{F_y} \cdot \rho_P$$

$$V_{Cr} = (V_A^2 + V_{F_y}^2 + V_P^2)^{1/2}$$

II: For Intermediate Columns: $0.15<\lambda\leq 3.6$

$$\rho_{Cr} = \rho_A \cdot \rho_F \cdot \rho_P$$

$$V_{Cr} = (V_A^2 + V_F^2 + V_P^2)^{1/2}$$

$$\text{where } V_F = \frac{(P_1^2 V_{F_y}^2 + P_2^2 V_r^2 + V_E^2)^{1/2}}{f(\lambda)}$$

where $f(\bar{\lambda}) = 1.035 - 0.202\bar{\lambda} - 0.222\bar{\lambda}^2$ for $0.15<\lambda\leq 1.0$

and $P_1 = 1.035 - 0.303\bar{\lambda} - 0.444\bar{\lambda}^2$

$P_2 = 0.202\bar{\lambda} + 0.444\bar{\lambda}^2$

$P_3 = 0.101\bar{\lambda} + 0.222\bar{\lambda}^2$

where $f(\bar{\lambda}) = -0.111 + 0.636\bar{\lambda}^{-1} + 0.087\bar{\lambda}^2$ for $1.0<\lambda<2.0$

and $P_1 = -0.111 + 0.318\bar{\lambda}^{-1}$

$P_2 = 0.636\bar{\lambda}^{-1} + 0.174\bar{\lambda}^{-2}$

$P_3 = 0.318\bar{\lambda}^{-1} + 0.087\bar{\lambda}^{-2}$

where $f(\bar{\lambda}) = 0.009 + 0.877\bar{\lambda}^{-2}$ for $2.0<\lambda<3.6$

and $P_1 = 0.0009$

$P_2 = 1.754\bar{\lambda}^{-2}$

$P_3 = 0.877\bar{\lambda}^{-2}$

III: For Long Columns: $\lambda>3.6$

$$\rho_{Cr} = \rho_I \cdot \rho_E \cdot \rho_P$$

$$V_{Cr} = (V_I^2 + V_E^2 + V_P^2)^{1/2}$$

[2.35] In accordance to clause 13.3.2

I: For Short Columns: $0 \leq \lambda \leq 0.15$

$$\rho_{Cr} = \rho_A \cdot \rho_{F_y} \cdot \rho_P$$

$$V_{Cr} = (V_A^2 + V_{F_y}^2 + V_P^2)^{1/2}$$

II: For Intermediate Columns: $0.15 < \lambda \leq 3.6$

$$\rho_{Cr} = \rho_A \cdot \rho_F \cdot \rho_P$$

$$V_{Cr} = (V_A^2 + V_F^2 + V_P^2)^{1/2}$$

where: $$V_F = \frac{(P_1^2 V_{F_y}^2 + P_2^2 V_r^2 + V_E^2)^{1/2}}{f(\lambda)}$$

where $f(\bar{\lambda}) = 0.990 - 0.122\bar{\lambda} - 0.367\bar{\lambda}^2$ for $0.15 < \lambda \leq 1.2$

and $P_1 = 0.990 - 0.187\bar{\lambda} - 0.734\bar{\lambda}^2$

$P_2 = 0.122\bar{\lambda} + 0.734\bar{\lambda}^2$

$P_3 = 0.061\bar{\lambda} + 0.367\bar{\lambda}^2$

where $f(\bar{\lambda}) = 0.051 + 0.801\bar{\lambda}^{-2}$ for $1.2 < \lambda \leq 1.8$

and $P_1 = 0$

$P_2 = 1.602\bar{\lambda}^{-2}$

$P_3 = 0.801\bar{\lambda}^{-2}$

where $f(\bar{\lambda}) = 0.008 + 0.942\bar{\lambda}^{-2}$ for $1.8 < \lambda \leq 3.6$

and $P_1 = 0$

$P_2 = 1.884\bar{\lambda}^{-2}$

$P_3 = 0.942\bar{\lambda}^{-2}$

III: For Long Columns: $\lambda > 3.6$

$$\rho_{Cr} = \rho_I \cdot \rho_E \cdot \rho_P$$

$$V_{Cr} = (V_I^2+V_E^2+V_P^2)^{1/2}$$

Chapter 3

Computer Aided Analysis of Column Behaviour and Strength

3.1. General

With the application of ultimate strength theories and progressively advancing techniques in structural analysis, such as the finite difference and finite element methods, the analysis of column behaviour has been reduced to the problem of establishing the mathematical model that truly reflects the behaviour of the material and the member. This is confirmed by verifying computer simulations against experimental results.

3.2. Ultimate strength analysis

The ultimate strength analysis is a method of determining the ultimate strength of a member (column, beam-column) by tracing its load-deflection response using incremental load steps. The ultimate strength of the member is that point on the load-deflection curve where the member can no longer sustain further increases in load and will proceed to deflect at reduced loads. At each load step, equilibrium between external loads and internal forces and moments is established

for each of the longitudinal elements into which the member is divided using an iterative procedure. Early techniques (Bjorhovde 1972) were restricted to evaluating the internal forces and moments at the mid-height cross-section, and thus the deflections at the mid-height cross-section.

Initial geometric imperfections are considered and thus the column begins to deflect with the onset of loading. The analysis also takes into account the initial residual stress pattern by subdividing the cross-section and setting an initial residual stress or strain for each subdivision. This subdivision of the cross-section permits the analysis of a non-homogeneous member and, in conjunction with the incremental load steps, permits progressive yielding across the cross-section to be taken into account. This, together with the longitudinal elements, permits progressive yielding along the length of the member to be taken into account as well.

3.3. Finite element method

The Finite element method is a sophisticated extension of numerical methods for matrix analysis (Liable 1985). It is a versatile method for analyzing structures that allows the evaluation of loads and displacements at any predetermined points along the structure. Thus, it is not restricted to mid-height displacements as with the earlier ultimate strength analysis techniques.

The principles of continuum mechanics are applied to a discretized structure. The structure is subdivided into "discrete" or "finite"

elements which are joined by a system of nodes. Each element is analyzed independently of the others with equilibrium enforced only at the nodes; stresses along the inter-element boundaries are not necessarily in equilibrium (Liable, 1985). Each node can have up to six degrees of freedom for each of the three translational and three rotational displacements.

The stiffness or displacement method of analysis is preferred in finite elements because it is easier to program (Chen and Atsuta 1977) than the flexibility or force method. The element stiffness matrices are developed using energy theorems relating the nodal forces and displacements (Ghali and Neville 1978), and thus enforcing equilibrium at the nodes. They are assembled into an "overall system matrix" by superimposing the element stiffness matrices at the common nodes (Willems and Lucas 1978). This system matrix is then used to solve for the unknown displacements at the nodes from which the stresses and strains can be determined (Willems and Lucas, 1978).

3.3.1. Finite element analysis of columns

The equilibrium equation for the elastic column takes the form

$$[3.1] \quad [K_s]\{U\} + [K_g]\{U\} = \{F\}$$

where $\{U\}$ and $\{F\}$ represent the nodal displacements and forces respectively. The material stiffness matrix, $[K_s]$, contains the elastic flexural stiffness matrices of the elements which are dependent on the material properties of the member, while the geometric stiffness matrix, $[K_g]$, is

dependent on the geom or displacement of the member (Chen and Atsuta, 1977).

For an initially perfectly straight column, the buckling phenomena is defined as the change in deflection at the constant load such that from [3.1] we get a homogeneous equation, such that

[3.2] $[K_s]\{\Delta U\} + [K_g]\{\Delta U\} = \{\Delta F\} = \{0\}$

and can be solved as an eigenvalue problem, such that

[3.3] $[K_s]\{\Delta U\} - \lambda[K_g]\{\Delta U\} = 0$

However, with the introduction of initial geometric imperfections, $\{U_i\}$, [3.1] takes the form

[3.4] $[K_s]\{U\} + [K_g]\{U\} + [K_g]\{U_i\} = \{F\}$

for which there is a unique solution.

The analysis of the plastic response is a more involved process than that of the elastic response. Detailed descriptions can be found in several texts dealing with plastic theories. Chen and Atsuta (1977) give a brief review on "Flow theory" which is the most widely used theorem in conjunction with finite elements. "Flow Theory" is a method of modeling the plastic stress-strain relationship which identifies the plastic strain as a function of the final state of stress, the plastic strain and the stress increment (Chen and Atsuta 1977). Elastic strain and plastic strain are dealt with independently, the sum of which, makes up the total strain. This theory is versatile and is capable of tracing the load-deformation response, even during load reversal.

3.3.2. Solution techniques

Because the geometric stiffness matrix is displacement dependent, it cannot be determined until the displacement is determined which, in turn, cannot be determined until the geometric stiffness matrix is determined. The nature of this problem requires an iterative solution technique which basically calculates successive increments of displacements for a given load step by updating the geometric stiffness matrix. The algorithms begin by setting the geometric stiffness matrix to zero and only using the material stiffness matrix in the first iteration cycle. The resulting increment in displacement is used to determine the geometric matrix which, in combination with the material stiffness matrix, is used, in turn, to calculate an additional increment in the displacements (Chen and Atsuta 1977; Willems and Lucas 1978). This routine is repeated until equilibrium is established at an acceptable level of precision.

There are several iteration techniques. The Newton-Raphson technique uses the tangent stiffness matrix, while the modified Newton-Raphson technique saves computer power by using the initial stiffness matrix and thus omits the calculations required to modify the stiffness matrix at each cycle. Because the latter technique does not update the stiffness matrix, it requires additional iterations. Figs. 3.1a and 3.1b illustrate the difference between the two techniques.

The above mentioned solution techniques fail as they approach the critical or ultimate load because the stiffness matrix becomes "soft" or,

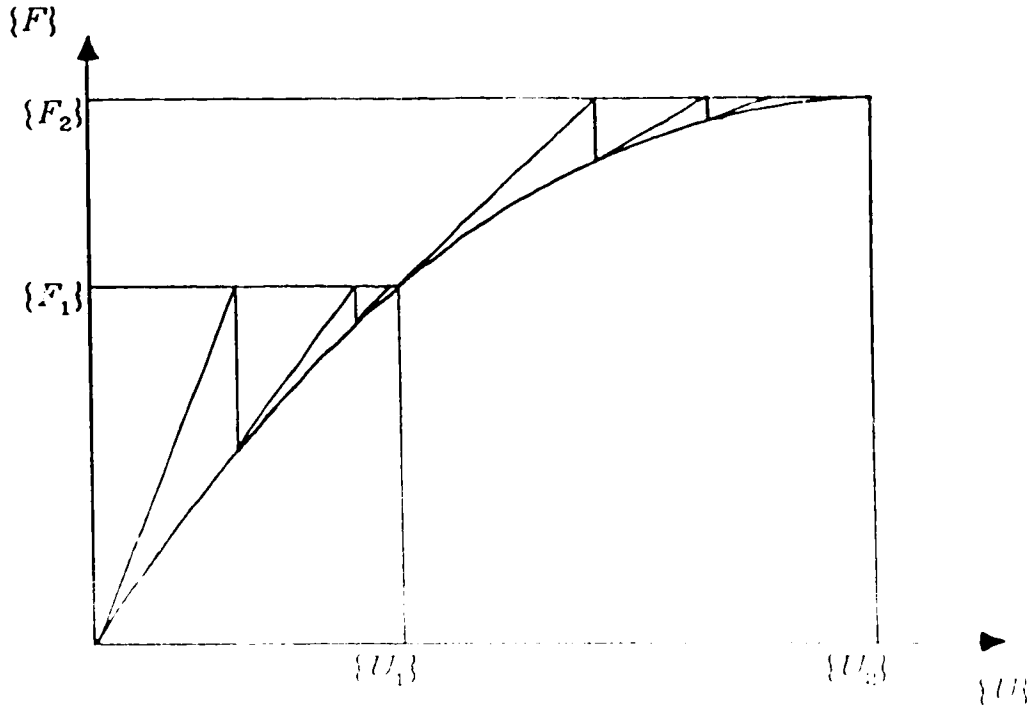

Fig. 3.1a Schematic diagram of the Newton-Raphson iteration technique

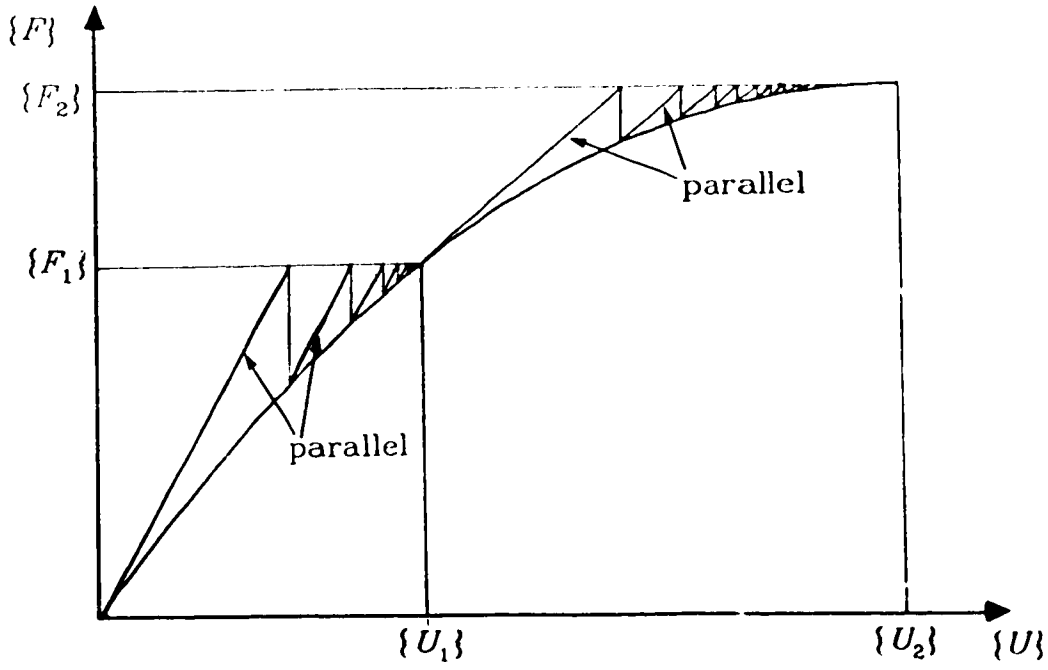

Fig. 3.1b Schematic diagram of the modified Newton-Raphson iteration technique

mathematically speaking, approaches singularity. Beyond the ultimate load, the solution techniques diverge and therefore cannot trace post buckling behaviour.

Solution strategies successful in tracing the post-buckling behaviour are discussed and analyzed by Ramm (1980). Two powerful techniques are the displacement-control method and the constant-arc-length method. The displacement control method avoids the problem of singularity by making displacement the dependent variable and load the independent variable. The constant arc-length-method, also known as the Riks-Wempner method (Riks 1972, 1979; Wempner 1971) basically sets the arc length of the tangent stiffness matrix to a prescribed value and converges by following a path normal to the tangent (Ramm 1980).

3.1. NISA

The program NISA is a multi-element, non-linear, finite element program of which the thin-walled open cross-section beam element (Osterrieder 1983) was used. This program was chosen for its ability to analyze three-dimensional members in the plastic range, for its capability of large deformation analysis which follows into the post-buckling range, and for its capacity to include both out-of-straightness and residual strains in the analysis. As cross-sectional distortions have not been incorporated in the program yet, it was not possible to include the influence of local buckling. This is considered to be inconsequential because the $\frac{b}{t}$ ratios are selected to preclude premature local

buckling.

With this program, the principles of continuum mechanics are applied to the elastic-plastic analysis of welded wide flange columns. The column is discretized into two systems of subdivisions. The first system defines the cross-section which is degenerated to a set of one-dimensional line elements on a two dimensional grid as shown in Fig. 3.2. This system of points is used to define the geometry of the section, the plate thickness, and to assign the residual strains according to a chosen residual stress model. The program uses this set of points to calculate the cross-sectional properties and the locations of the geometric and shear centers. The second system of subdivisions defines nodes along the length. This permits the assignment of geometric imperfections along the length, such as out-of-straightness for the three translational and three rotational displacements.

A type of beam-column behaviour particular to thin-walled open cross-sections is twisting due to the small torsional rigidity these sections possess. Rajaskaran and Murray (1973) were the first to introduce the concept of representing the element displacements by nodal displacements and assigning a seventh degree of freedom to each node to account for warping displacements (Chen and Atsuta 1977). However, this seventh degree of freedom, was restrained in this study on the premise that the axial loads in conjunction with the initial out-of-straightness about a single axis of symmetry would preclude warping, and the column would remain untwisted. Although it is true, in prac-

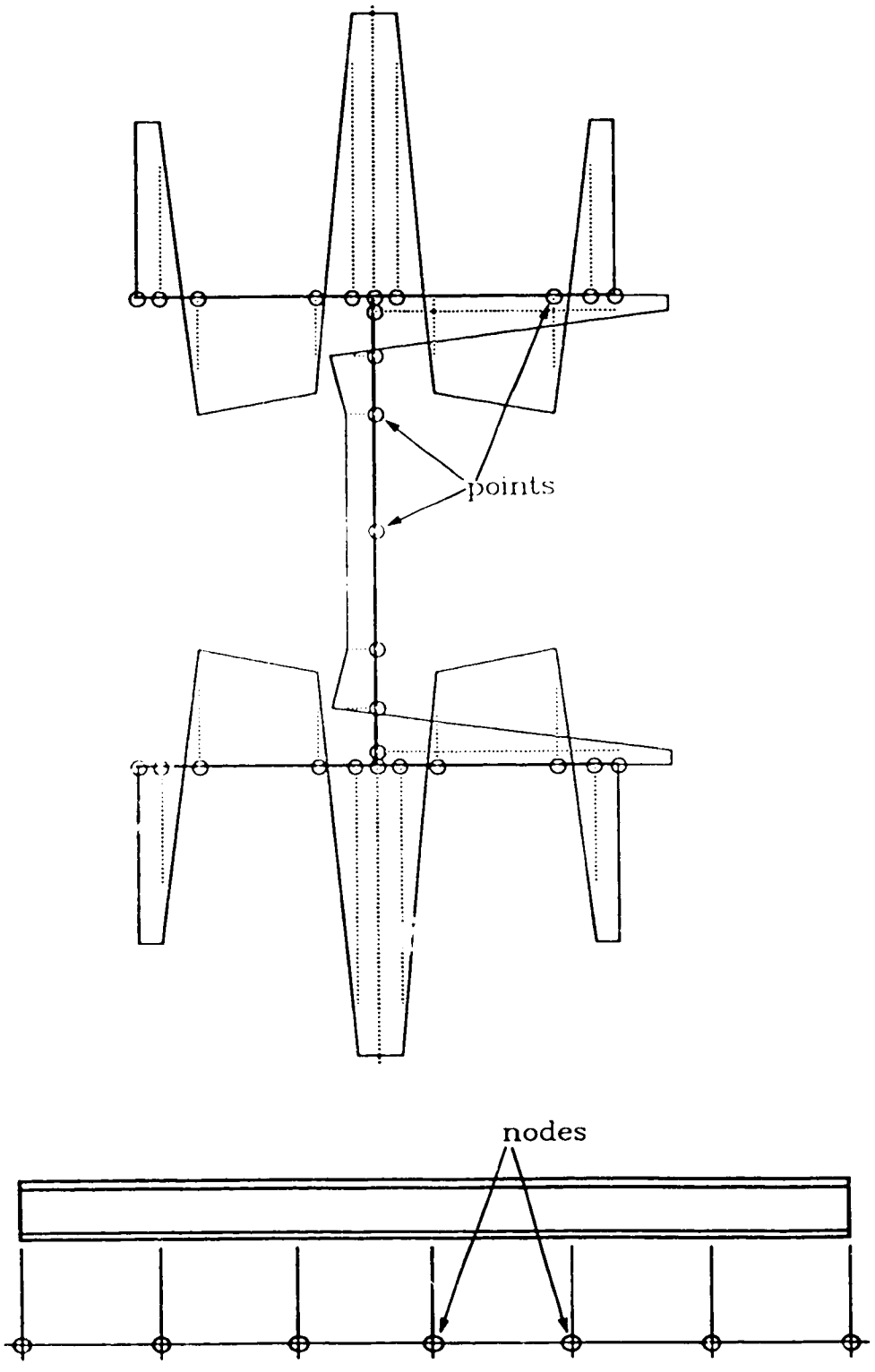

Fig. 3.2 Typical node system and cross-sectional points

tice, that some degree of out-of-straightness exists concurrently about both axes which could lead to biaxial buckling, this was considered to be outside the scope of this study.

The length of the column was represented by six elements (seven nodes) and the cross-sectional geometry was defined by as many as twenty-nine points. Rajasekaran in Chen and Atsuta (1977), illustrates the typically rapid convergence characteristics of the finite element method for a column buckling problem. The error in the critical load is less than 1% for a four element member and decreases with more elements. Increasing the number of elements increases the computer time without significant benefits as was confirmed by testing two identical columns with one divided into six elements and the other into ten elements. The ten element approximation only altered the sixth significant digit, unnecessarily exceeding the accuracy of any other data. This rapid convergence, characteristic of the finite element method, distinguishes it from other methods such as the finite difference method which can yield a 5% error for a four element approximation and converges relatively slowly toward the exact solution. The number of points used to define the geometry of the cross-section strictly depends on the complexity of the residual stress model.

The ultimate buckling load for a given column is determined by following the load-deflection response through a sequence of load steps. Two iteration techniques were used; the modified Newton-Raphson iteration technique was used in the elastic range, and the constant-

arc-length method was used up to and beyond the ultimate buckling load. When convergence at a particular load step was not obtained, a restart file containing the last column configuration was used and the loading parameters were reset.

3.4.1. Computer simulation programme

The computer testing programme consisted of a total of fifty simulations of column compression tests. The objective of the testing programme was to establish quantitatively the individual and combined effects of out-of-straightness and residual stresses and thus these parameters were varied. The simulations were conducted on steels with yield strengths based on McFalls and Tall (1969) except for two simulations which were run on steel with a yield strength of 300 MPa as currently used in Canada. Six experimental tests reported by McFalls and Tall (1969) and Bjorhorde (1972) were used as the benchmarks for the study.

Table 3.1 gives the details of the geometric and material properties for each of the computer simulations, together with the yield (compressive) loads and ultimate loads obtained. In addition, the maximum mid-height deflection at the ultimate load is given for a majority of the computer simulations. All tests are limited to the two cross-sections examined by McFalls and Tall (1969); the typical light section, 12H79, and the typical heavy section, 12H202. The various residual stress patterns are identified by two or three letter codes as discussed subsequently. The magnitude of out-of-straightness investigated ranged from $0.0000182 \simeq$

Table 3.1. Details of the computer analysis programme

Test no.	Section	Residual stress σ_r (code)	Modulus of elasticity E (ksi)	Yield stress σ_y (ksi)	Length L (inch.)	λ	O.O.S. Buckling Δ/L	axis	Axial load P_{max} (kips)	Yield load P_y (kips)	$\frac{P_{max}}{P_y}$ (NISA)	Δmax (inch.)
1	14X202	WB	29,500	35.8	122	0.336	1/1110	W	2100	2165	0.9700	
2	14X202	WB	29,500	35.8	244	0.672	1/1680	W	1784	2165	0.8240	0.623
3	14X202	WB	29,500	35.8	366	1.008	1/5230	W	1439	2165	0.6647	0.541
4	14X202	F	29,500	35.0	121.8	0.336	1/1110	W	2038	2117	0.9627	
5	14X202	F	29,500	35.0	243.6	0.673	1/1680	W	1779	2117	0.8403	
6	14X202	W	29,500	35.8	122	0.336	1/1110	W	2080	2165	0.9607	0.2892
7	14X202	W	29,500	35.8	244	0.672	1/1680	W	1727	2165	0.7977	0.7092
8	14X202	W	29,500	35.8	366	1.008	1/5230	W	1436	2165	0.6633	0.4386
9	14X202	WNT	29,500	35.8	244	0.672	1/1680	W	1570	2165	0.7252	
10	14X202	WNT	29,500	35.8	366	1.008	1/5230	W	1395	2165	0.6443	
11	14X202	none	29,500	35.8	122	0.336	1/1110	W	2117	2165	0.9778	0.0751
12	14X202	none	29,500	35.8	244	0.672	1/1680	W	2013	2165	0.9298	0.1653
13	14X202	none	29,500	35.8	366	1.008	1/5230	W	1830	2165	0.8453	0.3857
14	14X202	WL	29,500	35.8	244	0.672	1/1680	W	1677	2165	0.7746	
15	14X202	WB	29,500	35.8	122	0.336	1/3400	W	2139	2165	0.9852	
16	14X202	WB	29,500	35.8	244	0.672	1/3400	W	1840	2165	0.8499	0.5263
17	14X202	WB	29,500	35.8	366	1.008	1/3400	W	1414	2165	0.6531	0.5731
18	14X202	WB	29,500	35.8	122	0.336	1/1000	W	2095	2165	0.9677	0.1924
19	14X202	WB	29,500	35.8	244	0.672	1/1000	W	1726	2165	0.7972	
20	14X202	WB	29,500	35.8	366	1.008	1/1000	W	1295	2165	0.5982	1.451

Table 3.1. Details of the computer analysis programme (continued)

Test no.	Section	Residual stress σ_r (code)	Modulus of elasticity E (ksi)	Yield stress σ_y (ksi)	Length L (inch.)	λ	O.O.S Δ/L	Buckling axis	Axial load P_{max} (kips)	Yield load P_y (kips)	$\frac{P_{max}}{P_y}$ (NISA)	Δmax (inch.)
21	14X202	WB	29,500	35.8	396	0.672	1/1700	S	1778	2165	0.8212	1.235
22	14X202	WB	29,500	35.8	594	1.008	1/1700	S	1365	2165	0.6305	2.412
23	14X202	WB	29,500	35.8	396	0.666	1/1000	S	1731	2165	0.7995	1.310
24	14X202	WB	29,500	35.8	594	1.000	1/1000	S	1310	2165	0.6051	0.2758
25	14X202	none	29,500	35.8	244	0.666	1/5155	W	2087	2165	0.9640	
26	14X202	none	29,500	35.8	366	1.000	1/1710	W	1625	2165	0.7506	0.7053
27	12X79	WL	29,500	36.8	91	0.335	1/6070	W	835	855.8	0.975	
28	12X79	WL	29,500	36.8	182	0.671	1/3030	W	6583	855.8	0.769	0.4626
29	12X79	WL	29,500	36.8	273	1.006	1/54,600	W	529.6	855.8	0.619	0.4319
30	12X79	WB	29,500	36.8	91	0.335	1/6070	W	848	855.8	0.991	0.0848
31	12X79	WB	29,500	36.8	182	0.671	1/3030	W	728	855.8	0.850	0.4011
32	12X79	WB	29,500	36.8	273	1.006	1/54,600	W	591	855.8	0.690	1.141
33	12X79	WL	29,500	36.8	91	0.335	1/3400	W	830.4	855.8	0.970	
34	12X79	WL	29,500	36.8	273	1.006	1/3400	W	509	855.8	0.595	
35	12X79	WL	29,500	36.8	91	0.335	1/1000	W	813.6	855.8	0.950	0.2802
36	12X79	WL	29,500	36.8	182	0.671	1/1000	W	620.4	855.8	0.725	0.5870
37	12X79	WL	29,500	36.8	273	1.006	1/1000	W	471.0	855.8	0.550	
38	12X79	WL	29,500	36.8	319.2	0.671	1/1700	S	670.6	855.8	0.783	1.262
39	12X79	WL	29,500	36.8	478.8	1.006	1/1700	S	505.0	855.8	0.590	1.819

Table 3.1. Details of the computer analysis programme (continued)

Test no.	Section	Residual stress σ_r (code)	Modulus of elasticity E (ksi)	Yield stress σ_y (ksi)	Length L (inch.)	λ	O.O.S. Δ/L	Buckling axis	Axial load P_{max} (kips)	Yield load P_y (kips)	$\frac{P_{max}}{P_y}$ (NISA)	Δmax (inch.)
40	12X79	WL	29,500	36.8	319.2	0.671	1/1000	S	651.1	855.8	0.761	1.416
41	12X79	WL	29,500	36.8	478.8	1.006	1/1000	S	486.1	855.8	0.568	2.374
42	12X79	F	27,500	36.7	91.5	0.349	1/6100	W	786.7	853.4	0.9685	
43	12X79	F	27,500	36.7	183.0	0.698	1/3050	W	667.0	853.4	0.8186	
44	12X79	F	27,500	36.7	274.5	1.047	1/54,950	W	557.0	853.4	0.6527	
45	14X202	WNR	29,500	35.8	244	0.666	1/1680	W	1763	2165	0.8143	
46	14X202	WB	29,500	35.8	244	0.672	1/2000	W	1799	2165	0.8309	
47	14X202	WB	29,500	49.3	207.6	0.672	1/1680	W	2552	2982	0.8558	
48	14X202	WB	29,500	49.3	311.4	1.008	1/5230	W	2182	2982	0.7317	
49	14X202	none	29,500	35.8	366.0	1.000	1/1000	W	1496	2165	0.6908	
50	14X202	none	29,500	35.8	122.0	0.333	1/3400	W	2151	2165	0.9935	

1/55,000 to the code tolerance limit of 0.001 = 1/1000. The value of the modulus of elasticity used in this study of 29,500 ksi = 203,400 MPa, was obtained from data reported by Huber and Beedle (1954), Fugita and Driscoll (1962), and Galambos (1965) in association with the data given by McFalls and Tall (1969) and Bjorhovde (1972) on the six experimental tests. The value of the modulus of elasticity was not given in the latter two references. The three values for the slenderness parameter, λ, the corresponding column lengths, and the initial out-of-straightness were based on the data reported by McFalls and Tall (1969) in conjunction with that reported by Bjorhovde (1972).

3.4.2. Evaluation of NISA

NISA's ability to simulate column behaviour accurately can be assessed, in part, by comparing the load-deflection response obtained using NISA to that of the six experimental tests reported by the Lehigh group (McFalls and Tall 1969; Bjorhovde 1972) as shown in Figs. 3.3 to 3.8 for simulations 1, 2, 3, 27, 28, and 29 respectively. The comparisons were somewhat restricted as the original data were reported to only two significant digits. Moreover, as the NISA simulations, in general, were not carried significantly beyond the maximum load, the extent of the flat portions of the curves in this region cannot be compared.

The ultimate loads predicted by the computer simulations are in good agreement with the test values with a mean test (experimental) / predicted ratio of 1.010 and a coefficient of variation of 0.046 for the six tests. Even the greatest difference, for simulation 29 with the

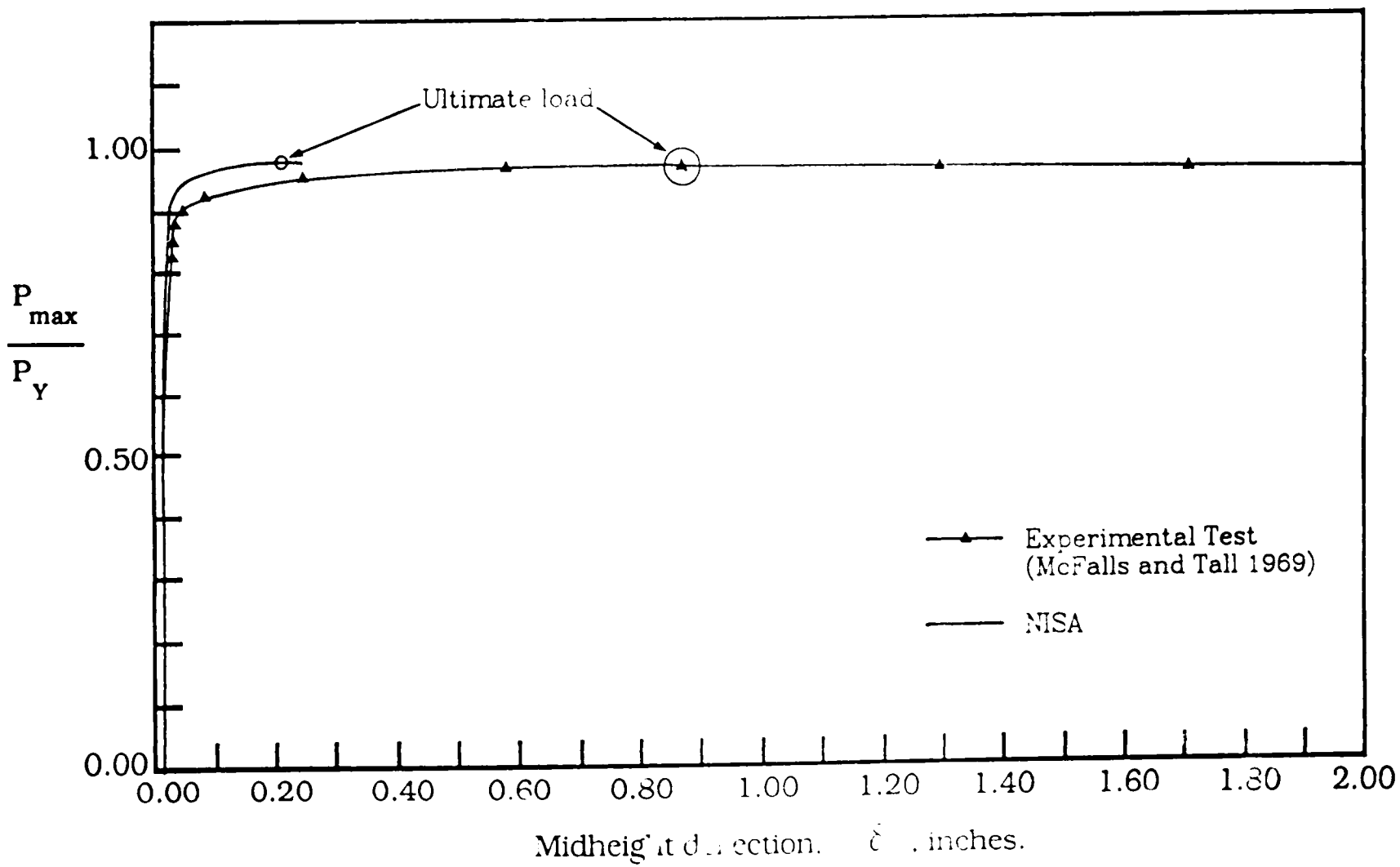

Fig. 3.3 Load-deflection curves for WWF 12x[illegible] at λ = 0.336

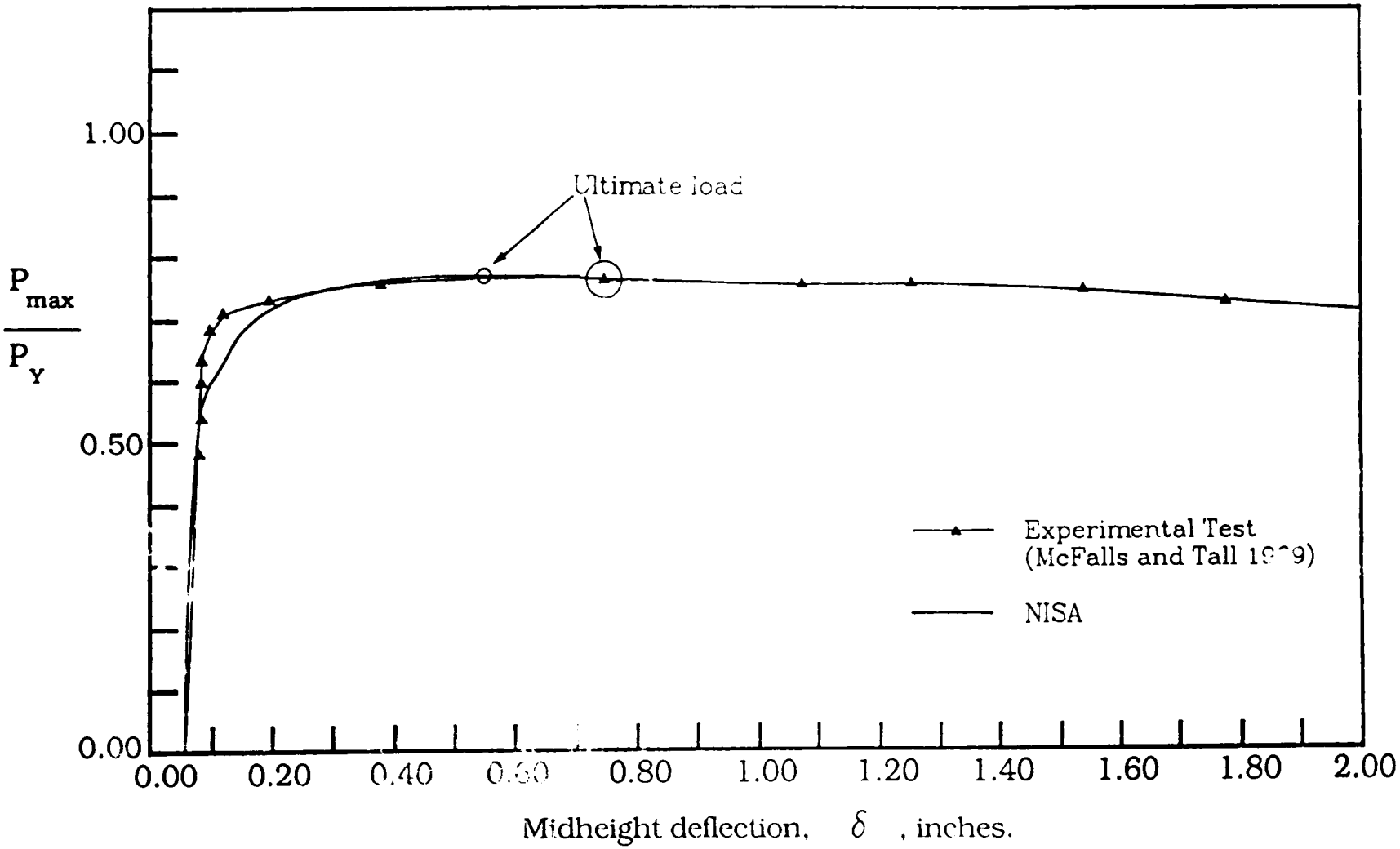

Fig. 3.4 Load-deflection curves for WWF 12x79 at $\lambda = 0.672$

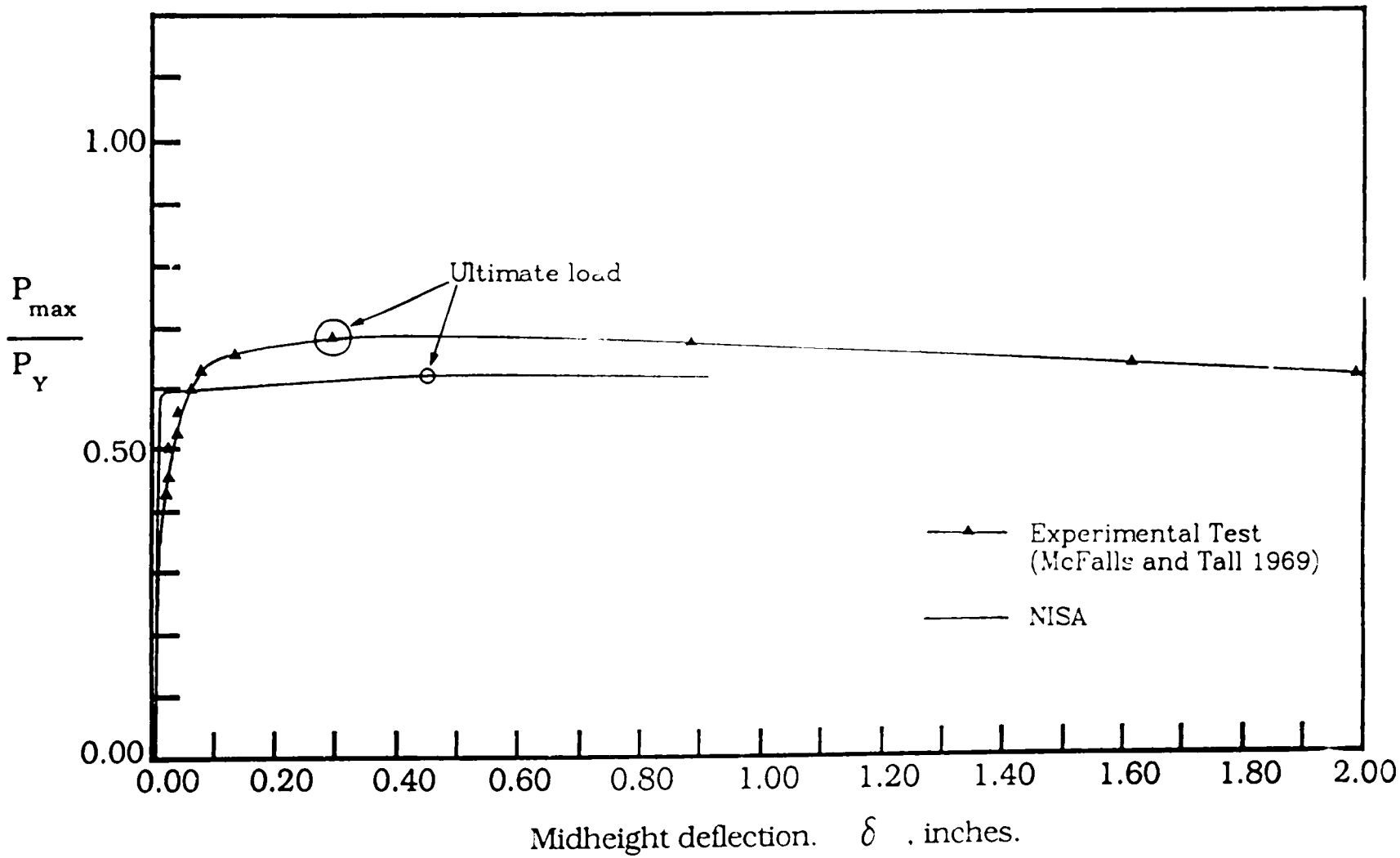

Fig. 3.5 Load-deflection cur[illegible] for WWF 12x79 at [illegible] = 1.007

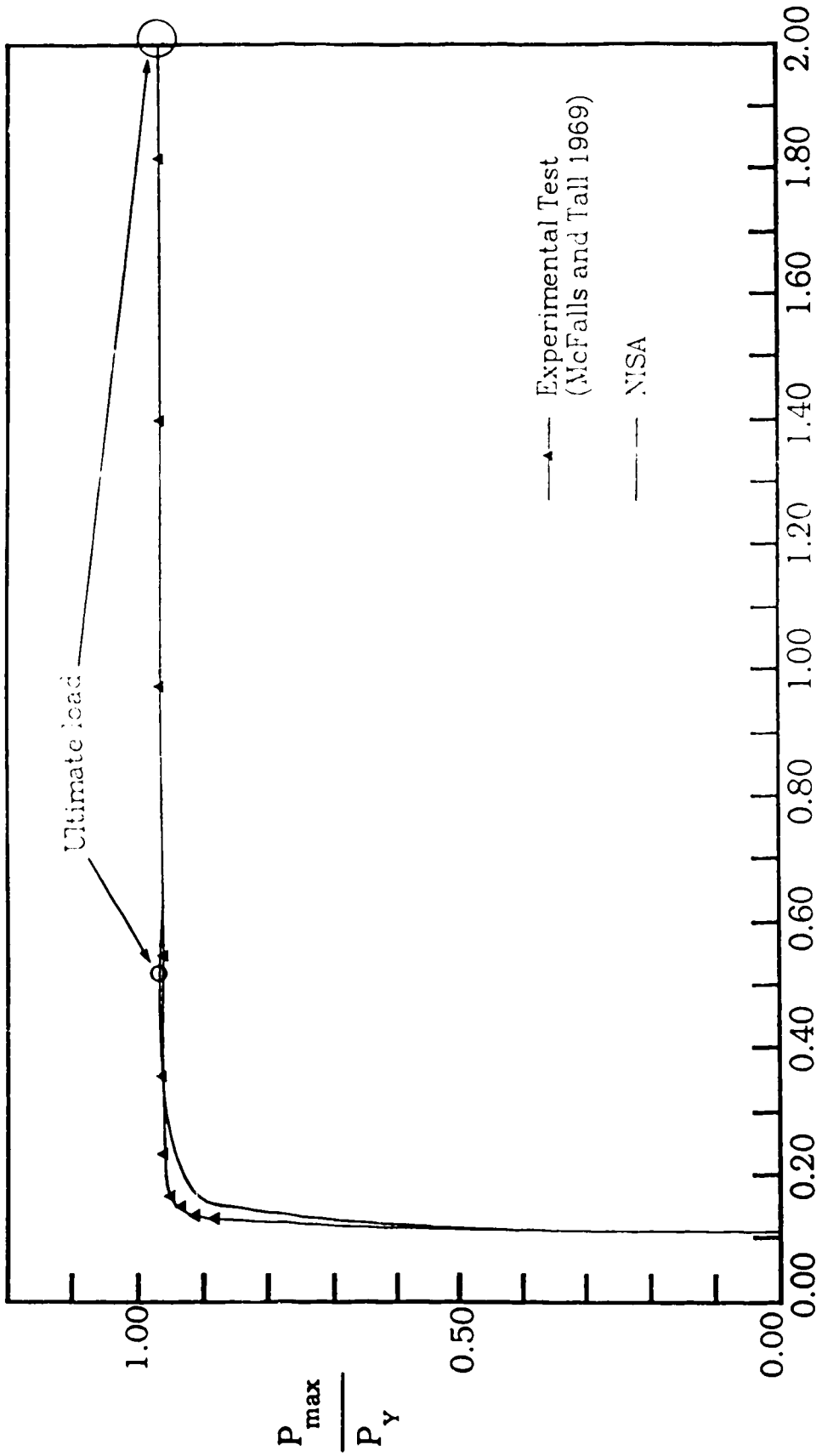

Fig. 3.6 Load-deflection curves for WWF 14x202 at $\lambda = 0.336$

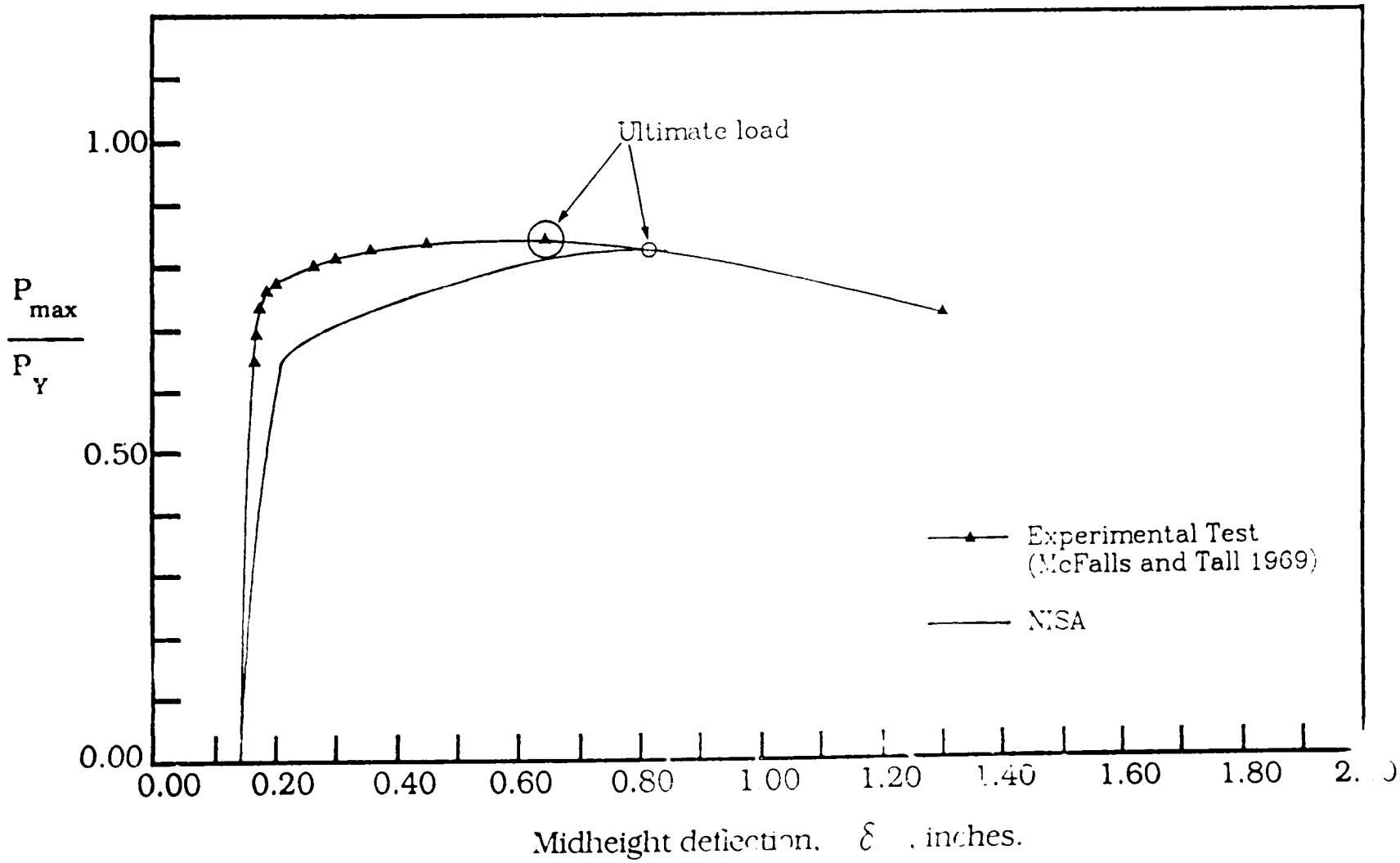

Fig 3.7 Load-deflection curves for WF 14x202 at λ = 0.672

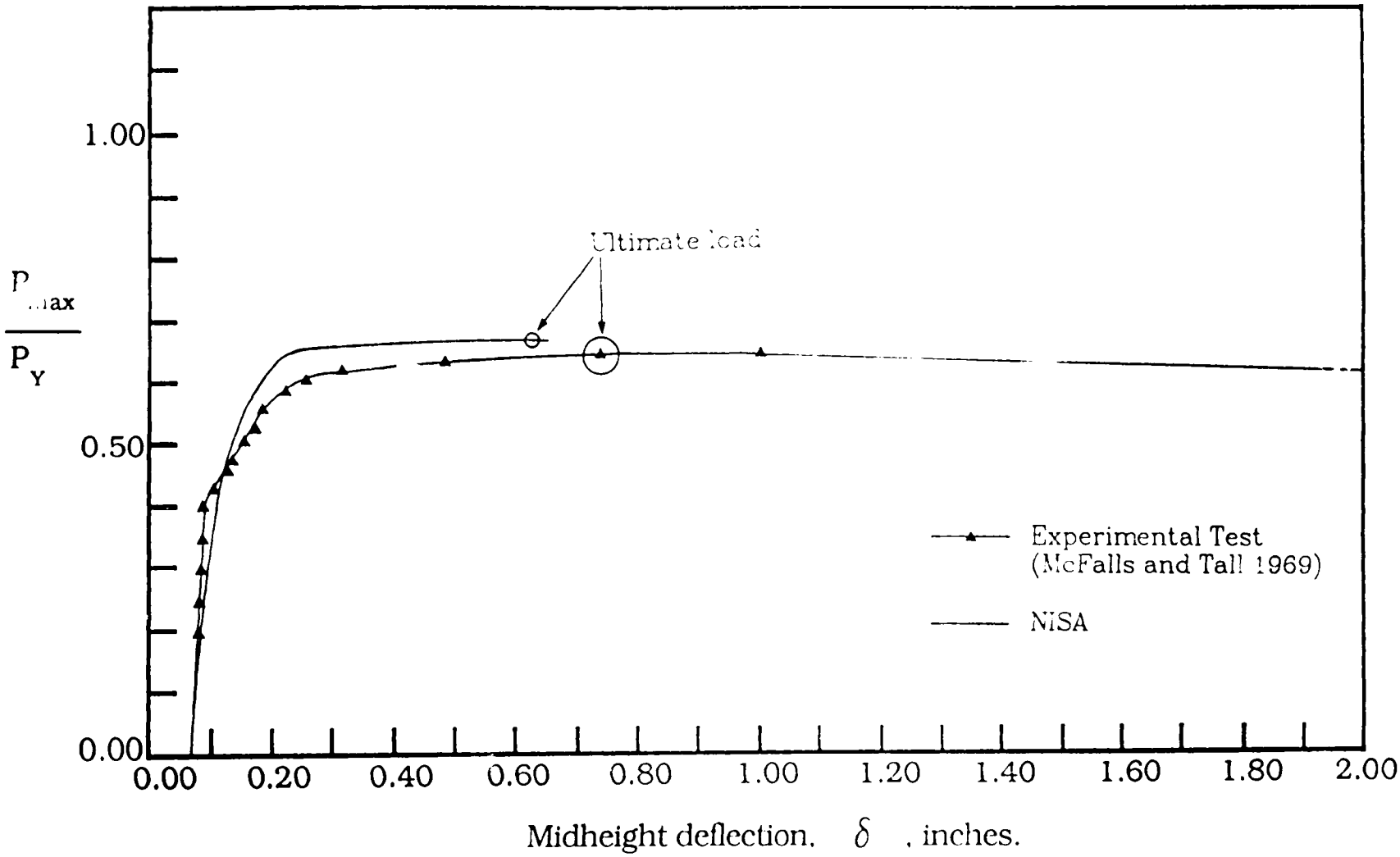

Fig. 3.8 Load-deflection curves for WWF 14x202 at λ = 1.007

experimental / predicted ratio is 1.098, did not exceed 10%. However, simulation 29 is believed to exhibit an excessive difference for a finite element analysis of this caliber and may be attributed to the fact that an insufficient number of significant digits were reported in the literature on the test results.

Although deflections of structural members, especially those related to inelastic stability, are more difficult to predict, the simulated load-deflection curves in Figs. 3.5 to 3.8 are in reasonable agreement with the test curves. They reflect the initial elastic behaviour, followed by progressive yielding until the maximum load is reached. The deflections at maximum load are also in reasonable agreement with the experimental values, but of greater significance, is that NISA, was able to model the behaviour at ultimate loads where the load remained virtually constant as deflections increased significantly (see Figs. 3.4, 3.5, and 3.8 in particular).

3.4.3. Models of residual stress patterns

In Figs. 3.9 and 3.10 typical residual stress patterns are shown by a solid line and variations by dashed lines. These patterns were used to examine the effects of residual stresses on column strength and behaviour. The solid patterns are modeled after those reported by McFalls and Tall (1969) shown in Figs. 2.3 and 2.4 and confirmed by Tall and Alpsten (1969) to be characteristic patterns for 14H202 (heavy) and 12H79 (light) sections, respectively. Besides linearizing the residual stress pattern, the minor modification of setting the maximum tensile

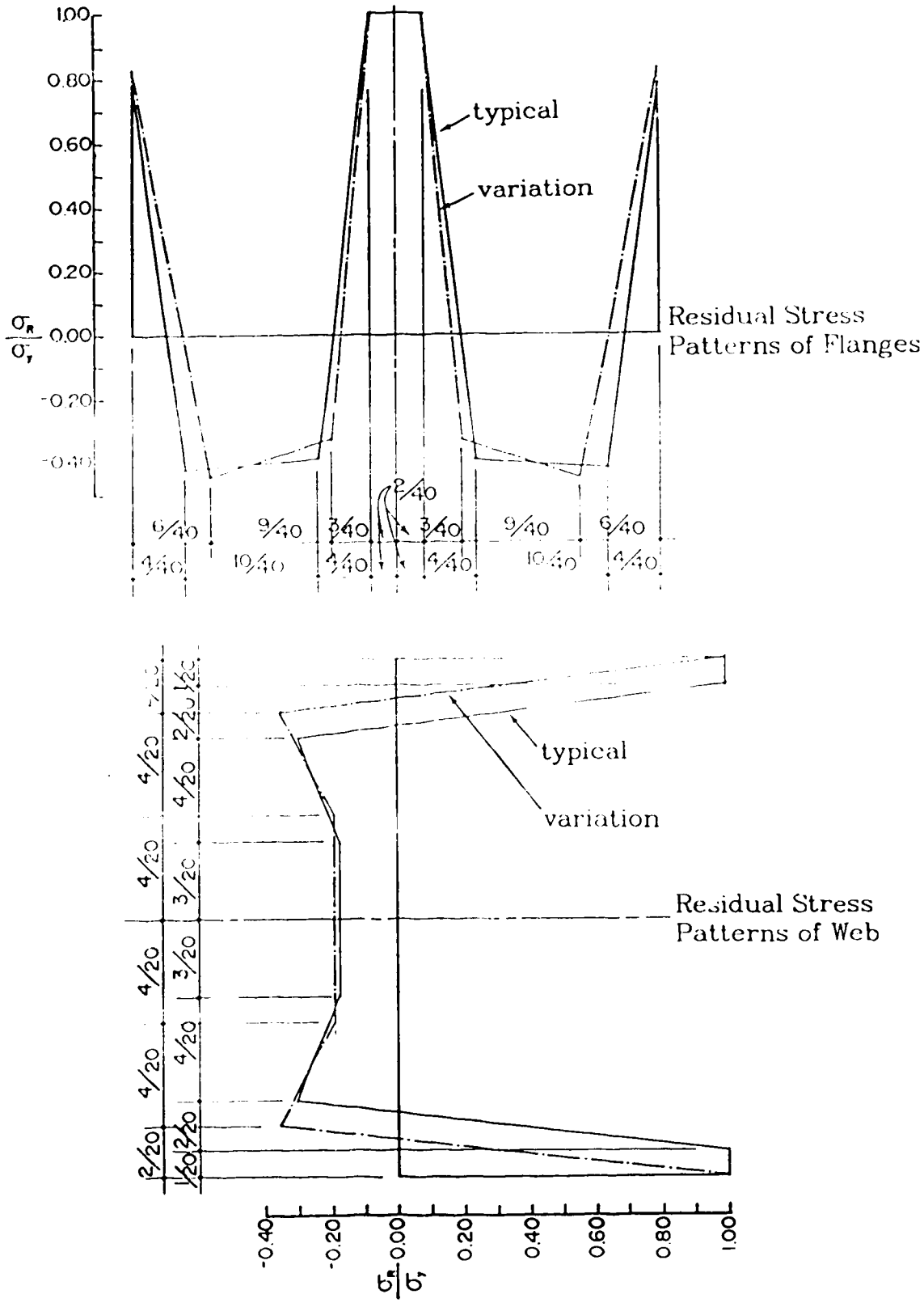

Fig. 3.9 **Models of residual stress distributions for WWF 12x79 (light) sections.**

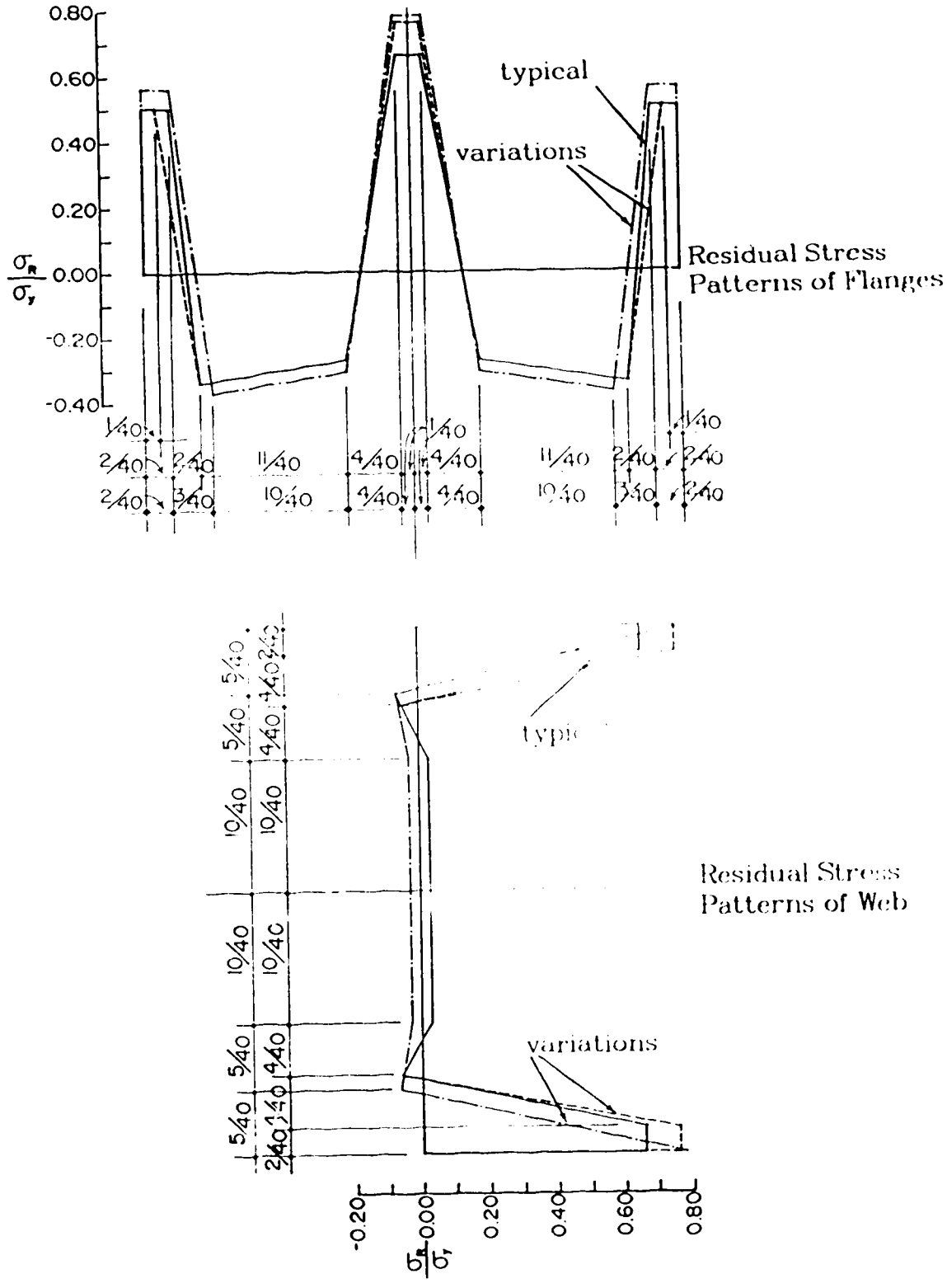

Fig. 3.10 Models of residual stress distributions for WWF 14x202 (heavy) sections.

residual stress at 1.0 times the yield strength was made because the program for the open beam cross-section element of NISA can analyze homogeneous structures only. Although this does not recognize the small volume of material in the tensile residual stress region at the web-flange junction which could experience property changes due to the high heat input and rapid cooling, it is believed to be inconsequential.

To broaden the spectrum of the residual stress patterns studied, that for light sections was used for heavy sections and vice versa. As well, heavy and light sections were investigated with no residual stresses, with tensile residual stresses at the flange tips ranging from $0.50\sigma_y$ to $0.82\sigma_y$, and with average compressive residual stresses in the flanges ranging from $0.275\sigma_y$ to $0.405\sigma_y$, extending over 0.450 to 0.550 of the flange width. As shown in Figs. 3.9 and 3.10, the tensile residual stress were either considered to be constant over a small region near the flange tip or to decrease rapidly from the maximum value. The maximum compressive residual stresses do not vary greatly. Fig. 3.11 read in conjunction with Table 3.2 gives a schematic presentation of the various proportions and magnitudes of the residual stress distributions investigated. They are identified by the two or three letter codes used in Table 3.1.

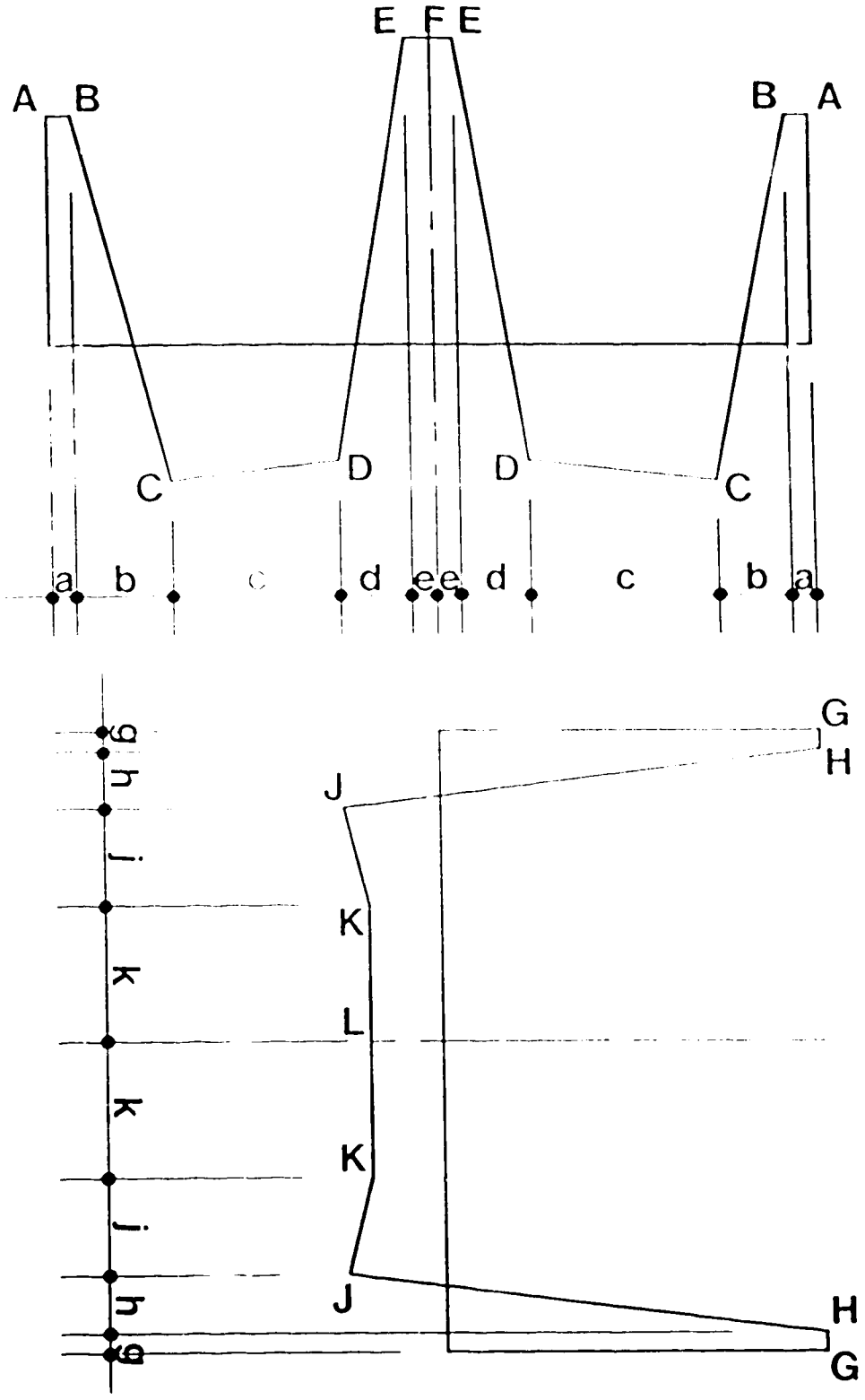

Fig. 3.11 Schematic diagrams of the residual stress distributions investigated

Table 3.2. Specifications for residual stress distributions illustrated in Fig. 3.11

Residual stress	Magnitudes at designated locations as a percentage of σ_Y										
	flanges						web				
code	A	B	C	D	E	F	G	H	J	K	L
WB	0.50	0.50	-0.34	-0.27	0.658	0.658	0.658	0.658	-0.06	0.03	0.03
F	0.56	0.56	-0.37	-0.31	0.78	0.78	0.78	N/A	-0.06	-0.03	-0.03
W	0.50	0.50	-0.34	-0.27	0.76	0.76	0.658	0.658	-0.06	0.03	0.03
WNT	0.0	0.0	-0.34	-0.27	0.98	0.98	0.980	0.980	-0.06	0.03	0.03
WL	0.78	N/A	-0.42	-0.39	1.0	1.0	1.0	1.0	-0.30	-0.18	-0.18
FL	0.82	N/A	-0.44	-0.33	1.0	1.0	1.0	N/A	-0.35	-0.19	-0.19
WNR	0.50	0.50	-0.31	-0.24	0.658	0.658	0.658		-0.06	0.04	0.03

Residual stress	Relative distances as a fraction of the plate width								
	flanges					web			
Code	a	b	c	d	e	g	h	j	k
WB	2/40	2/40	11/40	4/40	1/40	1/20	2/20	2/20	5/20
F	2/40	3/40	10/40	4/40	1/40	N/A	5/40	5/40	10/40
W	1/40	3/40	11/40	4/40	1/40	1/20	2/20	2/20	5/20
WNT	1/40	1/40	11/40	4/40	1/40	1/20	2/20	2/20	5/20
WL	N/A	2/20	5/20	2/20	1/20	1/20	2/20	4/20	3/20
FL	N/A	6/40	9/40	3/40	2/40	N/A	2/20	4/20	4/20
WNR	1/40	3/40	11/40	4/40	1/40	1/20	2/20	2/20	5/20

3.4.4. Analysis of the load deflection curves from the parametric study

The variations in out-of-straightness and in residual stress distributions affect the load deflection curves. Initially, the response of the columns is elastic with departures from linearity due to second order geometric effects. With the onset of plastic deformations, the columns lose stiffness and the load-deflection curves maximum loads are reached. Fig. 3.12 shows that for the columns investigated, the increase in load after the onset of yielding is only about 2.5 percent of the total. The overall shape of the load-deflection curves is typical of members attaining an ultimate strength, as distinct from those associated with the buckling of members. The large increase in deflections as the ultimate load is approached indicates that the behaviour is ductile and, in a structure, would provide warning of failure.

3.4.4.1. Effect of out-of-straightness

In Fig. 3.12, for columns with a slenderness parameter of 0.672, the load-deflection curves are drawn for three different magnitudes of initial out-of-straightness with other parameters affecting column strength held constant. All three curves are similar in shape and with increasing out-of-straightness:

(1) the initial slope of the curve increases,

(2) inelastic action begins earlier,

(3) the ultimate load decreases, and

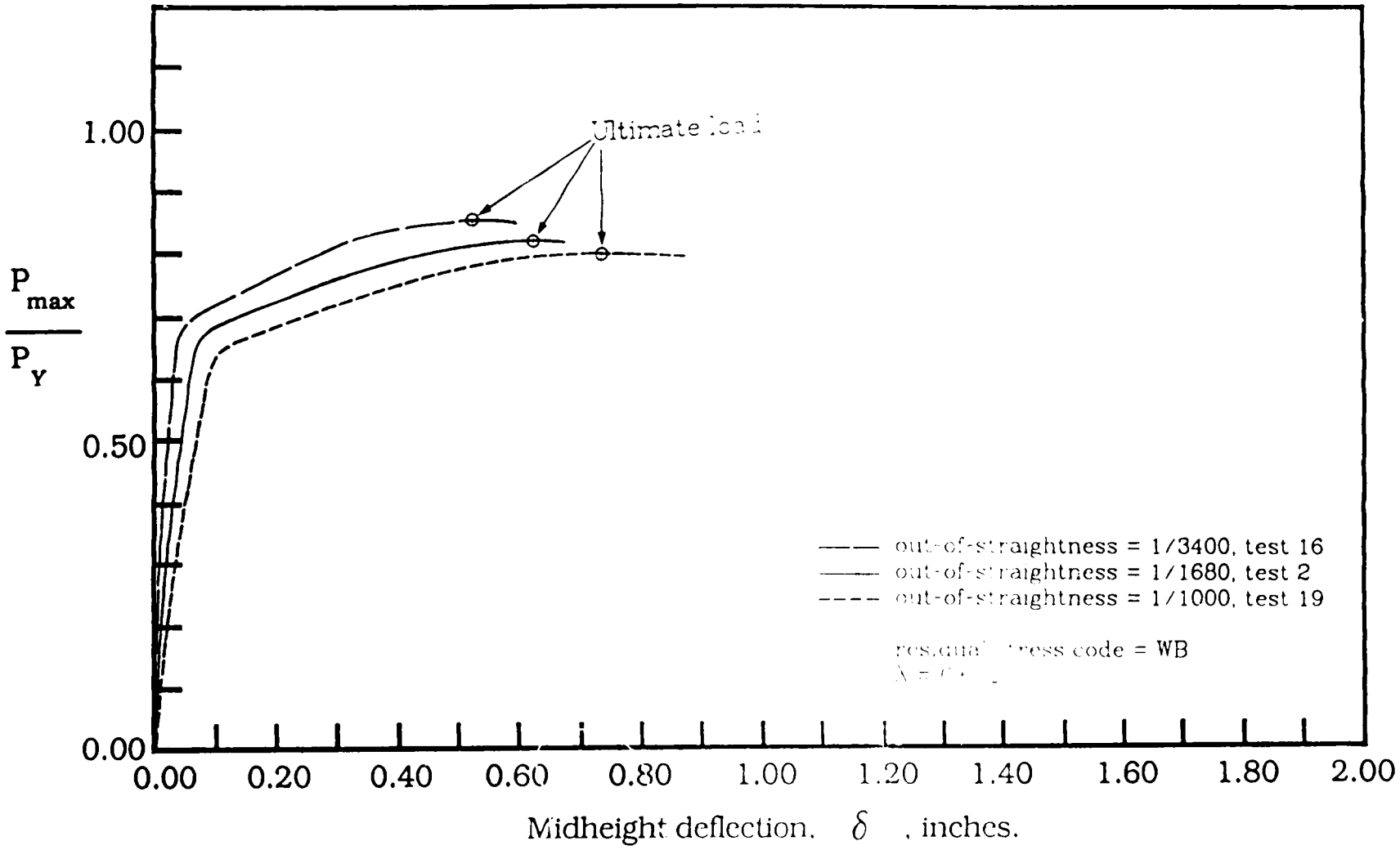

Fig. 3.12 Effect of out-of-straightness on load-deflection response

(4) the mid-height deflection at ultimate load increases.

Although the ultimate load decreases with out-of-straightness, the increase in mid-height deflection prior to reaching the ultimate load, results in greater deformation at the maximum load. The load-deflection response for the column with an out-of-straightness of 1/1000 attained a total mid-height deflection of 0.98 inches (0.74 inches plus initial out-of-straightness of 0.24 inches) at maximum load as compared to 0.60 inches (0.53 inches plus initial out-of-straightness of 0.07 inches) for the column with an initial out-of-straightness of 1/3400.

3.4.4.2. Effect of residual stresses

The effect of residual stresses on the load-deflection curves is illustrated in Fig. 3.13 with other parameters affecting column strength held constant. The four residual stress patterns represented are WB for the pattern typical of heavy sections, W for a variation of this pattern, WNT for the pattern typical of heavy sections modified to have no tensile residual stresses at the flange tips, and WL for the pattern typical of light sections. The initial elastic portion of the load-deflection curve remains the same, as would be expected. However, the onset of inelastic action occurs earlier with increased residual stresses as seen by comparing the curve WL for a column with a maximum compressive residual stress of $0.405\sigma_y$ with the remaining three curves all having a maximum compressive residual stress of $0.305\sigma_y$.

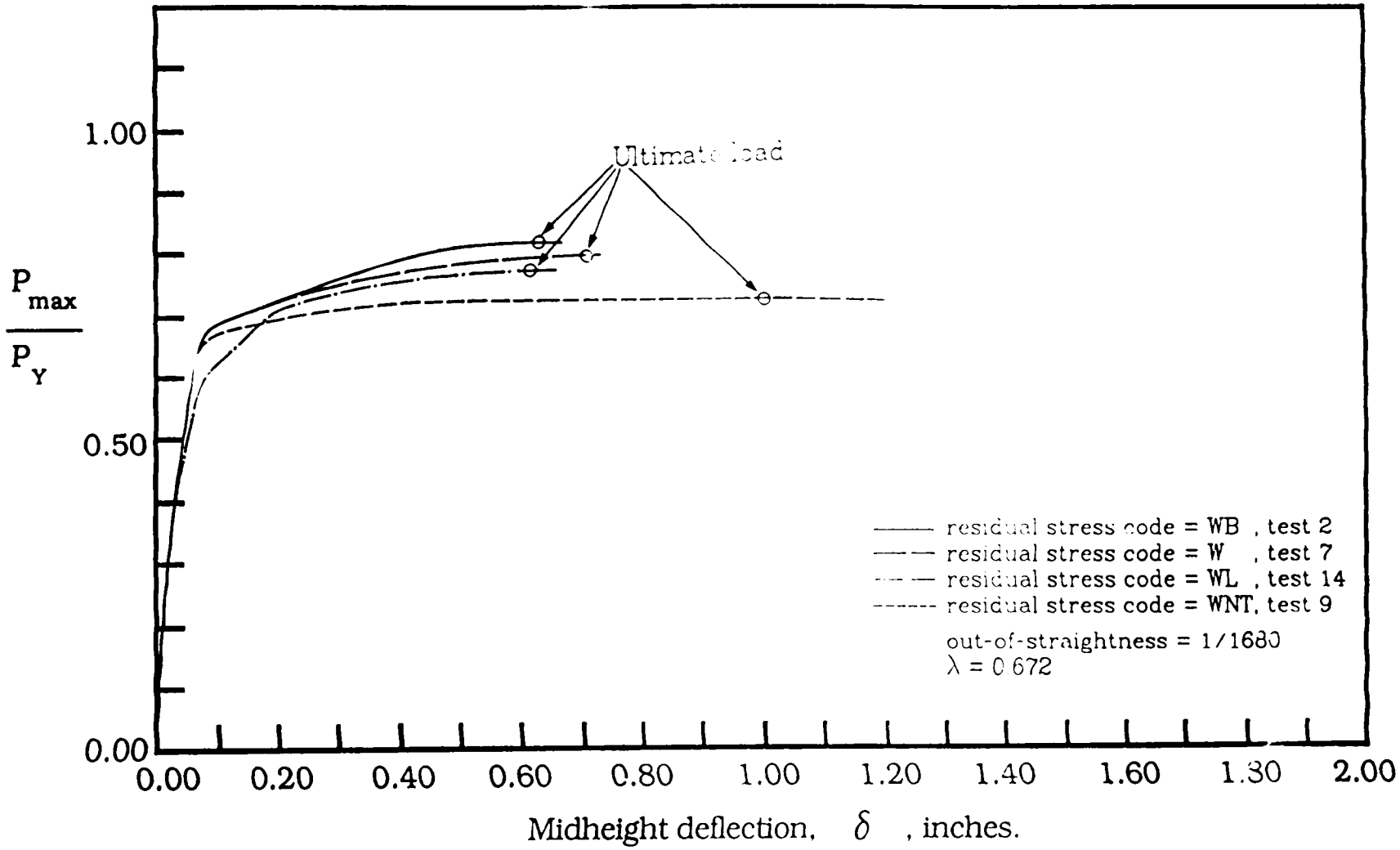

Fig. 3.13 Effect of residual stresses on load-deflection response

The curves with residual stress codes WB, W, and WNT all have the same maximum compressive residual stress of $0.305\sigma_y$ with the only difference being the maximum tensile residual stresses at the flange tips and the residual stress pattern. The differences in the maximum load observed between residual stress codes WB and W must be attributed to this pattern. The column with no tensile residual stresses at the flange tips (curve WNT) has its strength reduced by about 10% but with increased deflection at maximum load, improving ductility

Chapter 4

Statistical Parameters

4.1 General

The statistical data required to determine the factored resistance of WWF sections consist of that related to the variations of the geometric properties, material properties, and the professional factor, that is, the ratio of experimental test strengths to that predicted by the appropriate design code. Data related to geometric and material properties were collected during a site visit to Algoma Steel Corporation Limited in Sault Ste. Marie in April, 1986. These data were substantiated with a limited number of coupon tests conducted at the University of Alberta. Additional data necessary to establish the professional factor were obtained from the parametric study on column behaviour and from data reported in various publications.

4.2. Geometric variations

The term geometric variations is used to describe the variations in the dimensions of the plates used to manufacture WWF members, the cross-sectional properties of the WWF's, and includes the alignment of the plates with respect to each other (tilt and skewness) and the out-of-straightness of the member. These variations are depicted in Fig. 4.1. Visible tilt or skewness of the assembled plates rarely occurs as the manufacturing process is designed to minimize this occurrence. The magnitudes of the imperfections are believed to be inconsequential although no data supporting this assumption was available. Out-of-straightness, that is, camber and sweep is discussed subsequently.

The cross-sectional properties of concern are the area, A, the moment of inertia about both principal axes, I_x, and I_y, and the corresponding radii of gyration, r_x and r_y. Variations in these geometric properties were derived from measurements of the flange and web plate thicknesses t and w, respectively, the flange widths, b, and the cross-sectional depth, d.

4.2.1. Plate thickness

Plate thickness, monitored in the plate mill by a computer aided production system, allows plates to be rolled to very close tolerances. A quality assurance team performs spot checks to avoid gross errors and to ascertain that the computer monitoring equipment is functioning correctly. A second set of spot checks, conducted by the quality assurance team of the mill's welded-beam division, are reported in this

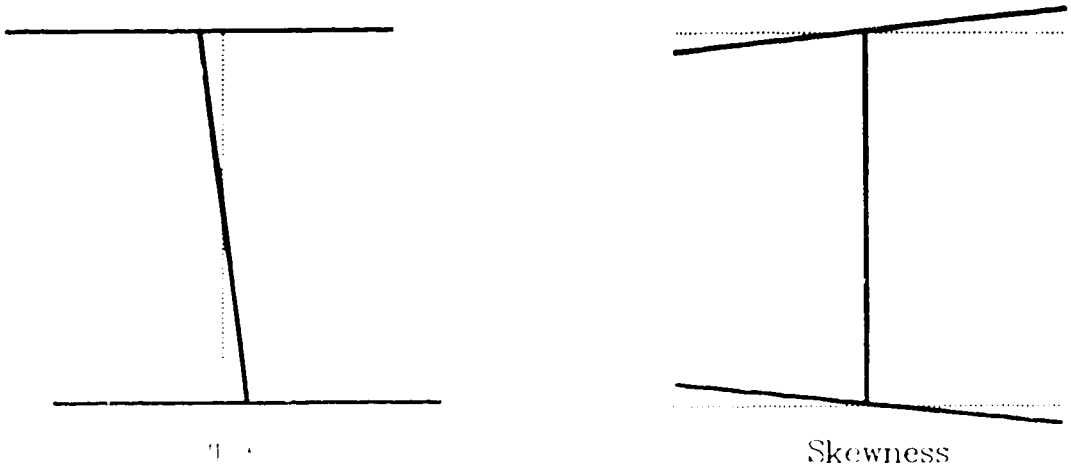

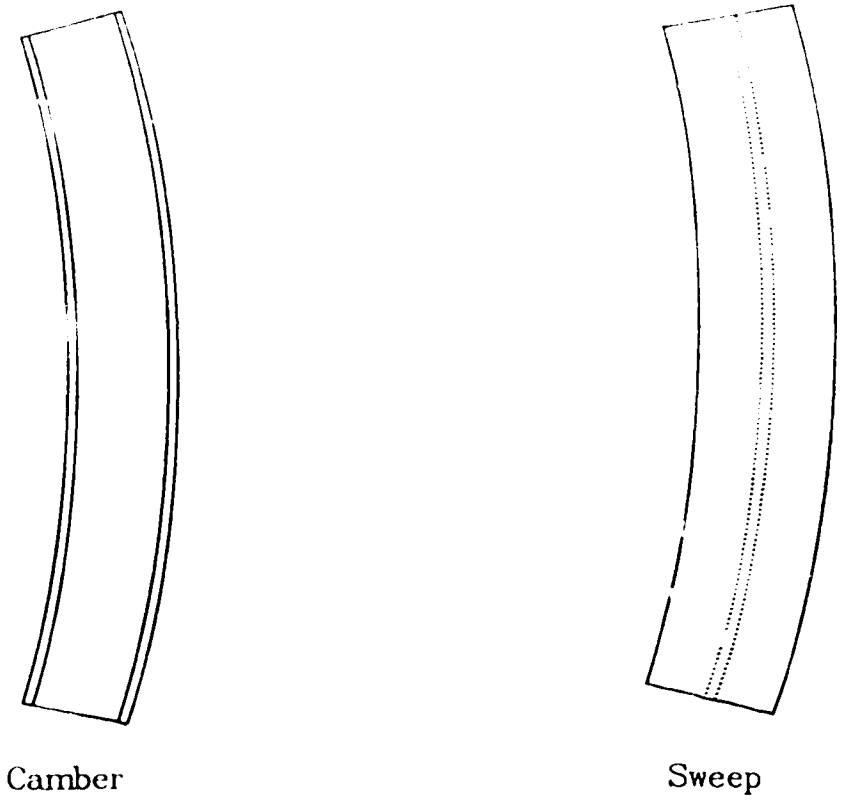

Fig. 4.1 Geometric variations in plate alignment

study.

The mean or mode of three measurements, taken at different locations when the member is cold with a micrometer having a sensitivity of 0.001 inches, is recorded as the official plate thickness. Measurements taken by the author at different locations along the length of two plates with nominal thicknesses of 1.575 and 0.551 inches gave a coefficient of variation for the two sets of 13 measurements of 0.0036. This indicates that the variation of thickness within a plate is negligible.

Fig. 4.2 gives the frequency distribution of a sample of 92 values of the measured/nominal plate thicknesses obtained from the quality assurance files. No thickness is less than 0.9 of the nominal thickness, consistent with the practice of rolling plates slightly over nominal. The mean value of the measured/nominal ratio was found to be 1.010 with a coefficient of variation of 0.00784.

4.2.2. Plate width and cross-section depth

The variation in cross-sectional depth depends chiefly on variations in plate width as the plate thickness variations are small. A visual comparison of the data in Figs. 4.3 and 4.4 giving frequency distributions for the plate width, b, and cross-sectional depth, d, shows that the welding process does not have a significant additional effect.

The variation in plate width depends on the care taken in setting the torch heads. Distances between the heads are set, allowing for loss of width due to burn-off. A number of measurements between several combinations of torch heads are taken as an additional check. After the

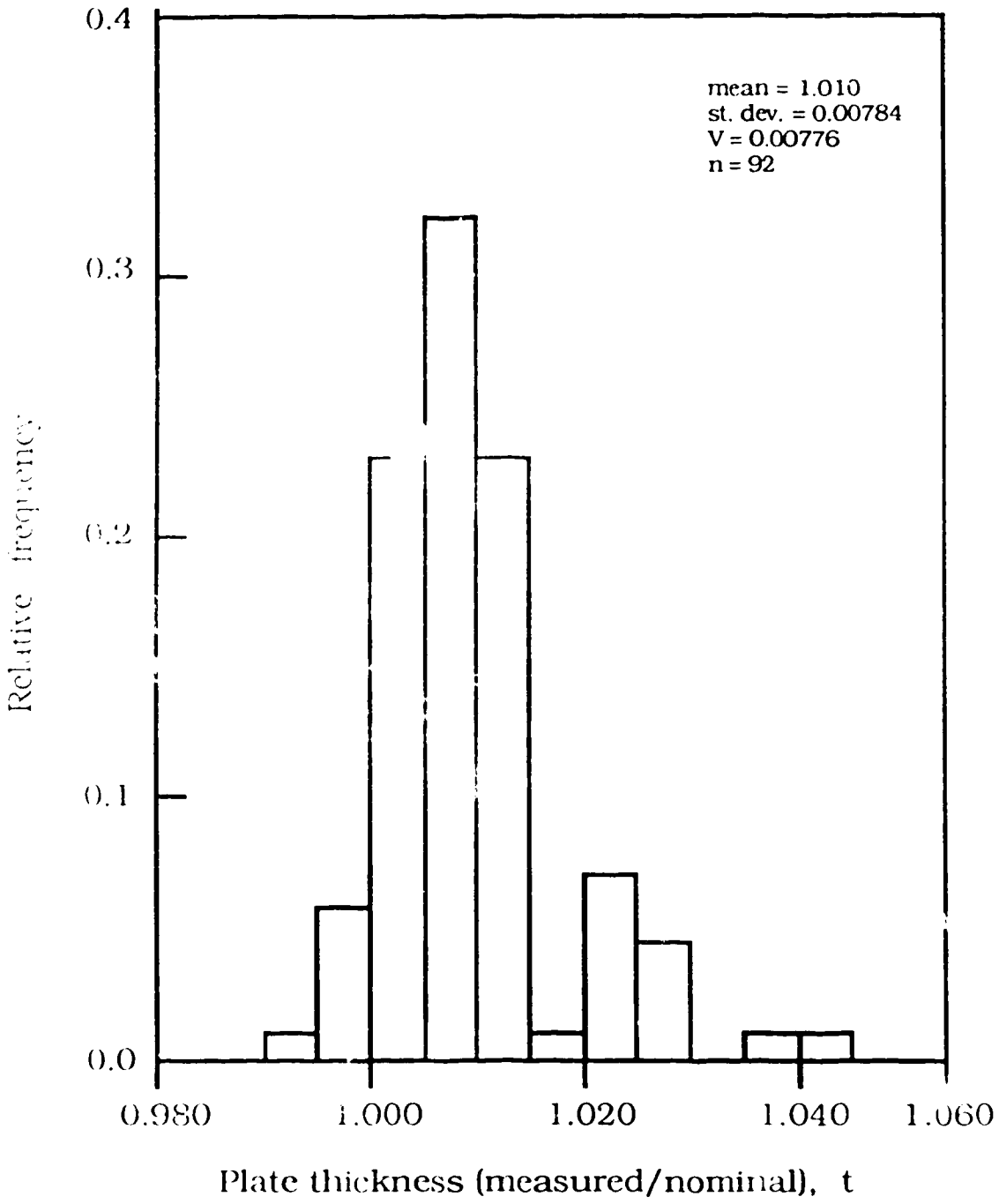

Fig. 4.2 Frequency distribution for plate thickness

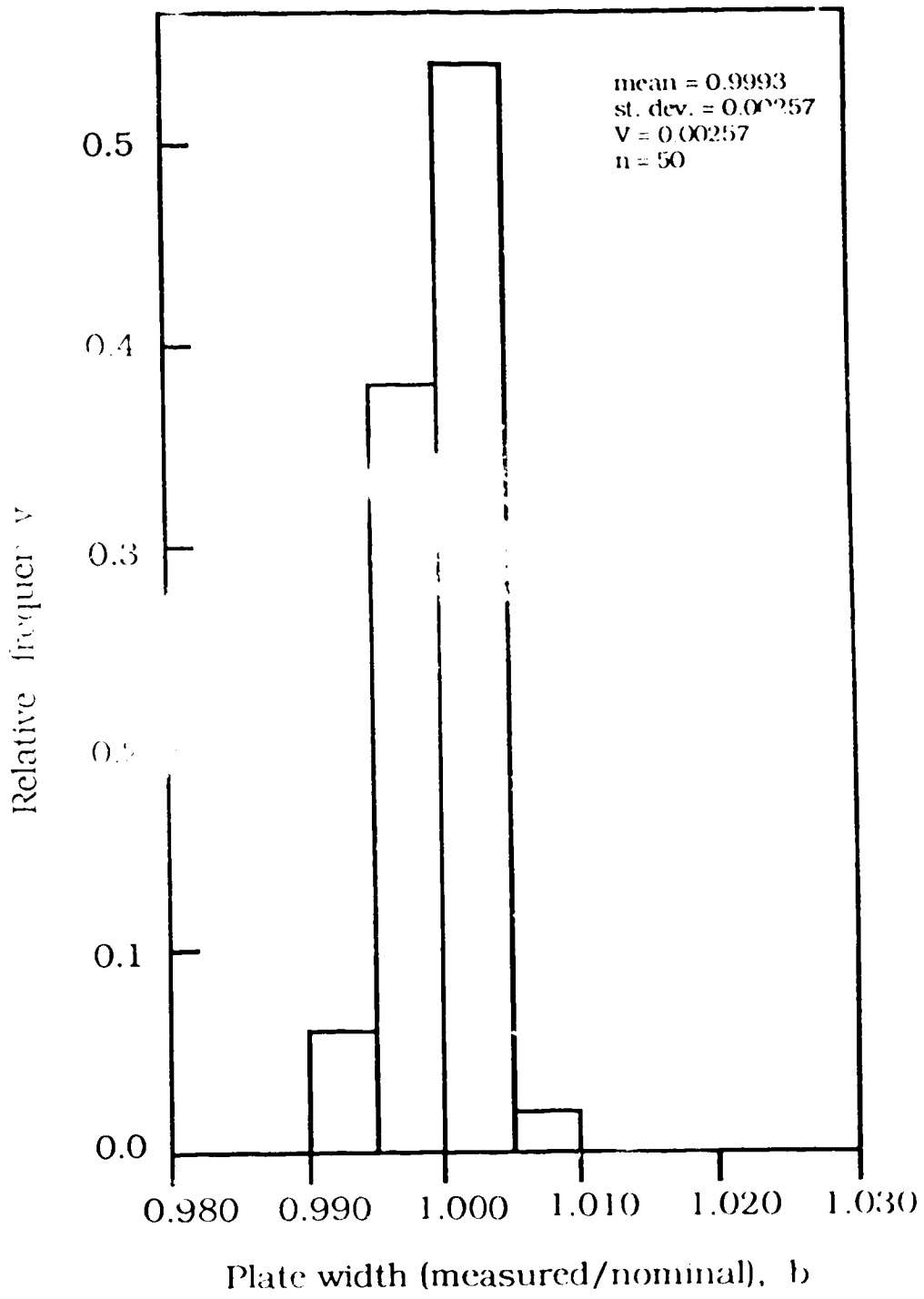

Fig. 4.3 Frequency distribution for plate width

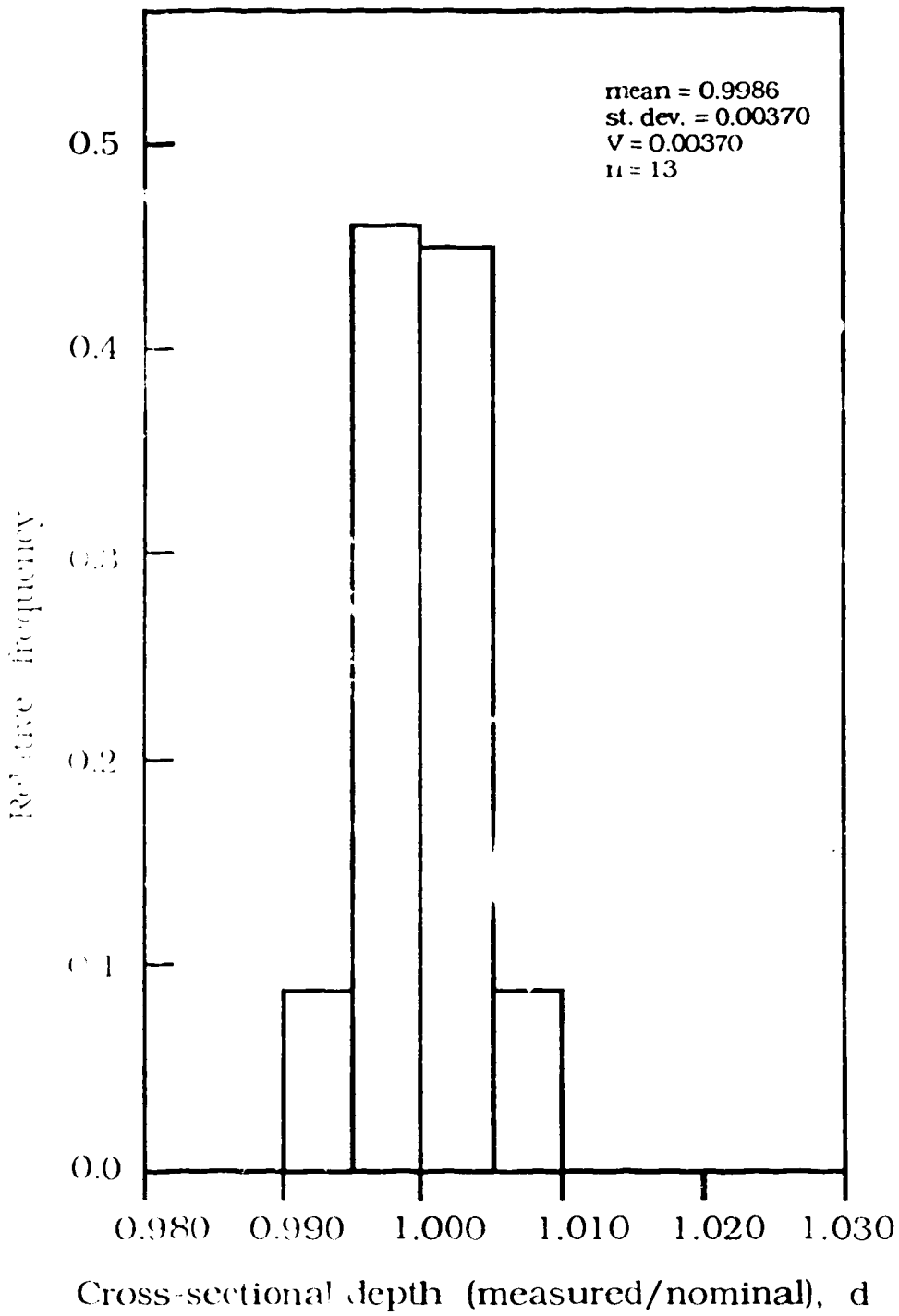

Fig. 4.4 Frequency distribution for cross-sectional depth

cutting process is started, a final check is made in the first foot of cutting and adjustments are made, if necessary, before cutting continues. This procedure produces exceptional control as clearly shown in Fig. 4.3 where the measured/nominal ratio is 0.9993 and the coefficient of variation is 0.00257. In cutting plates, negative tolerances are preferred to help avoid fitting problems in the field.

4.2.3 Cross sectional properties.

Complete data of all measurements for a given cross-section are not available because of the production process. The production of WW members involves several divisions of the mill, each with its own quality control tests. For any given element of the WW member, test samples are randomly chosen from a large population. Therefore, the statistical variation of geometric properties must be derived from the measurements taken of plate thicknesses, plate widths, and cross-sectional depths.

For any geometric property, the ratio of the measured to the nominal value is

$$[4.1] \quad \rho_G = \frac{\bar{G}}{G}$$

Thus, the mean value for the area of a given section is

$$[4.2] \quad \bar{A} = 2\bar{b}\,\bar{t} + (\bar{d}-2\bar{t})\bar{w} + 2\bar{g}^2$$

where the last term represents the area of the fillet welds joining the web to the flanges.

The mean value for the moment of inertia about the major and minor axes, $\bar{I}_x$ and $\bar{I}_y$, for a given section are

$$[4.3] \quad I_x = \tfrac{1}{6}\bar{b}\,\bar{t}^3 + \tfrac{1}{2}\bar{b}\,\bar{t}(\bar{d}-\bar{t})^2 + \tfrac{1}{12}\bar{w}(\bar{d}-2\bar{t})^3 + \tfrac{1}{9}\bar{g}^4 + 2\bar{g}^2(\tfrac{1}{2}\bar{d}-\bar{t}-\tfrac{1}{3}\bar{g})^2$$

and,

$$[4.4] \quad I_y = \tfrac{1}{6}\bar{t}\,\bar{b}^3 + \tfrac{1}{12}(\bar{d}-2\bar{t})\bar{w}^3 + \tfrac{1}{9}\bar{g}^4 + \bar{g}^2(\bar{w}+\tfrac{2}{3}\bar{g})^2$$

The corresponding radii of gyration are

$$[4.5] \quad r_x = \left(\frac{\bar{I}_x}{\bar{A}}\right)$$

and

$$[4.6] \quad r_y = \left(\frac{\bar{I}_y}{\bar{A}}\right)$$

As the geometric dimensions vary independently, the coefficient of variation for the cross-sectional properties is

$$[4.7] \quad V_{I_x} = \frac{1}{\bar{G}}\left[\left(\frac{\partial G}{\partial t}\right)^2\sigma_t^2 + \left(\frac{\partial G}{\partial w}\right)^2\sigma_w^2 + \left(\frac{\partial G}{\partial b}\right)^2\sigma_b^2 + \left(\frac{\partial G}{\partial d}\right)^2\sigma_d^2 + \left(\frac{\partial G}{\partial g}\right)^2\sigma_g^2\right]^{1/2}$$

where the partial derivatives are evaluated at the mean. Because actual measurements of weld sizes were not available, the variation in weld size has not been considered. The small cross-sectional area of the welds makes this approximation valid.

Tables 4.1 to 4.5 summarize the calculated means, measured-to-nominal ratios, and associated coefficients of variation of each pertinent geometric property for each standard member produced in

Table 4.1a. Statistical parameters of the geometric properties for WWF 350 series

Section	Flange		Web									
	b_n (mm)	t_n (mm)	d_n (mm)	w_n (mm)	A_n (mm^2)	$\bar{A}$ (mm^2)	ρ_A	V_A	I_{x_n} (10^6mm^4)	$\bar{I}_x$ (10^6mm^4)	ρ_{I_x}	V_{I_x}
350x385	350.	60.	350.	30.	49,100	49,480	1.0077	0.006666	928	926.2	1.0002	0.01034
350x315	350.	50.	350.	20.	40,200	40,520	1.0079	0.006917	82[illegible]	824.2	1.0002	0.01036
350x263	350.	40.	350.	20.	33,600	33,860	1.0078	0.006691	712	713.5	1.0021	0.01039
350x238	350.	35.	350.	20.	30,300	30,530	1.0077	0.006552	650.	651.5	1.0023	0.01040
350x212	350.	30.	350.	20.	27,000	27,210	1.0076	0.006393	583.	584.8	1.0031	0.01042
350x192	350.	28.	350.	16.	24,400	24,510	1.0046	0.006613	546.	544.6	0.9975	0.01047
350x176	350.	25.	350.	16.	22,400	22,490	1.0040	0.006560	502.	500.4	0.9969	0.01048
350x155	350.	22.	350.	14.	19,800	19,850	1.0027	0.006518	451.	449.6	0.9970	0.01051
350x137	350.	20.	350.	11.	17,500	17,560	1.0035	0.006678	412.	410.3	0.9958	0.01056

Table 4.1b. Statistical parameters of the geometric properties for WWF 350 Series

Section	r_{x_n} (mm)	$\bar{r}_x$ (mm)	ρ_{r_x}	V_{r_x}	I_{y_n} (10^6mm^4)	$\bar{I}_y$ (10^6mm^4)	ρ_{I_y}	V_{I_y}	r_y (mm)	$\bar{r}_y$ (mm)	ρ_{r_y}	V_{r_y}
350x385	137.	137.0	0.9998	0.004279	429	432.5	1.0081	0.01098	93.5	93.49	0.9999	0.001954
350x315	143.	142.6	0.9974	0.004167	357	360.1	1.0086	0.01100	94.2	94.27	1.0007	0.002882
350x263	146.	145.2	0.9942	0.003971	286.	288.1	1.0074	0.01099	92.[illegible]	92.24	0.9994	0.002996
350x238	146.	146.1	1.0005	0.003880	250	252.1	1.0[illegible]	0.01099	90.6	90.87	1.0008	0.003077
350x212	147.	146.6	0.9974	0.003761	215	216.3	1.0[illegible]4	0.01099	89.2	89.14	0.9993	0.003184
350x192	150.	149.1	0.9938	0.003791	200	201.6	1.0081	0.01100	90.[illegible]	90.69	1.0021	0.003084
350x176	150.	149.2	0.9945	0.003742	179.	180.[illegible]	1.0[illegible]	0.01100	89.[illegible]	89.47	1.0008	0.003160
350x155	151.	150.5	0.9967	0.003712	157.	158.[illegible]	1.0089	0.01100	89.[illegible]	89.32	1.0036	0.003164
350x137	153.	152.9	0.9990	0.003708	143.	144.3	1.0088	0.01100	90.4	90.55	1.0016	0.003079

Table 4.2a. Statistical parameters of the geometric properties for WWF 400 series

Section	Flange		Web									
	d_n (mm)	t_n (mm)	d_n (mm)	w_n (mm)	A_n (mm^2)	A (mm^2)	ρ_A	V_A	I_x (10^6mm^4)	$\bar{I}_x$ (10^6mm^4)	ρ_{I_x}	V_{I_x}
400x444	400.	60.	400.	30.	56,600	57,600	1.0080	0.006376	1460	1461.7	1.0012	0.01035
400x362	400.	50.	400.	20.	46,200	46,680	1.0082	0.006426	1280	1284.9	1.0038	0.01039
400x303	400.	40.	400.	20.	38,600	38,910	1.0081	0.006426	1100	1103.1	1.0029	0.01042
400x273	400.	35.	400.	20.	34,800	35,060	1.0080	0.006371	1000	1003.1	1.0031	0.01044
400x243	400.	30.	400.	20.	31,000	31,250	1.0080	0.006413	894.	896.8	1.0031	0.01045
400x220	400.	28.	400.	16.	28,000	28,270	1.0096	0.006504	834.	837.3	1.0039	0.01049
400x202	400.	25.	400.	16.	25,700	25,950	1.0097	0.006460	765.	767.9	1.0038	0.01049
400x178	400.	22.	400.	14.	22,700	22,910	1.0093	0.006492	686.	688.6	1.0038	0.01052
400x157	400.	20.	400.	11.	20,100	20,260	1.0080	0.006347	625.	627.4	1.0039	0.01056

Table 4.2b. Statistical parameters of the geometric properties for WWF 400 series

Section	r_{x_n} (mm)	$\bar{r}_x$ (mm)	ρ_{r_x}	V_{r_x}	I_{x_n} (10^6mm^4)	$\bar{I}_x$ (10^6mm^4)	ρ_{I_y}	V_{I_y}	r_{y_n} (mm)	$\bar{r}_y$ (mm)	ρ_{r_y}	V_{r_y}
400x444	161.	160.1	0.9942	0.004156	641.	645.6	1.0071	0.01099	106.	106.37	1.0035	0.002969
400x362	166.	166.1	1.0005	0.004067	534.	537.6	1.0067	0.01100	108.	107.43	0.9949	0.002892
400x303	169.	168.4	0.9963	0.003901	427.	430.1	1.0074	0.01100	105.	105.14	1.0013	0.003005
400x273	170.	169.1	0.9947	0.003825	374.	376.4	1.0065	0.01100	104.	103.59	0.9960	0.003086
400x243	170.	169.4	0.9965	0.003754	320.	322.7	1.0094	0.01100	102.	101.62	0.9963	0.003192
400x220	173.	172.1	0.9947	0.003754	299.	301.1	1.0069	0.01100	103.	103.19	1.0018	0.003098
400x202	173.	172.0	0.9944	0.003712	267.	268.8	1.0068	0.01100	102.	101.78	0.9979	0.003174
400x178	174.	173.4	0.9964	0.003687	235.	236.5	1.0065	0.01100	102.	101.61	0.9962	0.003178
400x157	176.	176.0	0.9998	0.003686	213.	215.0	1.0094	0.01100	103.	103.01	1.0001	0.003093

Table 4.3a. Statistical parameters of the geometric properties for WWF 450 series

Section	Flange		Web									
	b_n (mm)	t_n (mm)	d_n (mm)	w_n (mm)	A_n (mm^2)	$\bar{A}$ (mm^2)	ρ_A	V_A	I_{x_n} (10^6mm^4)	$\bar{I}_x$ (10^6mm^4)	ρ_{I_x}	V_{I_x}
450x503	450.	60.	450.	30.	64,100	64,630	1.0083	0.006692	[illegible]	2169.2	1.0042	0.010363
450x409	450.	50.	450.	20.	52,200	52,640	1.0084	0.006941	1,890.	1891.9	1.0010	0.010417
450x342	450.	40.	450.	20.	43,600	43,960	1.0083	0.006720	1,610.	1613.9	1.0024	0.010451
450x308	450.	35.	450.	20.	39,300	39,630	1.0083	0.006585	1,460.	1462.9	1.0020	0.010465
450x274	450.	30.	450.	20.	35,000	35,290	1.0082	0.006429	1,300.	1303.6	1.0028	0.010475
450x248	450.	28.	450.	16.	31,500	31,910	1.0098	0.006606	1,210.	1215.1	1.0042	0.010517
450x228	450.	25.	450.	16.	29,000	29,280	1.0098	0.006493	1,110.	1112.4	1.0022	0.010521
450x201	450.	22.	450.	14.	25,600	25,840	1.0093	0.006504	991.	995.3	1.0044	0.010543
450x177	450.	20.	450.	11.	22,600	22,840	1.0106	0.006654	901.	905.3	1.0048	0.010582

Table 4.3b. Statistical Parameters of the Geometric Properties for WWF 450 Series

Section	r_{x_n} (mm)	$\bar{r}_x$ (mm)	ρ_{r_x}	V_{r_x}	I_{y_n} (10^6mm^4)	$\bar{I}_y$ (10^6mm^4)	ρ_{I_y}	V_{I_y}	r_{y_n} (mm)	$\bar{r}_y$ (mm)	ρ_{r_y}	V_{r_y}
450x503	184.	183.2	0.9957	0.004066	912.	919.2	1.0079	0.001099	119.	119.3	1.0022	0.002980
450x409	190.	189.6	0.9978	0.003994	760.	765.6	1.0074	0.001100	121.	120.6	0.9967	0.002899
450x342	192.	191.6	0.9979	0.003851	608.	612.6	1.0075	0.001100	118.	118.0	1.0003	0.003012
450x308	193.	192.1	0.9956	0.003785	532.	536.0	1.0078	0.001100	116.	116.3	1.0026	0.003092
450x274	193.	192.2	0.9959	0.003722	456.	459.5	1.0077	0.001100	114.	114.1	1.0010	0.003198
450x248	196.	195.1	0.9956	0.003724	425.	428.7	1.0088	0.001100	116.	115.9	0.9992	0.003103
450x228	196.	194.9	0.9944	0.003687	380.	382.8	1.0074	0.001100	114.	114.3	1.0030	0.003179
450x201	197.	197.3	0.9963	0.003666	334.	336.9	1.0085	0.001100	114.	114.2	1.0016	0.003182
450x177	200.	199.1	0.9955	0.003666	304.	306.2	1.0071	0.001100	116.	115.8	0.9982	0.003

Table 4.4a. Statistical parameters of the geometric properties for WWF 500 series

Section	Flange		Web									
	b_n (mm)	t_n (mm)	d_n (mm)	w_n (mm)	A_n (mm^2)	$\bar{A}$ (mm^2)	ρ_A	V_A	I_{x_n} ($10^6 mm^4$)	$\bar{I}_x$ ($10^6 mm^4$)	ρ_{I_x}	V_{I_x}
500x651	500.	60.	500.	60.	83,000	83,070	1.0008	0.000821	3,200.	3211.7	1.0036	0.01034
500x561	500.	60.	500.	30.	71,600	72,210	1.0085	0.010705	3,070.	2075.2	1.0017	0.01038
500x456	500.	50.	500.	20.	58,200	58,700	1.0086	0.008619	2,660.	2665.4	1.0020	0.01045
500x381	500.	40.	500.	20.	48,600	49,020	1.0086	0.008631	2,220.	3262.2	1.0054	0.01048
500x343	500.	35.	500.	20.	43,600	44,170	1.0085	0.008736	2,010.	2045.4	1.0027	0.01049
500x306	500.	30.	500.	20.	39,000	39,330	1.0084	0.006110	1,810.	1818.1	1.0045	0.01050
500x276	500.	28.	500.	16.	35,200	35,550	1.0099	0.006615	1,680.	1692.4	1.0074	0.01054
500x254	500.	25.	500.	16.	32,300	32,620	1.0098	0.006603	1,540.	1547.0	1.0046	0.01054
500x223	500.	22.	500.	14.	28,500	28,770	1.0094	0.006614	1,370.	1381.8	1.0086	0.01056
500x197	500.	20.	500.	11.	25,200	25,420	1.0085	0.006682	1,250.	1255.1	1.0041	0.01050

Table 4.4b. Statistical Parameters of the Geometric Properties for WWF 500 Series

Section	r_{x_n} (mm)	$\bar{r}_x$ (mm)	ρ_{r_x}	V_{r_x}	I_{y_n} ($10^6 mm^4$)	$\bar{I}_y$ ($10^6 mm^4$)	ρ_{I_y}	V_{I_y}	r_{y_n} (mm)	$\bar{r}_y$ (mm)	ρ_{r_y}	V_{r_y}
500x651	196.	195.9	0.9996	0.003867	1,260.	1267.5	1.0059	0.01093	123.	123.08	1.0007	0.003441
500x561	207.	206.4	0.9970	0.003997	1,250.	1261.0	1.0088	0.01099	132.	132.15	1.0012	0.002988
500x456	214.	213.1	0.9957	0.003938	1,040.	1050.4	1.0100	0.01100	134.	133.77	0.9983	0.002904
500x381	215.	214.8	0.9992	0.003812	834.	840.4	1.0077	0.01100	131.	130.94	0.9996	0.003017
500x343	216.	215.2	0.9962	0.003754	729.	735.4	1.0088	0.01100	129.	129.03	1.0002	0.003098
500x306	215.	215.0	1.0001	0.003698	625.	630.4	1.0086	0.01100	127.	126.89	0.9989	0.003203
500x276	218.	218.2	1.0009	0.003701	583.	588.2	1.0089	0.01100	129.	129.[illegible]	[illegible]	0.003107
500x254	218.	217.8	0.9990	0.003668	521.	525.2	1.0081	0.01100	127.	126.96	[illegible]	[illegible]
500x223	219.	219.2	1.0008	0.003650	458.	462.1	1.0091	0.01100	127.	126.75	0.9[illegible]	[illegible]
500x197	223.	222.2	0.9966	0.003651	41[illegible]	420.1	1.0074	0.01100	129.	[illegible].57	0.9966	0.003098

Table 4.5a. Statistical parameters of the geometric properties for WWF 550 Series

Section	Flange		Web									
	b_n (mm)	t_n (mm)	d_n (mm)	w_n (mm)	A_n (mm^2)	$\bar{A}$ (mm^2)	ρ_A	V_A	I_{x_n} ($10^6 mm^4$)	$\bar{I}_x$ ($10^6 mm^4$)	ρ_{I_x}	V_{I_x}
550x721	550.	60.	550.	60.	92,000	92,760	1.0082	0.005924	4390.	4402.5	1.0029	0.01035
550x620	550.	60.	550.	30.	79,100	79,780	1.0086	0.006716	4190.	4204.4	1.0034	0.01041
550x503	550.	50.	550.	20.	64,200	64,760	1.0088	0.006956	3610.	3625.7	1.0043	0.01047
550x420	550.	40.	550	20.	53,600	54,070	1.0087	0.006739	3050.	3064.6	1.0048	0.01050
550x217	550.	20.	550.	11.	27,700	27,990	1.0105	0.006669	1680.	1685.1	1.0030	0.01062

Table 4.5b. Statistical parameters of the geometric properties for WWF 550 series

Section	r_{x_n} (mm)	$\bar{r}_x$ (mm)	ρ_{r_x}	V_{r_x}	I_{y_n} ($10^6 mm^4$)	$\bar{I}_y$ ($10^6 mm^4$)	ρ_{I_y}	V_{I_y}	r_{y_n} (mm)	$\bar{r}_y$ (mm)	ρ_{r_y}	V_{r_y}
550x721	218.	217.9	0.9994	0.003825	1670.	1685.8	1.0095	0.01094	135	134.8	0.9986	0.003457
550x620	230.	229.6	0.9981	0.003943	1660.	1678.6	1.0112	0.01100	145	145.0	1.0003	0.002996
550x503	237.	236.6	0.9984	0.003894	1390.	1398.3	1.0059	0.01100	147	146.9	0.9996	0.002909
550x420	239.	238.1	0.9962	0.003782	1110.	1118.7	1.0078	0.01100	144	143.8	0.9989	0.003022
550x217	246.	245.4	0.9974	0.003639	555.	559.2	1.0076	0.01100	142	141.3	0.9954	0.003100

Canada, using [4.1] to [4.6]. Nominal values listed have been taken from the Handbook of Steel Construction (CISC 1985).

For all sections taken as a whole, the mean value of the measured-to-nominal ratios and the coefficients of variation are calculated from

$$[4.8] \quad \bar{\rho}_G = \sum_{i=1}^{i=n} \rho_{G_i} = \rho_{G_1} + \rho_{G_2} + \cdots + \rho_G$$

and

$$[4.9] \quad V_G = \frac{1}{\bar{\rho}_G} \frac{1}{(n-1)^{1/2}} \left[\sum_{i=1}^{n} (V_{G_i} \rho_{G_i})^2 + \sum_{i=1}^{n} (\bar{\rho}_G \rho_{G_i})^2 \right]^{1/2}$$

A summary of the measured-to-nominal ratios and the coefficients of variation are given in Table 4.6. The mean values range from 0.997 to 1.010 of the nominal value with coefficients of variation ranging between 0.00257 to 0.0113. This indicates extremely close control on the manufacturing process.

Table 4.6. Statistical quantities, ρ_G and V_G, for geometric variations.

Geometric property G	Sample size n	ρ_G	V_G
t,w	92	1.010	0.00784
b,h	50	0.999	0.00257
d	13	0.999	0.00370
A		1.008	0.00690
I_x		1.003	0.0109
I_y		1.008	0.0111
r_x		0.997	0.0044
r_y		1.000	0.00386
J		1.005	0.0113
r		0.998	0.00432

4.3. Material variations

The material properties of significance, with respect to column strength, are the static yield strength, σ_y, and the modulus of elasticity, E.

4.3.1. Yield strength

The statistical evaluation of the yield strength was determined in a two-step process. Figs. 4.5 and 4.6 give the probability density functions of the mill test yield strengths on 300W steel from Algoma's quality assurance tests for two samples of plate thicknesses ranging between 0.20 and 0.75 inches (5 and 19 mm) and between 0.75 and 1.50 inches (19 and 38 mm), respectively. The overall mean mill test yield strength for the two populations taken together, representing thicknesses of 5 to 38 mm, is 53.9 ksi or 371.7 MPa with a coefficient of variation of 0.0644.

Recognizing that the mill tests do not provide static yield strengths, ten coupons were tested at the University of Alberta to obtain static yield strengths to correlate with the mill test strengths of sister coupons conducted by Algoma Steel. The stress-strain curves for the tests conducted at the University of Alberta are given in Figs. 4.7 to 4.15 except for plate number 56943, which failed prematurely due to a laminar flaw. The results of the tests are shown in Table 4.7. Static yield strengths were obtained from seven of the ten coupons. In addition to the plate that failed prematurely, in the tests on plates 56400 and 56723 the load was carried beyond the yield point inadvertently.

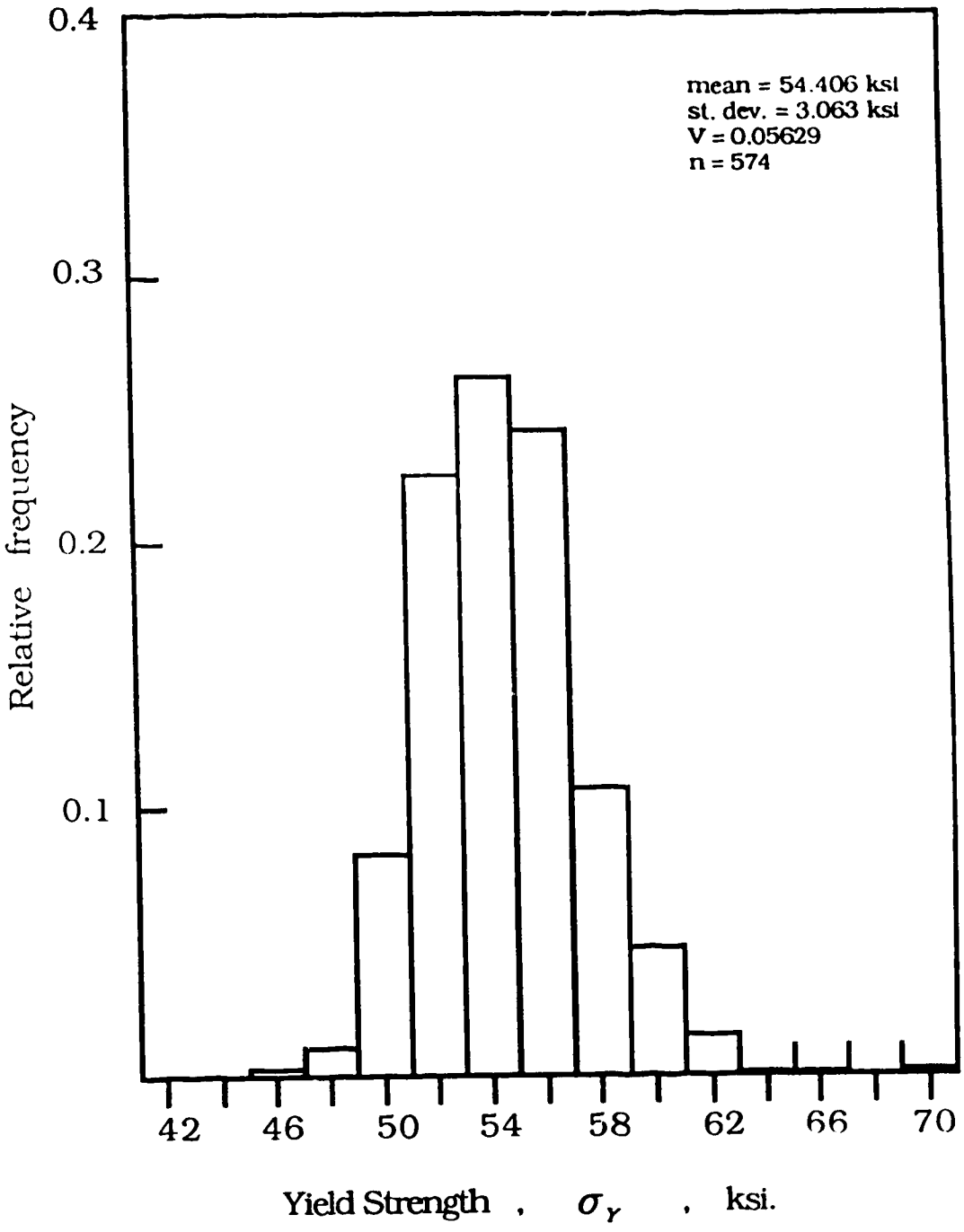

Fig. 4.5 Frequency distribution for the yield strength of mill tests plates ranging in thickness from 0.20 to 0.75 inches

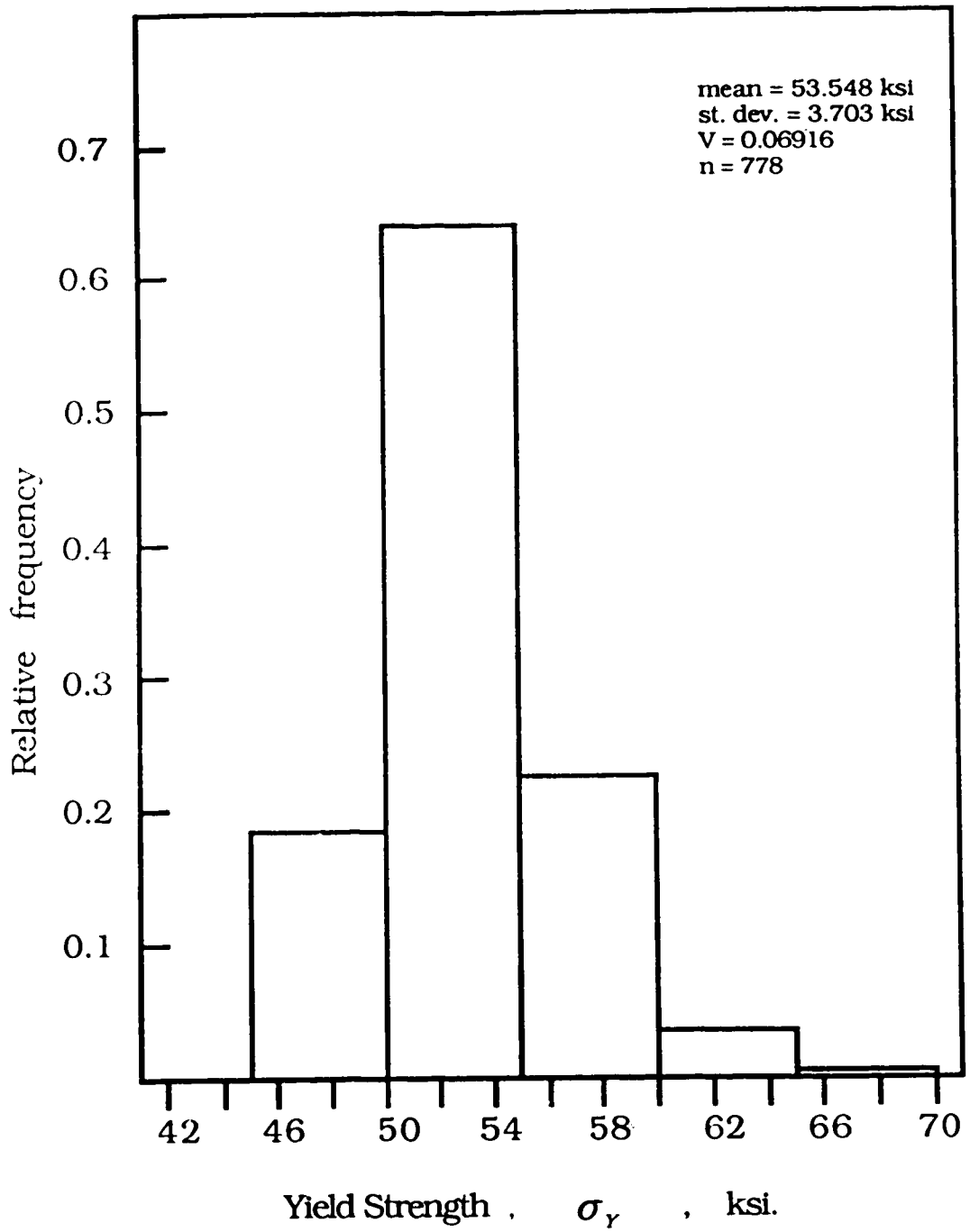

Fig. 4.6 Frequency distribution for the yield Strength of mill tests plates ranging in thickness from 0.75 to 1.50 inches

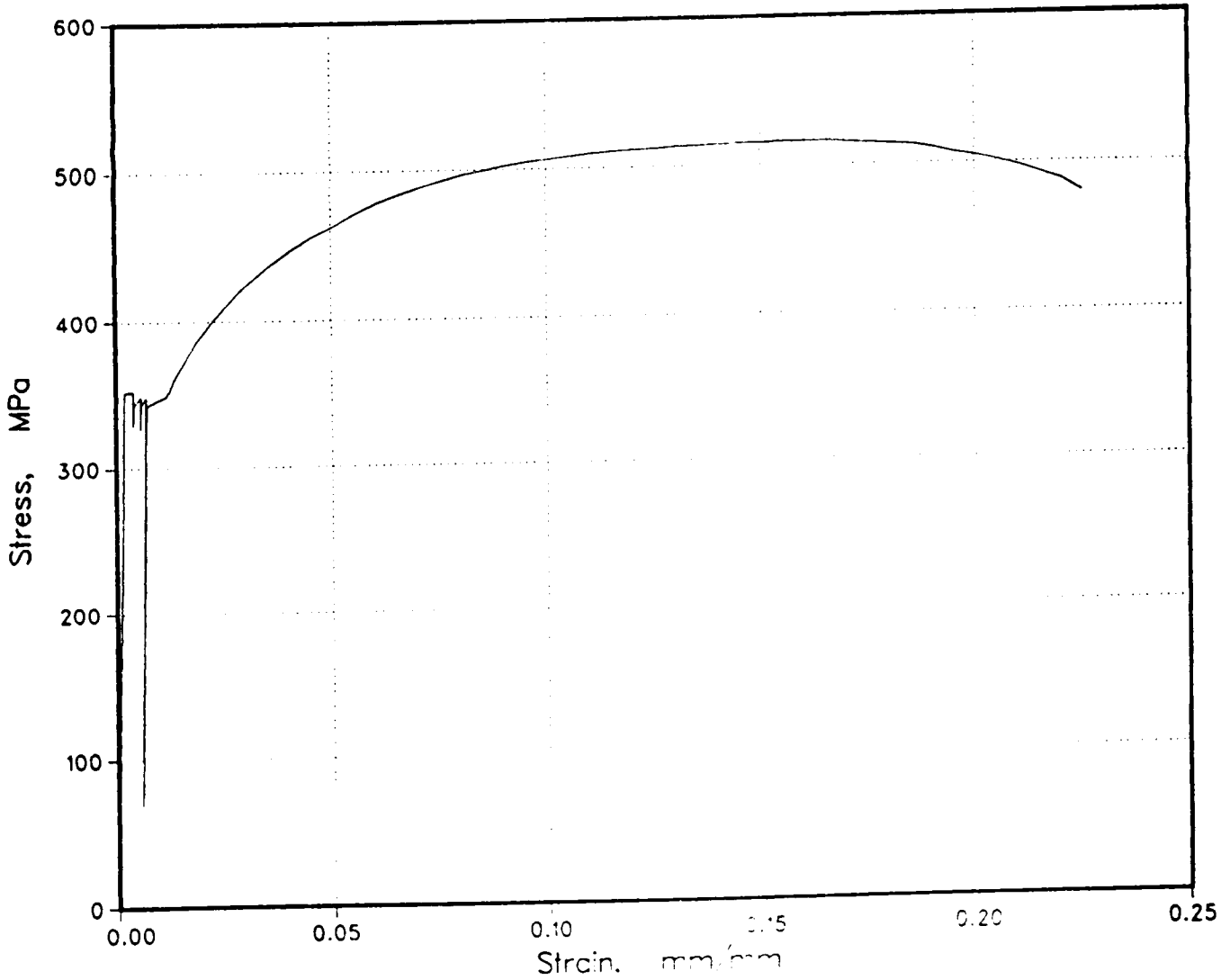

Fig. 4.7 Stress-strain curve of Algoma coupon: plate number 55372, plate thickness t=35mm

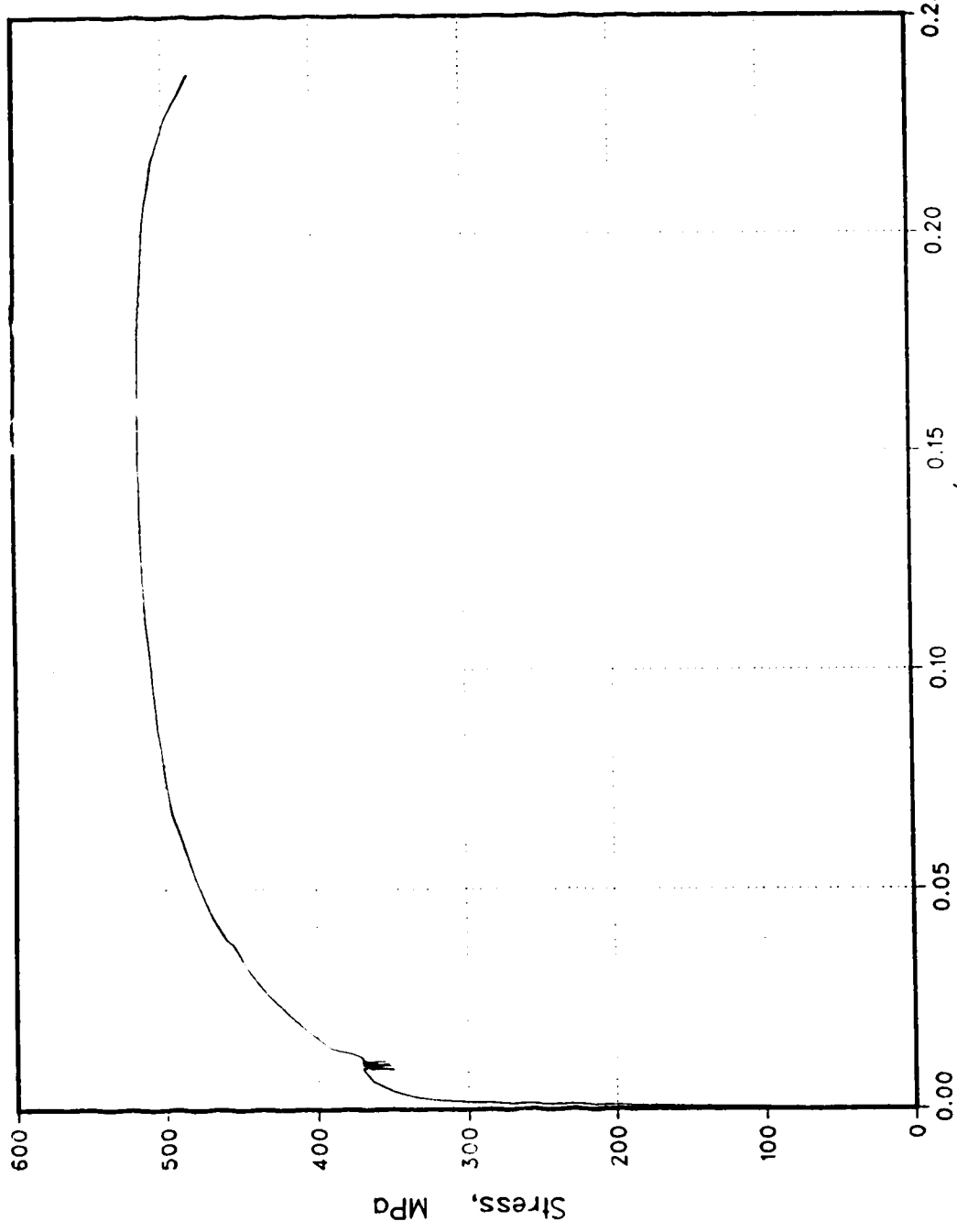

Fig. 4.8 Stress-strain curve of Algoma coupon: plate number 56162, plate thickness t=20mm

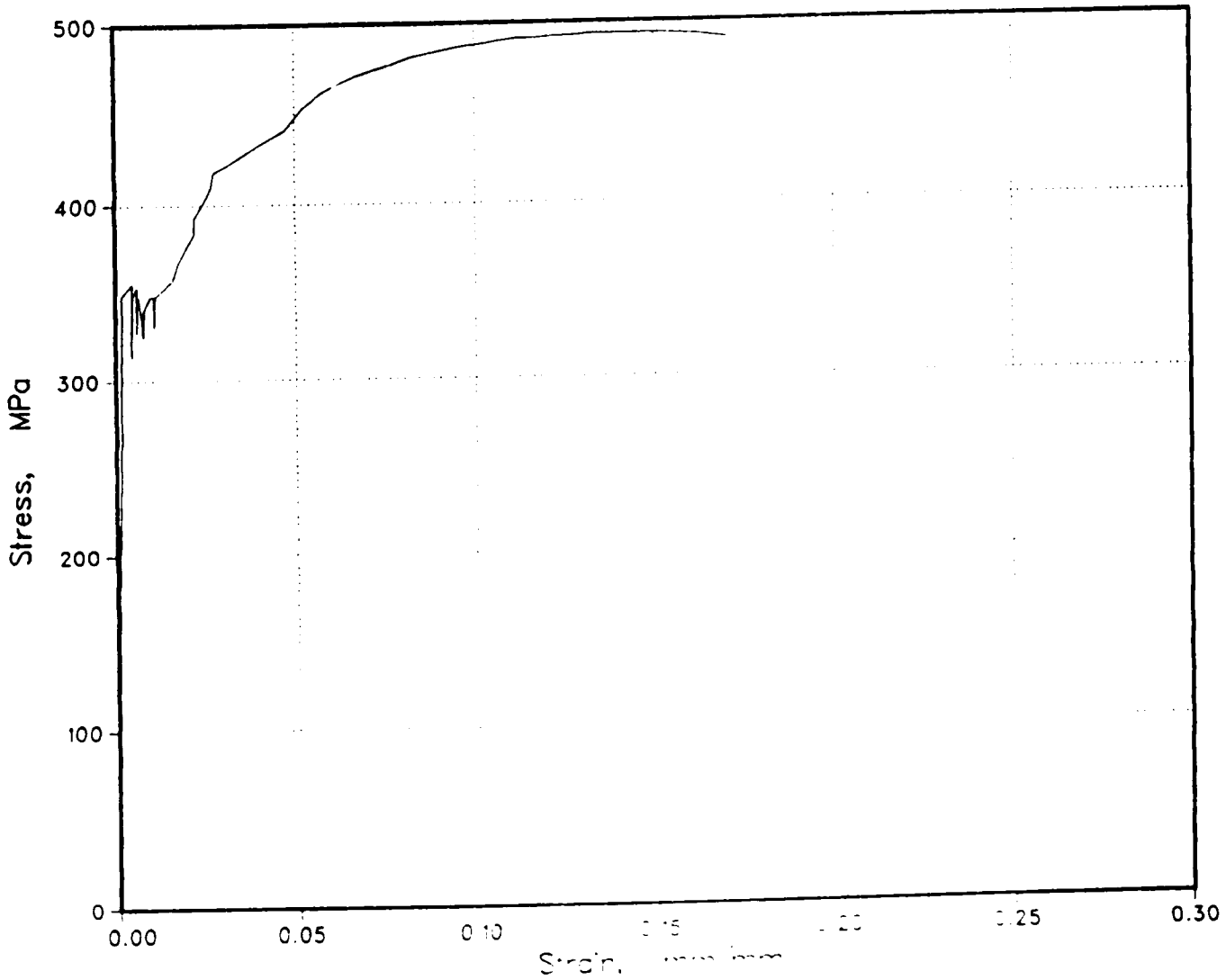

Fig. 4.9 Stress-strain curve of Algoma coupon plate number 30247, plate thickness t=35mm

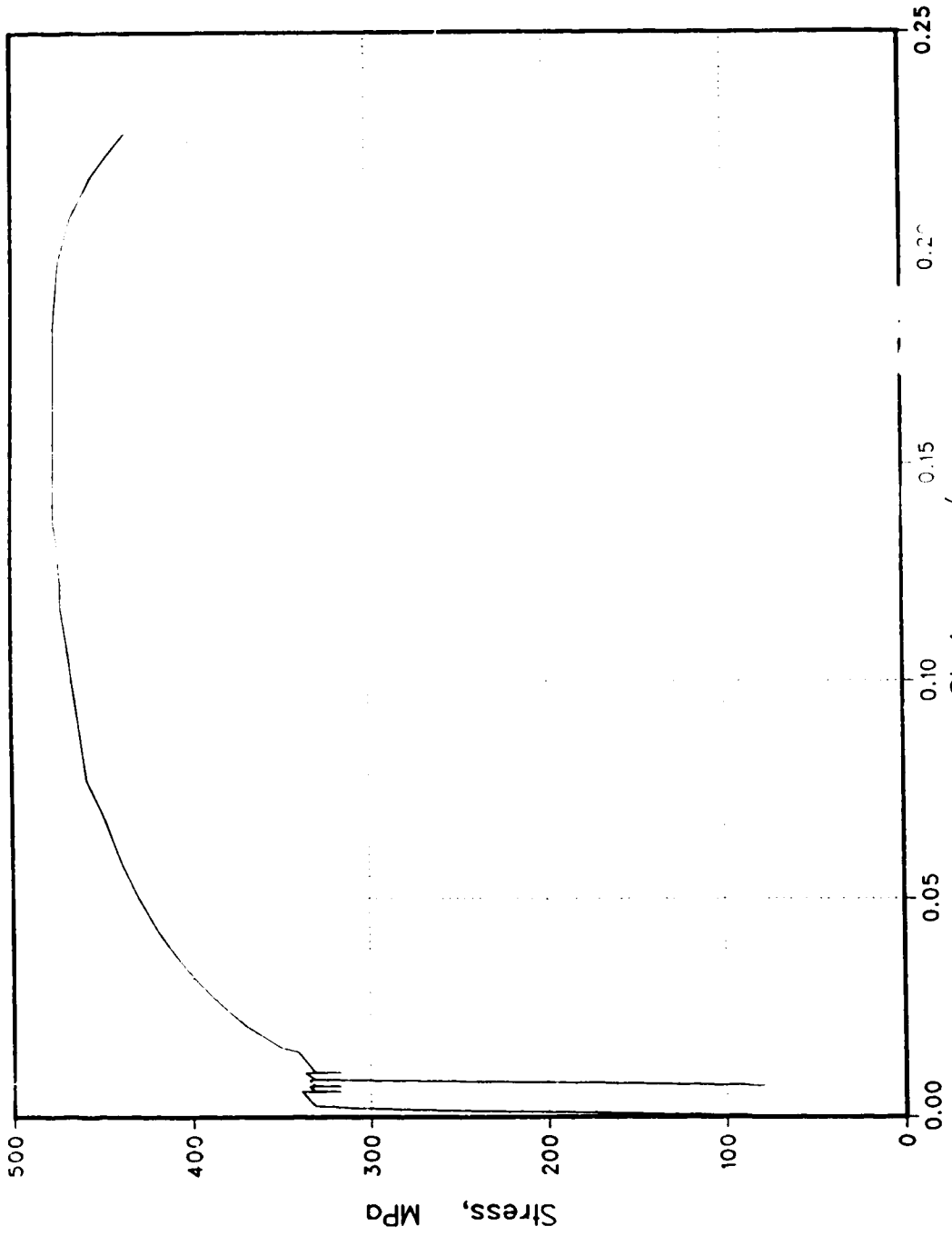

Fig. 4.10 Stress-strain curve of Algoma coupon: plate number 56296, plate thickness t=14mm

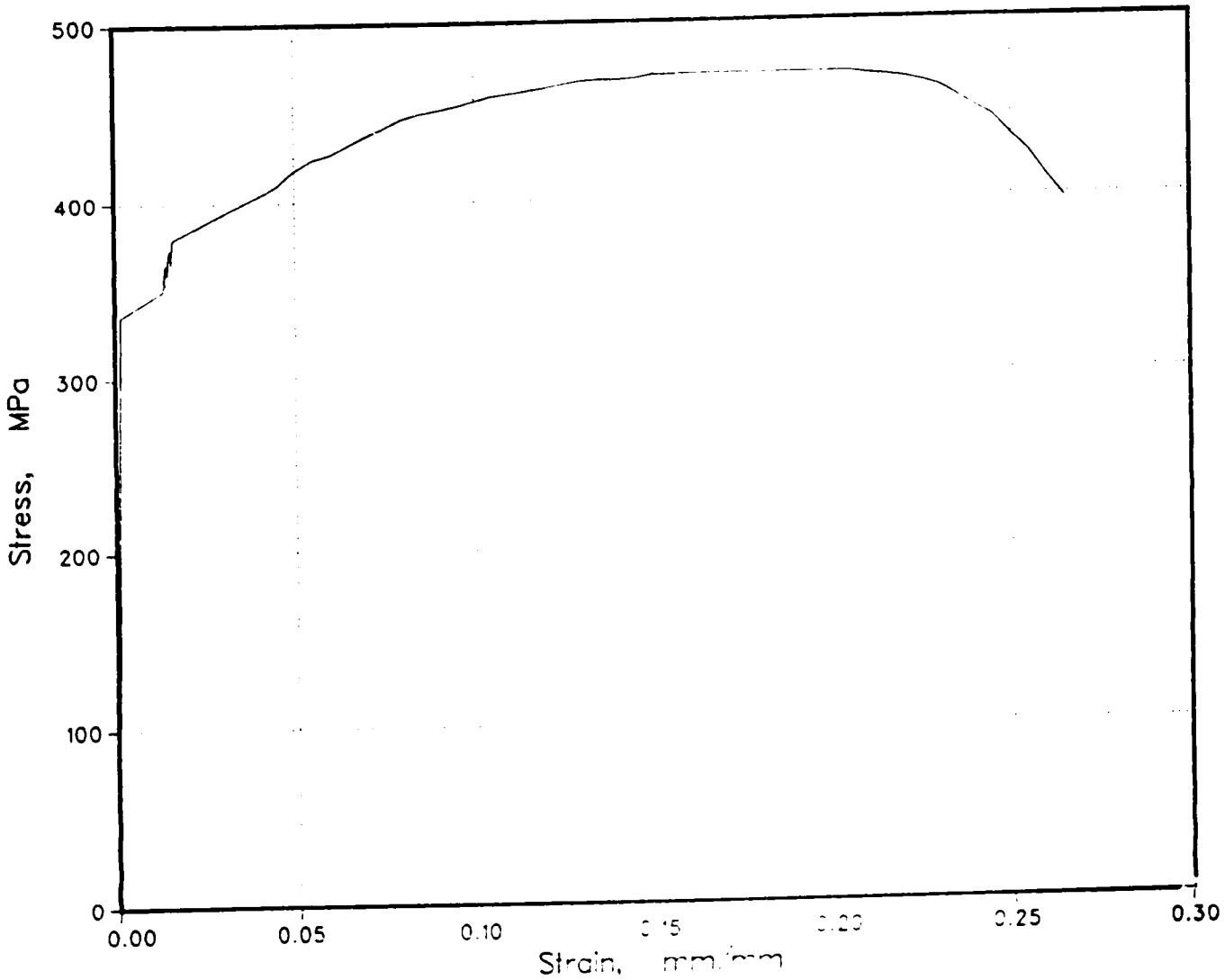

Fig. 4.11 Stress-strain curve of Algoma coupon plate number 56400, plate thickness t=9mm

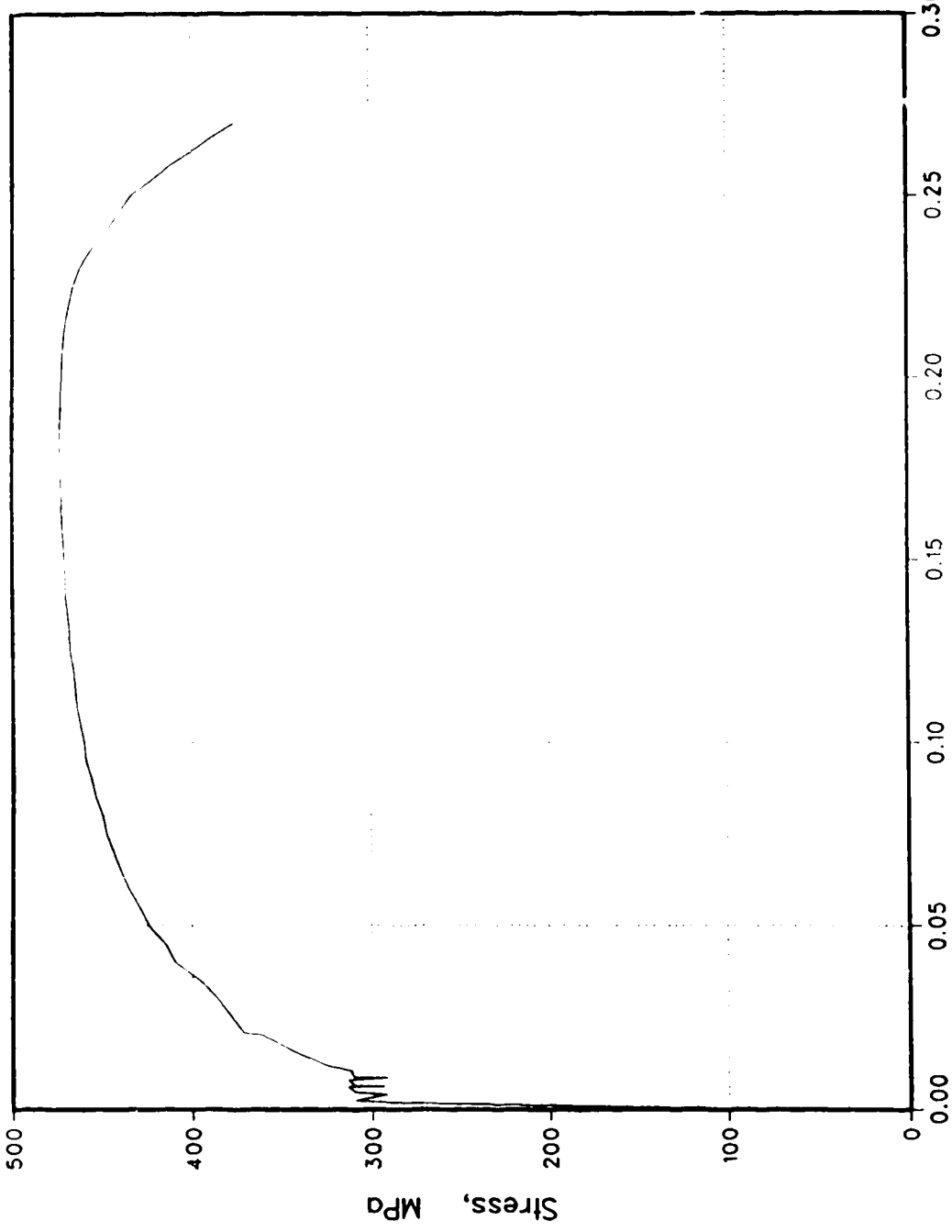

Fig. 4.12 Stress-strain curve of Algoma coupon: plate number 56401, plate thickness t=14mm

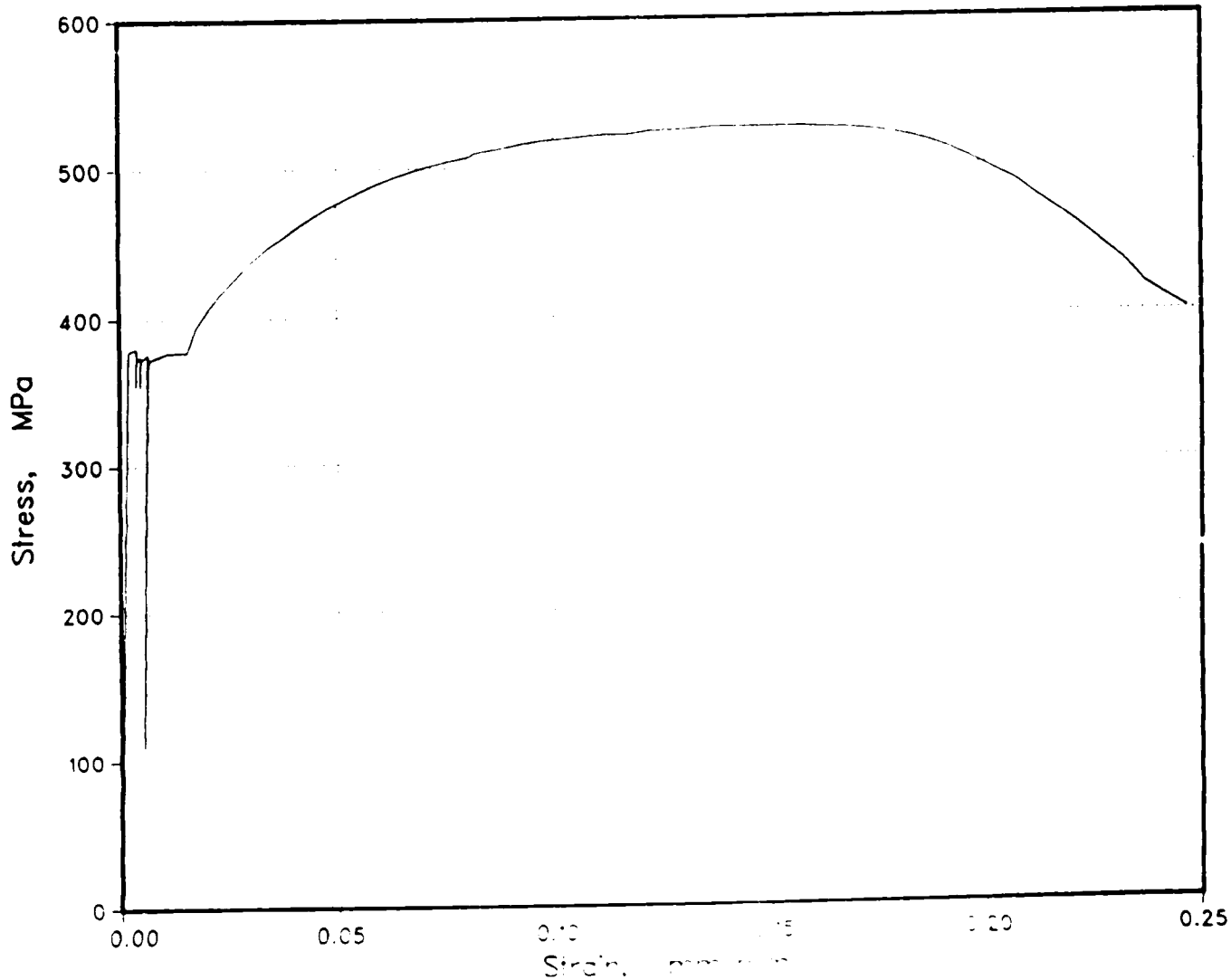

Fig. 4.13 Stress-strain curve of Algoma Coupon [illegible] plate thickness t=28mm

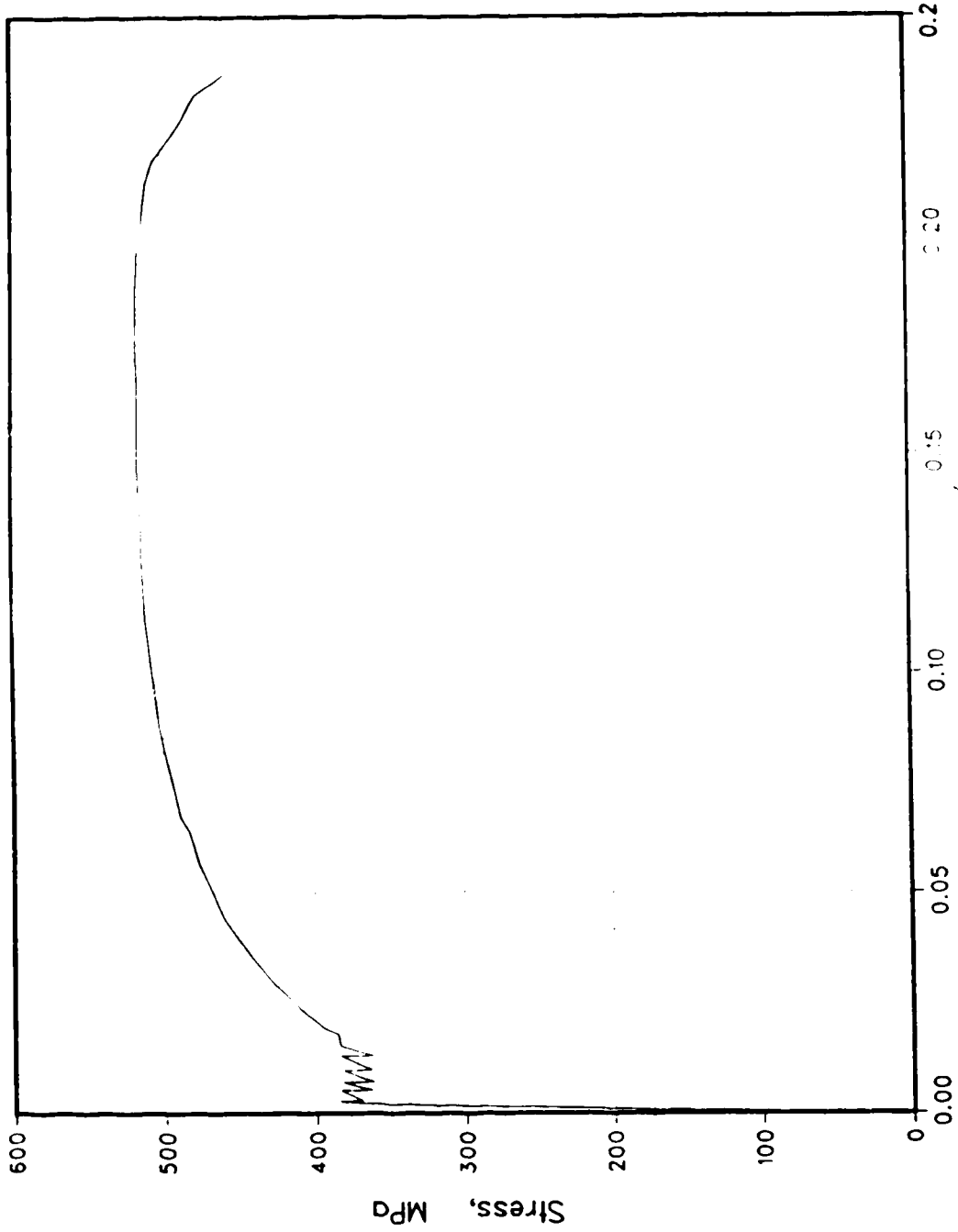

Fig. 4.14 Stress-strain curve of Algoma coupon: plate number 56660, plate thickness t=9mm

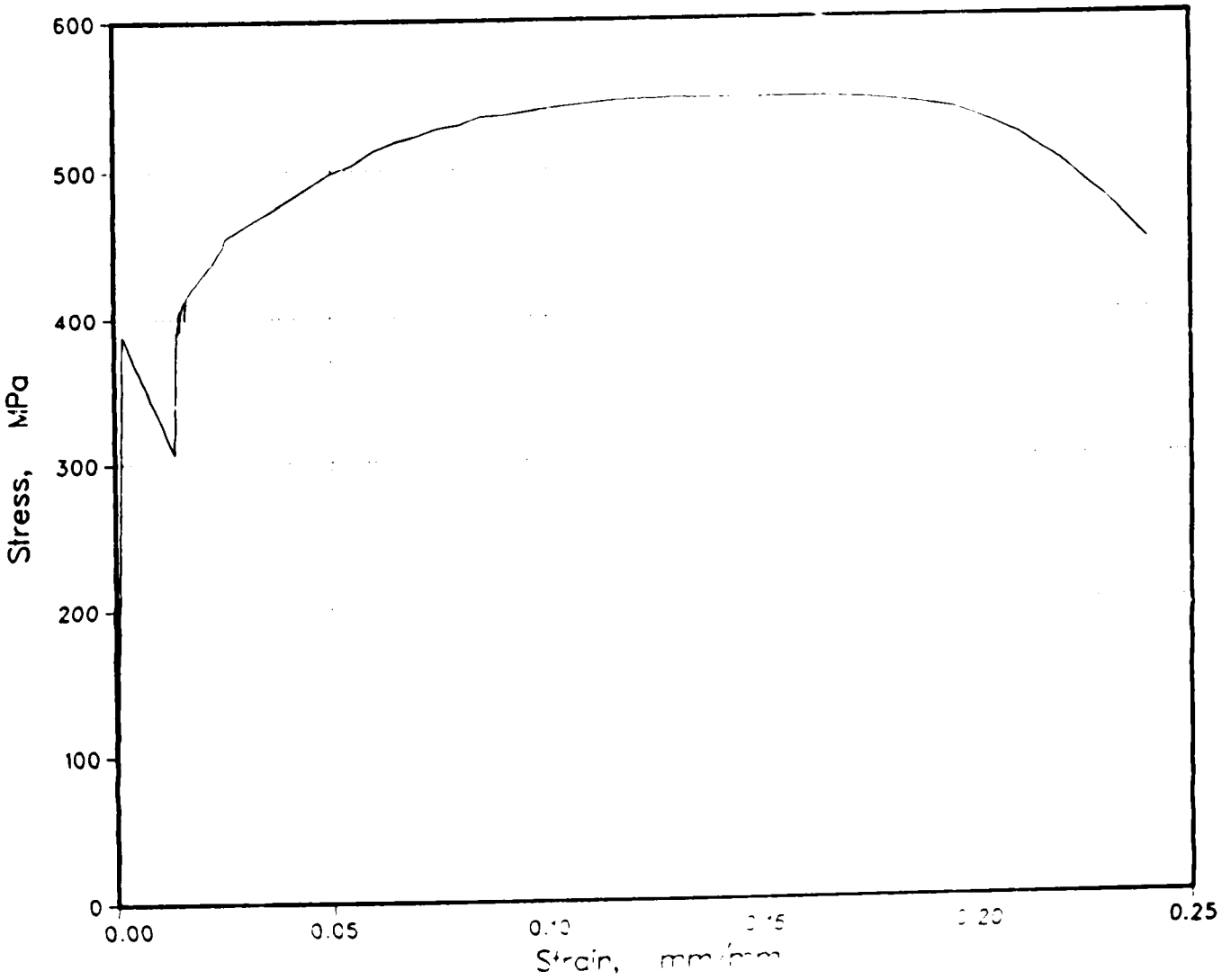

Fig 4.15 Stress-strain curve of Algoma coupon plate number 56723, plate thickness t=20mm

Table 4.7. Comparison of UofA coupon tests with Algoma coupon tests:

Plate number	Plate thickness t, mm	Yield Strength, σ_y Algoma MPa	UofA MPa	UofA / Algoma	Ultimate Stress, σ_u Algoma Mpa	UofA Mpa	UofA / Algoma	Mod. of elasticity E, MPa
55372	35	373.5	327.1	0.8758	532.6	515.7	0.9683	202,700
56162	20	369.2	350.7	0.9499	493.7	517.0	1.0472	217,200
56247	35	356.0	324.5	0.9115	504.9	493.4	0.9772	-
56296	14	340.5	316.8	0.9304	480.9	475.7	0.9892	205,800
56400	9	350.9	-	-	456.6	470.3	1.0300	212,000
56401	14	326.0	291.1	0.8929	480.3	473.8	0.9865	205,200
56461	28	377.1	354.4	0.9398	528.0	525.8	0.9958	201,600
56660	9	401.3	362.2	0.9026	513.7	515.8	1.0041	205,700
56723	20	406.4	-		548	546.7	0.9980	211,200
56943	11	386.1	-		516.9	-	-	-
μ			0.9147		0.9996			207,700
σ			0.0266		0.0250			5310
V			0.0291		0.0250			0.0255

When the seven test results are compared to the mill tests, a mean value of the ratio of the static yield to the mill test yield of 0.915 and a coefficient of variation of 0.0291 are obtained. The mean difference between the static yield and the mill test yield strength is 31.6 MPa. Combing the results of the two sets of tests gives a ratio of the measured-to-nominal yield strengths of $371.7 \times 0.915 / 300 = 1.133$.

Before combining the coefficients of variations, they must be adjusted to account for the errors in experimental testing. The true coefficient of variation of experimental measurements is less than the apparent one as the latter reflects errors in the measurements themselves as well as the natural variation of the test results (Ellingwood *et al.* 1980). The errors in the coefficient of variation can be represented as (Mirza and MacGregor 1982; Kennedy and Baker 1984)

$$[4.10] \quad V_e = \left[V_s^2 + V_t^2\right]$$

where V_s is due to:

(1) the variations between the test and control specimens, and

(2) the variations of actual specimen dimensions from those measured,

and V_t, a result of uncertainties in the test loads, is due to:

(1) inaccuracies in the load monitoring devices,

(2) inaccuracies in the recording procedure, and

(3) differences in the definition of failure.

The breakdown of errors in measurement are shown in Table 4.8. For WWF sections comprised of plates, it is considered that the variations between the yield strength measured in the coupons and in the plates is inconsequential provided that the coupons are obtained from the column cross-section. Several measurements were taken of each coupon dimension to establish the second item under V_s. The variations listed under V_t are obtained from equipment specifications or estimated. The magnitudes of the errors in the coefficient of variation for the Algoma coupon tests are estimated, in part, according to observations made during the site visit.

The coefficients of variation for the error in measurement of the yield strengths are estimated to be 0.0175 for the tests conducted at the University of Alberta and 0.035 for the mill tests conducted at Algoma. The latter figure reflects the fact that the strain rate, known to have a profound effect on the yield strength, may vary below the

Table 4.8. Corrections for errors in testing

Location of test	V_s (1)	V_s (2)	V_t (1)	V_t (2)	V_t (3)	V_e
University of Alberta	-	0.00282	0.01	0.01	0.01	0.0175
Algoma	-	0.0111	0.01	0.01	0.03	0.0350

upper limit specified in the standards code. This introduces a random variation that is not a function of the material per se. Thus the coefficient of variation of the yield strength is estimated as

$$[4.11]\quad V_{F_y} = \left((0.0644^2 - 0.035^2) + (0.0291^2 - 0.0175^2)\right)^{\frac{1}{2}} = 0.0588$$

rather than 0.0707 if no errors in measurement were acknowledged.

The American Iron and Steel Institute (1974) shows that the yield strength for ingot cast steel varies within a given heat and within a given plate depending on the location of the coupon across the width and along the length of a plate. Strand cast steel, to which Algoma is currently converting, should display less variability. One factor not taken into account, however, is that the coupons were acquired from the tail end of the plate which, being cooler, are subject to more cold working than the remainder of the plate.

4.3.2. Modulus of elasticity

The mean value of the modulus of elasticity for the eight tests given in Table 4.7 is 207,700 MPa with a coefficient of variation of 0.0255. The mean value of the measured-to-nominal ratio is 1.038. Because the value for the coefficient of variation is relatively small in itself, no adjustment has been made for errors in measurement.

4.4. Professional factor

The professional factor relates the test strength of a member to that predicted by the appropriate equation given in the design standard. The column equations given in S16.1-M84 reflect the variation in column capacity as function of the slenderness ratio and, on the average, take into account the effects of out-of-straightness and residual stresses. The professional factor accounts for variations in column capacity other than those considered as geometric and material properties. These include variations in out-of-straightness, residual stress distributions, cross-sectional geometry, axes of bending, and non-linear interaction of the above parameters. However, for WWF columns, out-of-straightness and residual stresses are primarily responsible for the variations in column capacity that can occur for a given slenderness ratio.

Chernenko and Kennedy (1988) proposed that the effect on column strength due to statistical variations in out-of-straightness and residual stresses be assessed sequentially and finally that the effects of different residual stress patterns, axes of buckling and whether the

sections are heavy or light, be considered. This method has the advantage that the effects of out-of-straightness and residual stresses can be assessed independently and the statistical variations of these parameters can be used directly to obtain the statistical variation in the strength. It is, of course, necessary to know the mean value and standard deviation of the out-of-straightness and average compressive residual stress. The professional ratio can be written as

$$[4.12] \quad \rho_P = \rho_{\bar{s}} \rho_n \rho_{ex}$$

In [4.12], $\rho_{\bar{s}}$ is the simulated professional ratio, that is, the ratio of the strength determined by the computer simulations divided by that predicted by the design equation (such as clause 13.3.1 of the S16.1-M84) for the mean value of out-of-straightness and average compressive residual stress, for a given value of λ. The second term, ρ_n, accounts for variations due to the different residual stress patterns and the like while the third term, ρ_{ex}, is the mean value of the ratio of strengths determined by experiment and that determined by computer simulations. Overall, the professional ratio, ρ_P, is the required test (experimental)/predicted ratio.

The third term is required as a computer simulation is only as good as the assumptions used in the program and therefore must be verified by physical experiment. Provided good correlations are obtained, it is advantageous to do computer simulations rather than physical tests for a number of reasons:

(1) the effects of specific parameters on column strength can be systematically examined,

(2) the input is programmed so that defined values of the parameters are used and thus the need for the sometimes tedious measurements of residual stresses, cross-sectional geometry, yield strength and out-of-straightness is eliminated,

(3) the cost of computer simulations is much less than physical tests, and,

(4) the physical size of the column simulated is not limited by the capacity of the testing machine.

Provided that the computer simulations cover the expected range of the parameters studied, it is of little consequence what particular welded wide flange column sections are used. The only restriction is that they should represent the correct ratios of the flange/web area and width/thickness of the plate elements. As nearly all WWF column sections in grade 300W steel meet the width/thickness ratio of Class 1 sections in compression, and as the variation of the flange/web area ratio is small, this study was limited to the use of two sections, a WWF 12x79 and a WWF 14x202. The corresponding S.I. designations are WWF 314x118 and WWF 400x301.

4.4.1. Effect of out-of-straightness and residual stresses

In Figs. 4.16, 4.17, and 4.18 the simulated professional ratio, ρ_s, for slenderness parameters, λ, of 0.336, 0.672, and 1.007, respectively, is plotted against out-of-straightness ranging from 0 to 0.001 (the maximum out-of-straightness permissible by CSA Standard G40.20) and for the various average compressive residual stresses indicated. The simulated professional ratio was calculated by dividing the maximum capacity of the column obtained in the computer simulations by the unfactored resistance given in clause 13.3.1 of CSA Standard S16.1. All the data used to plot the figures are given in Tables 4.9, 4.10, and 4.11. Most simulations were carried out for three levels of average compressive residual stress, that of $0.0\sigma_y$, $0.305\sigma_y$, and $0.405\sigma_y$ as shown in Figs. 4.16, 4.17, and 4.18. The few simulations conducted at other values of average compressive residual stresses are considered subsequently. Magnitudes in out-of-straightness investigated ranged from just above zero at $0.0000182 \simeq 1/55{,}000$ (so selected to give a strength rather than a bifurcation problem) to $0.001 = 1/1000$ (the code tolerance limit). Strong and weak axis bending were considered and a variety of residual stress patterns were investigated.

Also given in Tables 4.9, 4.10, and 4.11 are the simulated professional factors based on clause 13.3.2 of CSA Standard S16.1-M84. As only the predicted strengths change, the only effect on Figs. 4.16 to 4.18 would be to change the value of the ratio ρ_s, that is, the vertical scale. Thus, mean values and standard deviations of ρ_s would change but the

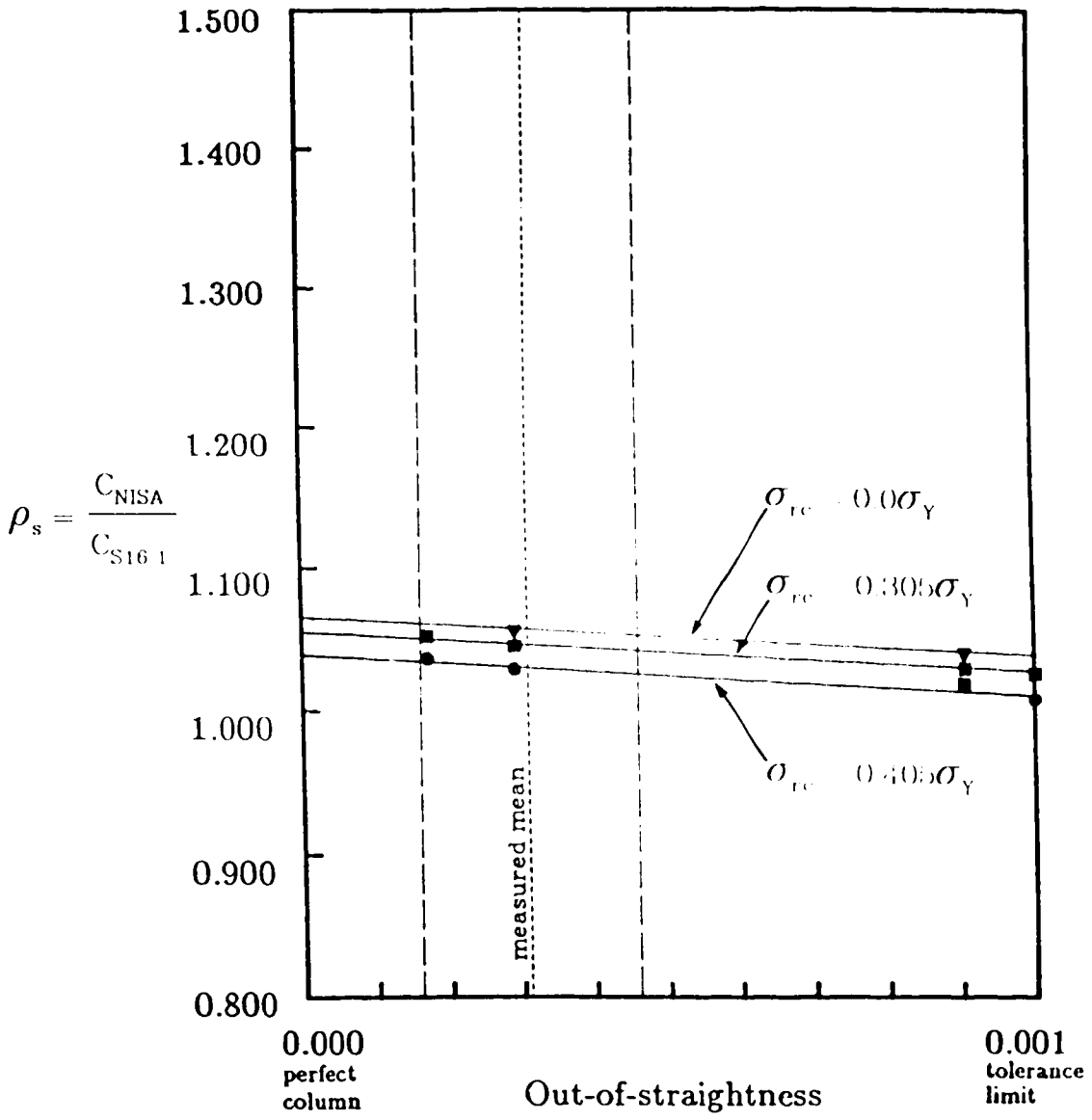

Fig. 4.16 Professional ratio vs. of out-of-straightness for λ=0.336

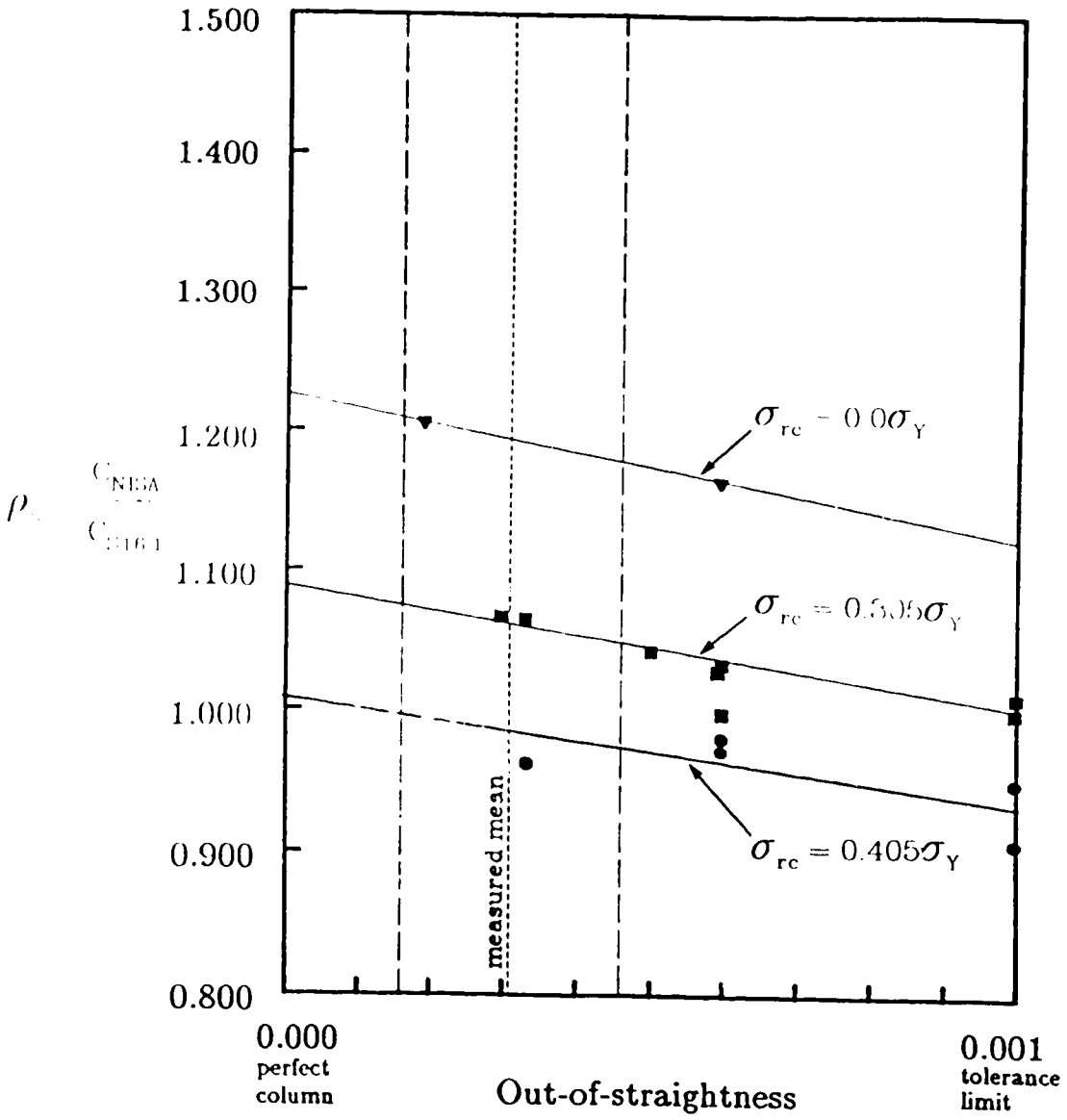

Fig. 4.17 Professional ratio vs. of out-of-straightness for λ=0.672

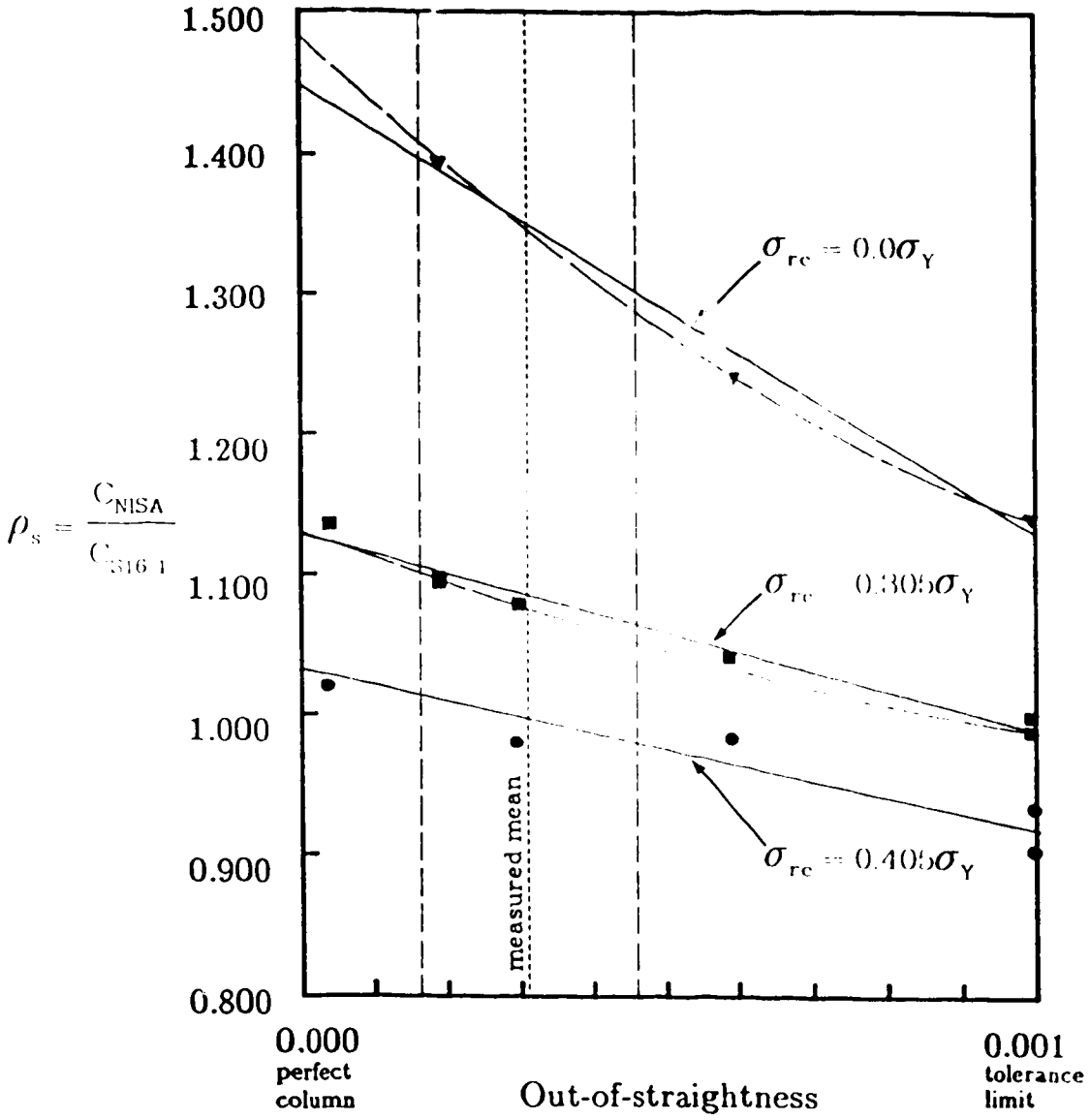

Fig. 4.18 Professional ratio vs. of out-of-straightness for λ=1.007

Table 4.9a. Simulated professional factor for λ=0.336 (Heavy section 14x202)

Test no.	λ	σ_r code	$\frac{\sigma_{rc}}{\sigma_y}$ (NISA)	Axis	$\rho_{NISA}=\frac{P_{max}}{P_y}$	OOS.	Cl. 1' $\rho_s=\frac{\rho_{NISA}}{\rho_{S16.1}}$ $\rho_{S16.1}$=0.9420	Cl. 13.3.2 $\rho_s=\frac{\rho_{NISA}}{\rho_{S16.1}}$ $\rho_{S16.1}$=0.9895
1	0.336	WB	0.305	W	0.9700	0.000901	1.0297	0.9803
4	0.336	F	0.340	W	0.9627	0.000901	1.0220	0.9729
6	0.336	W	0.305	W	0.9607	0.000901	1.0199	0.9709
11	0.336	none	0.0	W	0.9778	0.000901	1.0380	0.9882
15	0.336	WB	0.305	S	0.9852	0.000294	1.0459	0.9956
18	0.336	WB	0.305	S	0.9677	0.001000	1.0273	0.9780
50	0.336	none	0.0	W	0.9935	0.000294	1.0547	0.10041

Table 4.9b. Simulated professional factor for λ=0.336 (light section 12x79)

Test no.	λ	σ_r code	$\frac{\sigma_{rc}}{\sigma_y}$ (NISA)	Axis	$\rho_{NISA}=\frac{P_{max}}{P_y}$	OOS.	Cl. 13.3.1 $\rho_s=\frac{\rho_{NISA}}{\rho_{S16.1}}$ $\rho_{S16.1}$=0.9423	Cl. 13.3.2 $\rho_s=\frac{\rho_{NISA}}{\rho_{S16.1}}$ $\rho_{S16.1}$=0.9896
27	0.336	WL	0.405	W	0.975	0.000165	1.035	0.985
30	0.336	WB	0.305	W	0.991	0.000165	1.052	1.001
33	0.336	WL	0.405	S	0.970	0.000294	1.029	0.980
35	0.336	WL	0.405	S	0.950	0.001000	1.008	0.960
42	0.336	WL	0.385	W	0.9685	0.000164	1.0278	0.9787

Table 4.10a. Simulated professional factor for λ=0.672 (heavy section 14x202)

Test No.	λ	σ_r code	$\frac{\sigma_{rc}}{\sigma_y}$ (NISA)	Axis	$\rho_{NISA}=\frac{P_{max}}{P_y}$	OOS.	Cl. 13.3.1 $\rho_s=\frac{\rho_{NISA}}{\rho_{S16.1}}$ $\rho_{S16.1}$=0.7989	Cl. 13.3.2 $\rho_s=\frac{\rho_{NISA}}{\rho_{S16.1}}$ $\rho_{S16.1}$=0.9061
2	0.672	WB	0.305	W	0.8240	0.000595	1.0314	0.9094
5	0.673	F	0.340	W	0.8403	0.000595	1.0518	0.9274
7	0.672	W	0.305	W	0.7977	0.000595	0.9985	0.8804
9	0.672	WNT	0.305	W	0.7252	0.000595	0.9077	0.8004
12	0.672	none	0.0	W	0.9298	0.000595	1.1639	1.0262
14	0.672	WL	0.405	W	0.7746	0.000595	0.9696	0.8549
16	0.672	WB	0.305	W	0.8499	0.000294	1.0638	0.9380
19	0.672	WB	0.305	W	0.7972	0.001000	0.9979	0.8798
21	0.672	WB	0.305	S	0.8212	0.000588	1.0279	0.9063
23	0.672	WB	0.305	S	0.7995	0.001000	1.0008	0.8824
25	0.672	none	0.0	S	0.9640	0.000194	1.2067	1.0639
45	0.672	WNR	0.275	S	0.8143	0.000595	1.0193	0.8987
46	0.672	WB	0.305	W	0.8309	0.000500	1.0401	0.9171
47	0.672	WB	0.221	W	0.8558	0.000595	1.0712	0.9445

Table 4.10b. Simulated professional factor for λ=0.672 (light section 12x79)

Test No.	λ	σ_r code	$\frac{\sigma_{rc}}{\sigma_y}$ (NISA)	Axis	ρNISA= $\frac{P_{max}}{P_y}$	OOS.	Cl. 13.3.1 $\rho_s=\frac{\rho_{NISA}}{\rho_{S16.1}}$ $\rho_{S16.1}$=0.7996	Cl. 13.3.2 $\rho_s=\frac{\rho_{NISA}}{\rho_{S16.1}}$ $\rho_{S16.1}$=0.9067
28	0.671	WL	0.405	W	0.796	0.000330	0.962	0.848
31	0.671	WB	0.305	W	0.950	0.000330	1.063	0.937
36	0.671	WL	0.405	W	0.725	0.001000	0.907	0.800
38	0.671	WL	0.405	S	0.783	0.000588	0.979	0.864
40	0.671	WL	0.405	S	0.761	0.001000	0.952	0.839
43	0.671	F	0.385	W	0.8186	0.000328	1.0237	0.9028

Table 4.11a. Simulated professional factor for λ=1.007 (heavy section 14x202)

Test No.	λ	σ_r code	$\frac{\sigma_{rc}}{\sigma_y}$ (NISA)	Axis	$\rho_{NISA}=\frac{P_{max}}{P_y}$	OOS.	Cl. 13.3.1 $\rho_s=\frac{\rho_{NISA}}{\rho_{S16.1}}$ $\rho_{S16.1}$=0.6053	Cl. 13.3.2 $\rho_s=\frac{\rho_{NISA}}{\rho_{S16.1}}$ $\rho_{S16.1}$=0.7398
3	1.008	WB	0.305	W	0.6647	0.000191	1.0981	0.8985
8	1.008	W	0.305	W	0.6633	0.000191	1.0958	0.8966
10	1.008	WNT	0.305	W	0.6443	0.000191	1.0644	0.8709
13	1.008	none	0.0	W	0.8453	0.000191	1.3965	1.1426
17	1.008	WB	0.305	W	0.6531	0.000294	1.0790	0.8828
20	1.008	WB	0.305	W	0.5982	0.001000	0.9883	0.8086
22	1.008	WB	0.305	S	0.6305	0.000588	1.0416	0.8523
24	1.008	WB	0.305	S	0.6051	0.001000	0.9999	0.8179
26	1.008	none	0.0	W	0.7506	0.000585	1.2400	1.0146
48	1.006	WB	0.221	W	0.7317	0.000191	1.2088	0.9891
49	1.008	none	0.0	W	0.6908	0.001000	1.1413	0.9338

Table 4.11b. Simulated professional factor for λ=1.007 (light section 12x79)

Test No.	λ	σ_r code	$\frac{\sigma_{rc}}{\sigma_y}$ (NISA)	Axis	$\rho_{NISA}=\frac{P_{max}}{P_y}$	OOS.	Cl. 13.3.1 $\rho_s=\frac{\rho_{NISA}}{\rho_{S16.1}}$ $\rho_{S16.1}$=0.6069	Cl. 13.3.2 $\rho_s=\frac{\rho_{NISA}}{\rho_{S16.1}}$ $\rho_{S16.1}$=0.7418
29	1.006	WL	0.405	W	0.619	0.0000183	1.020	0.835
32	1.006	WB	0.305	W	0.690	0.0000183	1.137	0.931
34	1.006	WL	0.405	W	0.595	0.000294	0.980	0.803
37	1.006	WL	0.405	W	0.550	0.001000	0.906	0.742
39	1.006	WL	0.405	S	0.590	0.000588	0.972	0.796
41	1.006	WL	0.405	S	0.568	0.001000	0.936	0.766
44	1.006	F	0.385	W	0.6527	0.0000182	1.0755	0.8807

coefficients of variation would remain the same.

In each of Figs. 4.16, 4.17, and 4.18, three straight lines are drawn for sections with average compressive residual stresses of $0.0\sigma_y$, $0.305\sigma_y$, and $0.405\sigma_y$. The lines were obtained using the method of least squares. In general, the data for strong and weak axis bending were indistinguishable as examination of Tables 4.9 to 4.11 shows. Where a minor difference occurred, as was the case for an average compressive residual stress of $0.405\sigma_y$ for $\lambda = 0.672$ and 1.007, equal weight was given to each axis of bending.

For the most part, the data for an average compressive residual stress of $0.305\sigma_y$ were obtained from computer simulations using the 14H202 while the data for a residual stress of $0.405\sigma_y$ were obtained with a light section, the 12H79. Again the data were generally indistinguishable and in any event no distinction is currently made in the design standard. The data for zero residual stresses were obtained from computer simulations using the 14H202. The linear relationships for each ratio of average compressive residual stress and each value of the slenderness parameter, λ, are given in Table 4.12.

In two cases, in Fig. 4.18 for λ=1.007, with average compressive residual stresses of $0.0\sigma_y$ and of $0.305\sigma_y$, curved lines are also drawn. The curved lines were based on points where the only variable was the out-of-straightness; that is, the same section, the same axis of bending, and the same residual stress pattern were used. This indicated that the variation in the ratio, ρ_s, with out-of-straightness is slightly non-linear

Table 4.12. Best fit curves

Eqn No.	λ	$\frac{\sigma_{rc}}{\sigma_y}$	Eqn for Best Fit Curve $\rho_s = m \cdot \Delta/L + b$	ρ_s [Δ/L=0.000302]
1	0.336	0.0	ρ_s = -29.5xΔ/L+1.062	1.053
2		0.305	ρ_s = -28.6xΔ/L+1.056	1.047
3		0.405	ρ_s = -28.2xΔ/L+1.036	1.027
4	0.672	0.0	ρ_s = -107xΔ/L+1.227	1.195
5		0.305	ρ_s = -90.6xΔ/L+1.088	1.061
6		0.405	ρ_s = -82.1xΔ/L+1.008	0.983
7	1.007	0.0	ρ_s = -315xΔ/L+1.446	1.351
8		0.305	ρ_s = -135xΔ/L+1.126	1.085
9		0.405	ρ_s = -114xΔ/L+1.028	0.994

and the rate of decrease decreases with increasing out-of-straightness. However, a best-fit straight line is considered the most appropriate representation when differences in residual stress patterns, the use of heavy and light sections, and bending about both axes are taken into account. Furthermore, design standards generally give a single equation to cover all these situations. The deviations from the best-fit straight lines, therefore, reflect the different residual stress patterns, strong and weak axis bending, heavy and light sections, and the fundamental non-linearity (other parameters held constant)

Examination of Figs. 4.16, 4.17, and 4.18 shows, as would be expected, that the ratio of the test/predicted strength decreases with increasing out-of-straightness for given values of λ and compressive residual stress. The slope of the lines, that is the rate of decrease of strength with out-of-straightness, also increases with increased values of the slenderness parameter (compare Fig. 4.16 to Fig. 4.17 to Fig 4.18

for a given value of residual stress). Thus out-of-straightness has a greater effect in reducing the column strength for larger values of λ (within the range studied) than for smaller values. In fact, the slope of the lines approaches zero for λ =0.336, indicating that out-of-straightness has little effect on the strength of short columns. Based on this, an out-of-straightness of up to 0.001L is concluded to have negligible effect on the strength of WWF sections for λ less than 0.336.

It is also of interest to note, as can be seen particularly in Fig. 4.18 for λ = 1.007 and to a lesser extent in Fig. 4.17 for λ = 0.672 that the rate of decrease of strength with out-of-straightness, that is the slope of the straight lines, decreases as the residual stresses become larger (see also Table 4.12). A zero change in slope would indicate the two effects of out-of-straightness and residual stresses were simply additive. An increased slope with increased values in the compressive residual stress would indicate a multiplicative or synergistic effect with the combined effect greater than the sum of the individual effects. In fact, the data show that there is a negative synergistic effect and that the effect of increasing out-of-straightness is softened.

4.4.2. Out-of-straightness

To assess the effect of the variation in out-of-straightness on column strength, its mean value and coefficient of variation must be established. Fig. 4.19 gives the probability density distribution for 120 measurements of camber taken by Algoma personnel as obtained from the quality assurance files. The mean camber is 0.000530 (1/1890) with

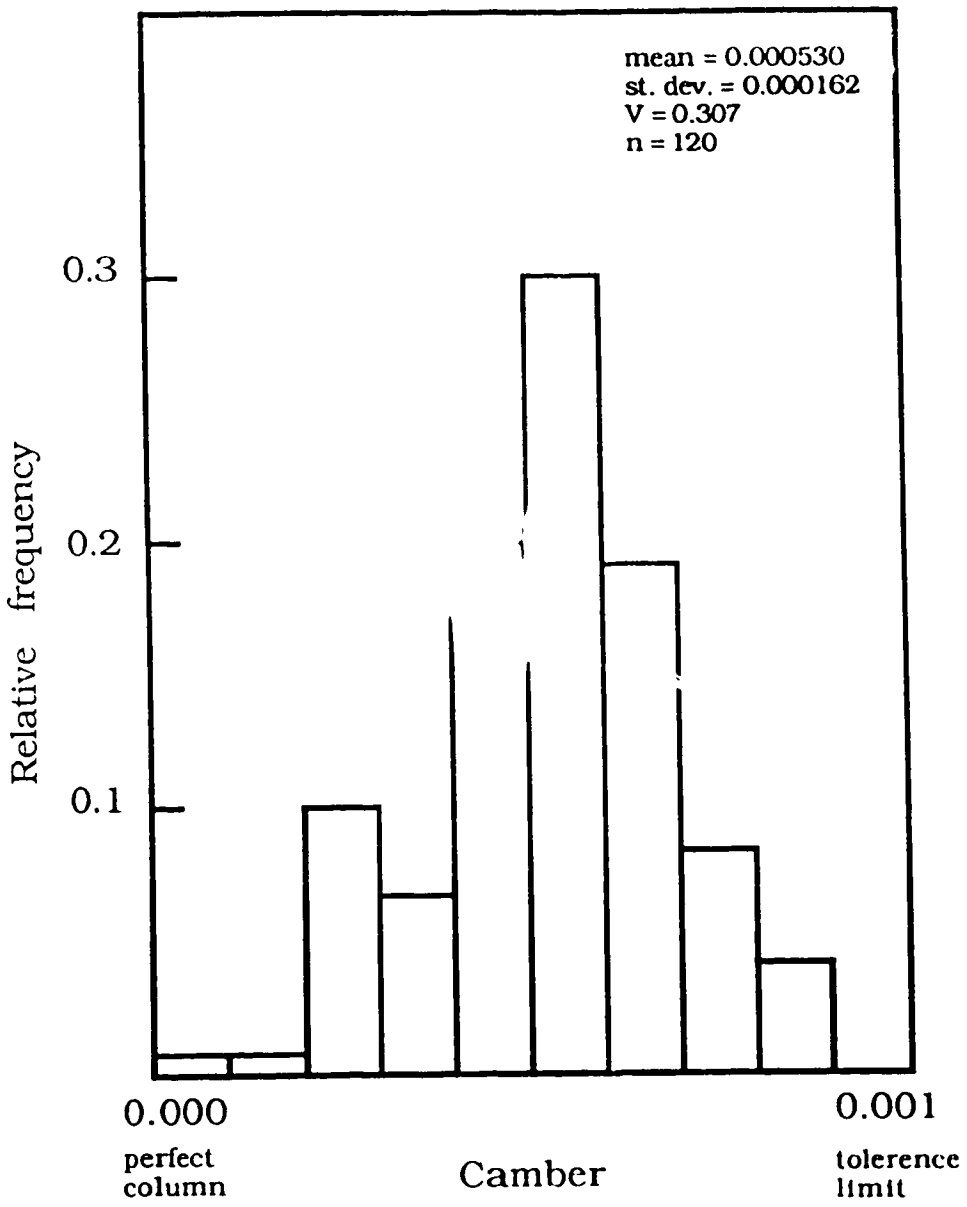

Fig. 4.19 Frequency distribution for camber

a coefficient of variation of 0.307. In no case does the camber exceed the tolerance of 1/1000 for, when members develop an excessive camber, they are straightened by heating to meet the limit and then included in the population. Members exceeding the tolerance limit seldom occur (less than 2% of all recorded measurements) and, in any case, are easily spotted. This prescribes the sampling procedure employed by the Algoma personnel; measurements are taken of those columns that appear to have the greater camber. It is estimated conservatively that the sample cited is 1/20 of the total population and furthermore that the remaining population of columns are, on the average, straighter with an estimated mean camber of 0.0003 and an estimated standard deviation of 0.0001, corresponding to a coefficient of variation of 0.33. Combining these two samples gives a mean camber of 0.000311 (1/3210) with a coefficient of variation of 0.370.

Fig. 4.20 gives the probability density function for 11 measurements of sweep made during the site visit. The mean value of sweep is 0.000293 with standard deviation of 0.000154 corresponding to a coefficient of variation of 0.525. These figures are substantiated by observations made by Algoma personnel that sweep rarely exceeds the tolerance limit of 1/1000 and generally exhibits smaller magnitudes in out-of-straightness than camber.

Giving equal weight to the sweep and camber measurements gives a mean out-of-straightness 0.000302, a standard deviation of 0.000136, and a coefficient of variation of 0.451. The large coefficient of variation

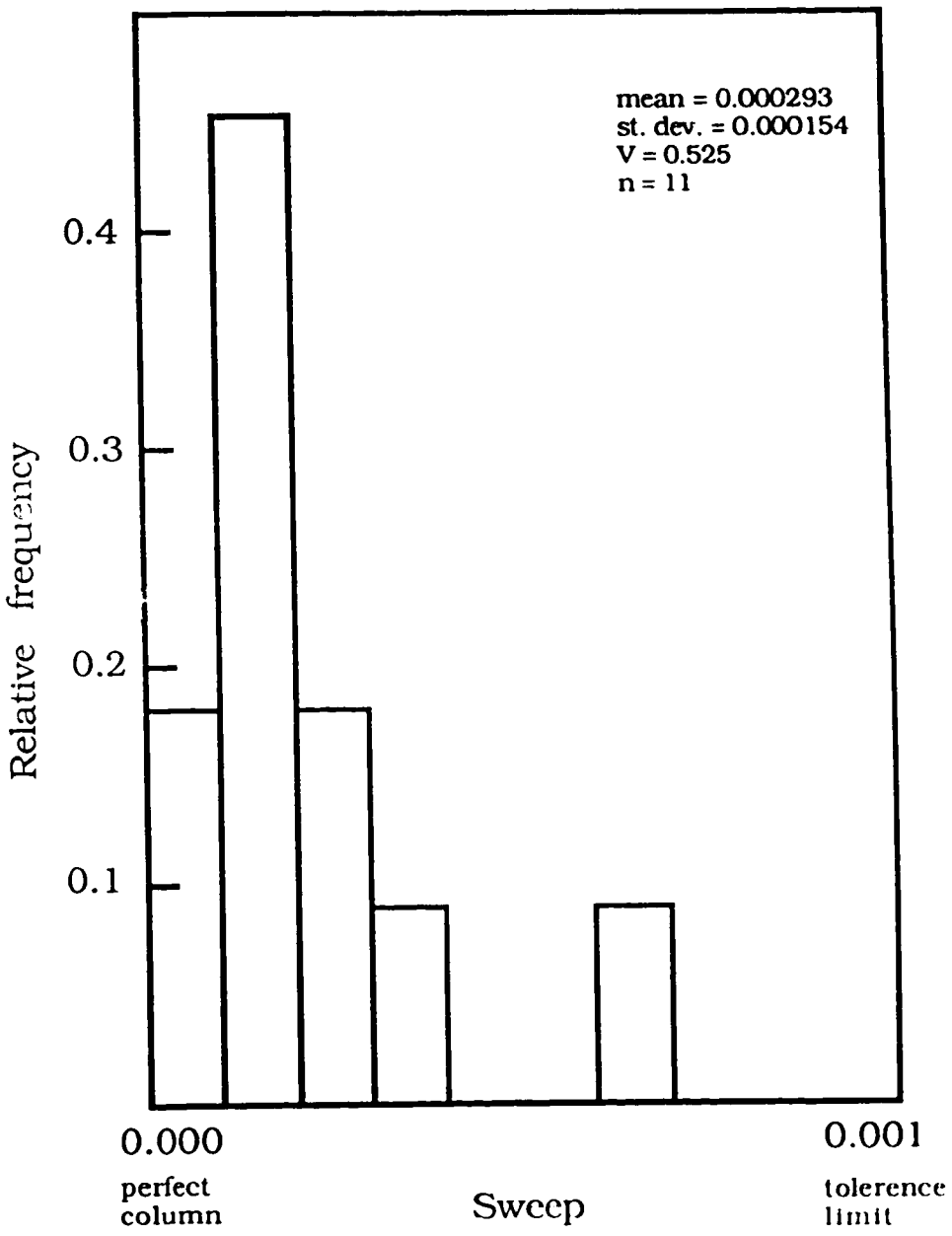

Fig. 4.20 Frequency distribution for sweep

is due to the fact that the mean value is so small.

On Figs. 4.16, 4.17, and 4.18 vertical lines are drawn at this mean value of out-of-straightness of $\Delta/L=0.000302$ and also at one standard deviation to the left and right of the mean, at out-of-straightness values of 0.000166 and 0.000438, respectively. The point were the vertical lin for the mean out-of-straightness intercepts the line for a particular value of residual stress gives the ratio ρ_s' for the mean out-of-straightness at that level of residual stress. The vertical distance between the intercepts of the right and left standard deviation lines, with the same residual stress line, is equal to two standard deviations of ρ_s' associated with out-of-straightness. Therefore, the standard deviation for the simulated professional ratio is computed by multiplying the slope of the equation for a given residual stress line by one standard deviation for out-of-straightness, that is, ' pe x 0.000136. From this, the coefficient of variation is computed a ay for the given residual stress level. Because the slope of the equations vary as the residual stress level varies, so does the coefficient of variation vary, for a given out-of-straightness. Therefore, the coefficient of variation for the professional factor as related to out-of-straightness, $V_{\Delta/L}$, is calculated in a subsequent section when the mean value of the average compressive residual stress is established. The variations in ρ_s' due to different residual stress patterns and like factors are considered in the following two sections.

4.4.3. Residual stresses

From Figs. 4.16, 4.17, and 4.18, or the equations given in Table 4.12, the values of ρ_s' corresponding to the mean out-of-straightness of 0.000302 for residual stress levels of $0.0\sigma_y$, $0.305\sigma_y$, and $0.405\sigma_y$ are determined for each value of λ studied. These are plotted in Fig. 4.21 against the average value of the compressive residual stress, σ_{rc}/σ_y. Fig. 4.21 is therefore a slice through Figs. 4.16, 4.17, and 4.18 combined, at a value of Δ/L of 0.000302. This is illustrated in Fig. 4.22, a composite of Figs. 4.16, 4.17, 4.18, and 4.21, giving a three dimensional plot of the simulated professional ratio ρ_s against out-of-straightness and average compressive residual stress. Figs. 4.16, 4.17, and 4.18, plotted originally for three separate slenderness parameters, are reformed, now appearing on planes of constant residual stress. The plane of $\sigma_{rc}/\sigma_y = 0.0$ depicts the variation of ρ_s with out-of-straightness for each of the three slenderness parameters as do the planes of $\sigma_{rc}/\sigma_y = 0.305$ and 0.405.

Fig. 4.21, evaluated at the mean out-of-straightness, is used to establish $\rho_{\bar{s}}$ given in [4.12], corresponding to the mean value of the out-of-straightness and the mean value of average compressive residual stress, as well as the standard deviation of $\rho_{\bar{s}}$ due to the variation of residual stresses as was done for out-of-straightness. In order to do so, the mean value of the average compressive residual stress and its standard deviation must first be established.

Table 4.13 gives the results of 10 sets of residual stress measurements reported by Tall and Alpsten (1969), McFalls and Tall (1969),

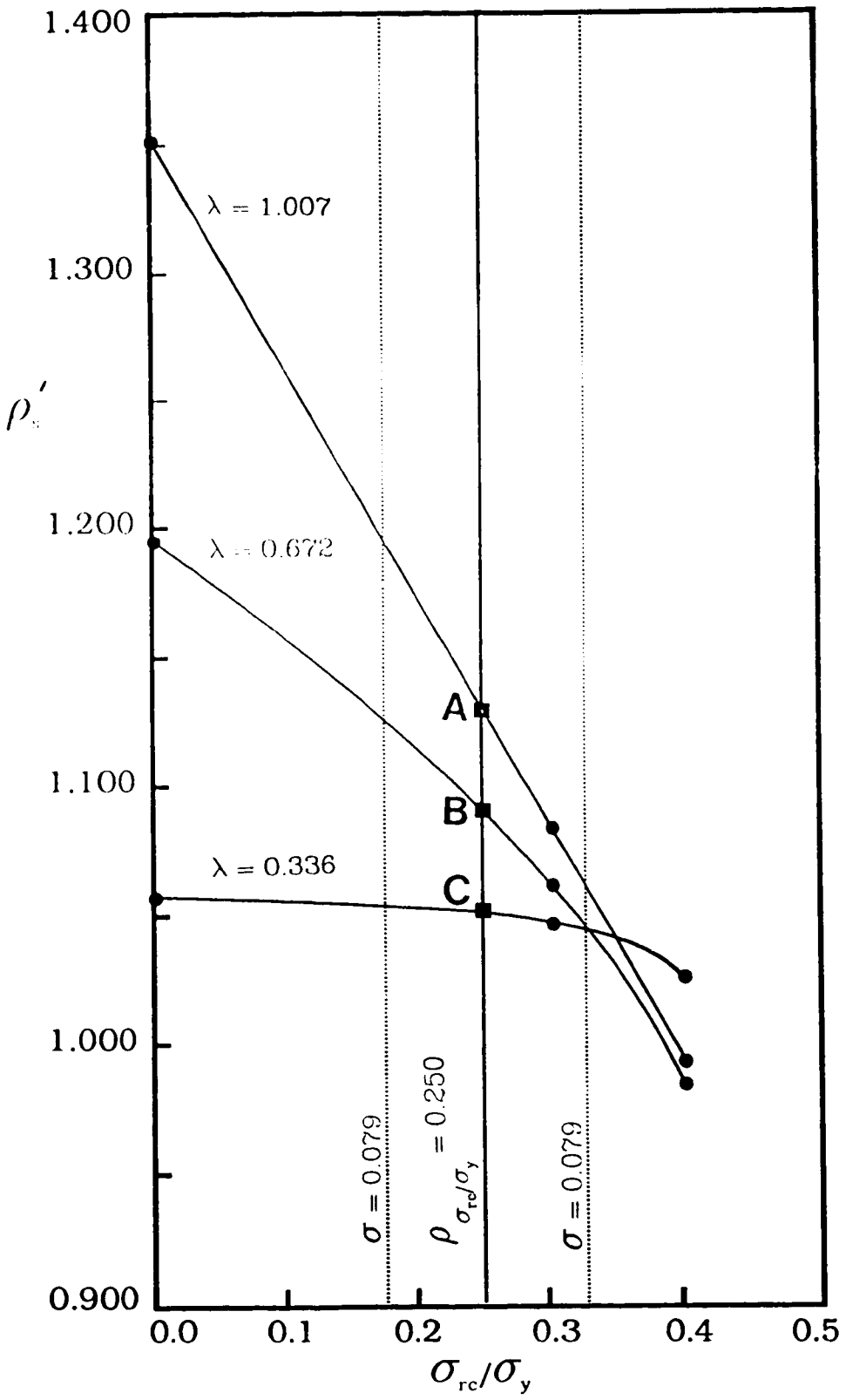

Fig. 4.21 Professional ratio vs. compressive residual stress at mean out-of-straightness

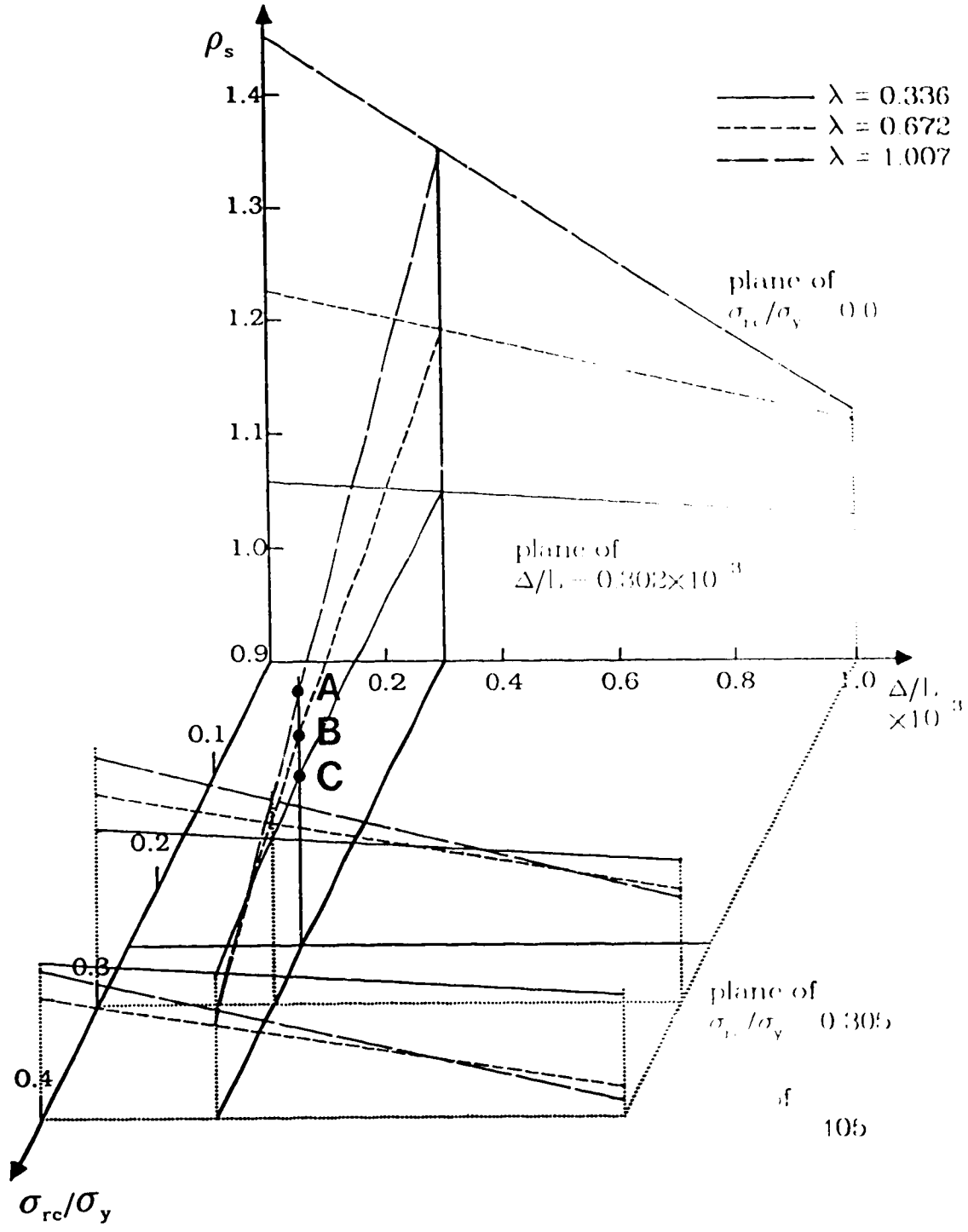

Fig. 4.22 Professional ratio vs. compressive resi ss and out-of-straightness

Table 4.13. Average compressive residual stress for various sections

Heavy Sections				Light Sections			
No.	Section	Section (Algoma)	$\bar{\sigma}_{rc}$ (ksi)	No.	Section	Section (Algoma)	$\bar{\sigma}_{rc}$ (ksi)
1	12H210	350x315	14.4	1	12H79	350x137	12.4
2	20H354	500x561	8.8	2	12H79	350x137	13.1
3	24H428	550x620	7.7				
4	24H1122		8.0				
5	14H202	350x315	9.2				
6	23H681		7.4				
7	15H290	400x444	7.6				
8	15H290	400x444	6.2				

Alpsten and Tall (1970), and Bjorhovde *et al.* (1972). Two of the sections are classified as light and the other eight as heavy sections. Equivalent S.I. sections manufactured by Algoma steel are also given. The mean value of the average compressive residual stress for the six heavy sections with Algoma equivalents is 8.98 ksi with standard deviation of 2.85 ksi and for the light sections the mean value is 12.75 ksi. (If all eight sections were used, the mean value becomes 8.66 ksi and the standard deviation becomes 2.49 ksi.) Assuming production to be equally distributed between heavy and light sections (the same distribution which was used previously), the mean value of residual stress is 10.87 ksi or 75 MPa. Lacking data, it is conservatively assumed that the standard deviation for light sections is the same as for heavy to give an overall standard deviation of 3.42 ksi or 23.6 MPa.

Although residual stresses are reported in the literature as decimal fractions of the yield value, as has been done here, it is argued that residual stresses per se are not a function of the yield stress. Unless residual strains due to uneven cooling exceed the yield level over a

significant portion of the cross-section, the average compressive residual stress, only a fraction of the residual stress, should not be a function of the yield stress at room temperature. This is substantiated by experimental results of McFalls and Tall (1969) and Alpsten and Tall (1969) on 12H79 sections made of steels with yield strengths of 36.8 ksi and 44.6 ksi which gave virtually the same average compressive residual stresses of 12.4 ksi and 13.1 ksi, respectively. Taking the ratio of the two yield strengths gives a value of 1.21 as compared to 1.06 for the ratio of the average compressive residual stresses, thus substantiating this argument. Therefore, for CSA G40.21 grade 300W steel, the most widely used steel, the ratio of the mean value of compressive residual stress to nominal is 75/300 = 0.250 with a standard deviation of 23.6/300 = 0.079.

In Fig. 4.21 vertical lines are drawn at the mean value of the compressive residual stress, $0.250\sigma_y$, and at one standard deviation to the left and right of the mean, that is at $0.171\sigma_y$ and $0.329\sigma_y$. By entering Fig. 4.21 or Fig. 4.22 at the mean value of the average compressive residual stress, the mean value of the simulated professional factor, $\rho_{\bar{s}}$, is established at the mean out-of-straightness and mean compressive residual stress, as found at points A, B, and C for λ's of 0.336, 0.672, and 1.007, respectively. The values for the ratio of the simulated professional factor are 1.049, 1.088, and 1.134 for slenderness parameters, λ, of 0.336, 0.672, and 1.007, respectively. The vertical distance between the left and right standard deviation lines represents two standard

deviations in the simulated professional ratio, leading to standard deviations (in the same order as above) of 0.0035, 0.038, and 0.070. The corresponding coefficients of variation are 0.00334, 0.0358, and 0.0617. The coefficients of variation, V_{σ_r}, and mean values for the simulated professional ratio, $\rho_{\bar{s}}$, are tabulated in Table 4.14.

Although one mean value has been determined for the professional factor related to both the mean value of out-of-straightness and the compressive residual stress, there are two coefficients of variation, one related to the residual stresses, V_{σ_r}, as found above, and the other related to out-of-straightness, $V_{\Delta/L}$. The latter is evaluated at the mean value of the average compressive residual stress of σ_{rc}/σ_y=0.250 by interpolating between the values for σ_{rc}/σ_y = 0.0 and σ_{rc}/σ_y = 0.305, using Fig. 4.23, to determine the slope of the best fit line for this residual stress level for the three values of the slenderness parameters. The values for $V_{\Delta/L}$ are 0.00373, 0.0117, and 0.0180 for λ's of 0.336, 0.672, and 1.007, respectively, as given in Table 4.14.

Table 4.14. Statistical parameters for the professional factor

Clause from S16.1	λ	$\rho_{\bar{s}}$	$V_{\Delta/L}$	V_{σ_r}	ρ_n	V_n	ρ_e	V_e	ρ_P	V_P
13.3.1	0.336	1.049	0.00373	0.00334	0.999	0.00362	0.993	0.0204	1.041	0.0213
	0.672	1.088	0.0117	0.0358	1.002	0.0194	0.993	0.0204	1.083	0.0470
	1.007	1.134	0.0180	0.0617	1.003	0.0134	0.993	0.0204	1.130	0.0688
13.3.2	0.336	0.999	0.00373	0.00334	0.999	0.00362	0.993	0.0204	0.991	0.0213
	0.672	0.959	0.0117	0.0358	1.002	0.0194	0.993	0.0204	0.955	0.0470
	1.007	0.928	0.0180	0.0617	1.003	0.0134	0.993	0.0204	0.925	0.0688

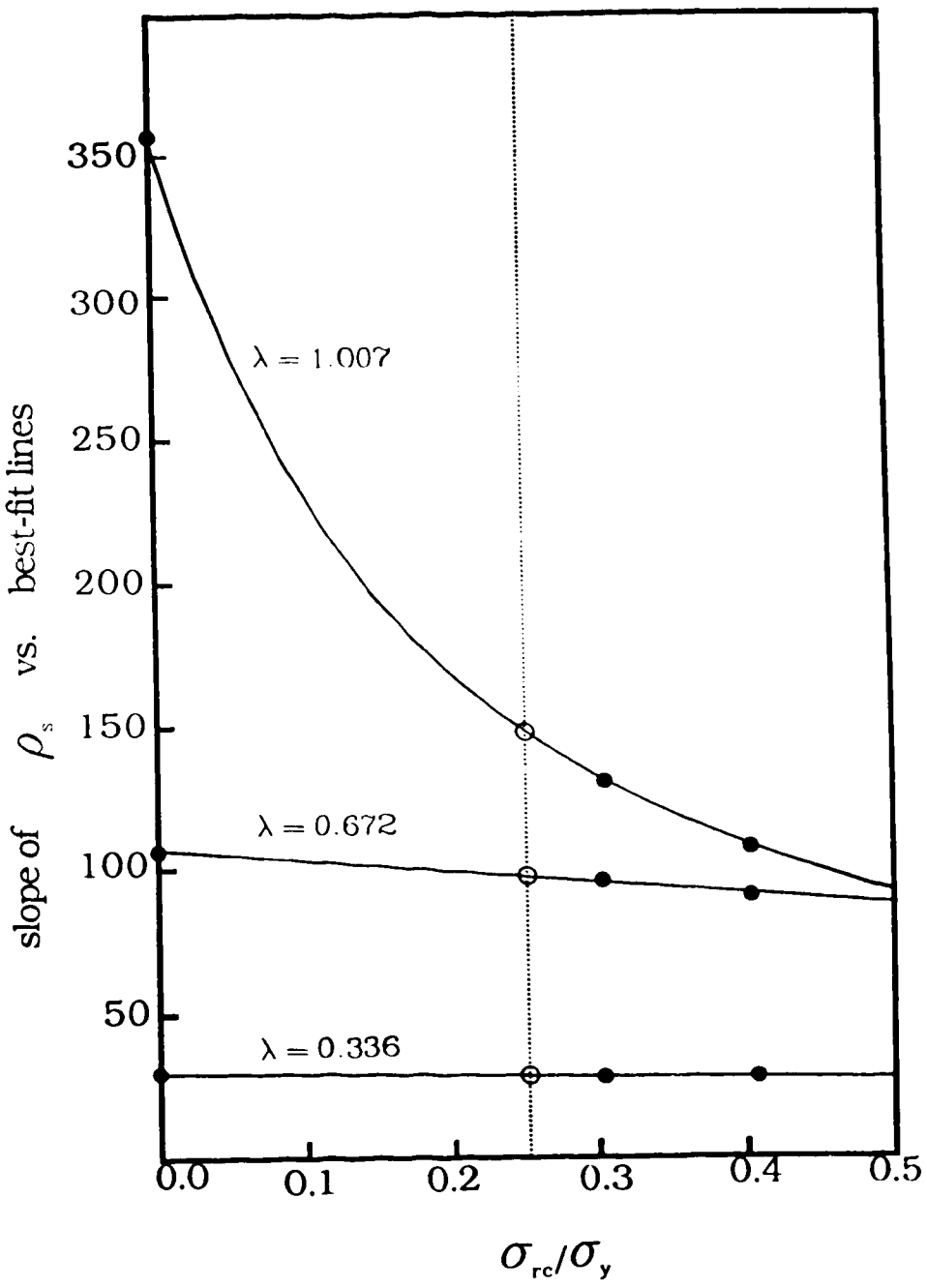

Fig. 4.23 Slope of best fit lines vs. compressive residual stress

4.4.4. Miscellaneous factors

In Figs. 4.16, 4.17, and 4.18 variations in the professional ratio about the best-fit straight lines exist that were attributed to factors such as different residual stress patterns, strong and weak axis bending, the heavy and light sections, and the fundamental non-linearity of the relation. The additional effect of these miscellaneous factors can be assessed by neutralizing the effect of both out-of-straightness and residual stresses. This is accomplished by normalizing the plotted professional ratio for any slenderness parameter and residual stress level by dividing by the value obtained from the linear expressions given in Table 4.12 for that specific residual stress level and slenderness parameter. For residual stress levels not represented by equations in Table 4.12, supplementary expressions were derived by interpolating between the slopes for residual stress levels using Fig. 4.23 and evaluating the coefficient for the intercept, b, such that for an out-of-straightness, Δ/L, of 0.000302 for which Fig 4.21 is plotted, the professional ratio given by the expression would coincide with that given in Fig. 4.21. All these data are given in Tables 4.15, 4.16, and 4.17 for the three λ values of 0.336, 0.672, and 1.007, respectively.

Of course, the average value of the normalized professional ratio, ρ_n, should equal 1.00 for any residual stress level for which a best-fit straight line has been used. The normalized professional ratio for λ = 0.336, 0.672, and 1.007 are plotted in Figs. 4.24, 4.25, and 4.26, respectively. The mean values and coefficients of variation for the three

Table 4.15. Normalized values of the simulated professional ratio for $\lambda = 0.336$

Test no.	Residual stress code	$\frac{\sigma_{rc}}{\sigma_y}$	Out-of-straightness Δ/L	ρ_s	$\rho_{s_{eq}} = m\Delta/L + b$	$\rho_{s_{eq}}$	$\rho_n = \frac{\rho_s}{\rho_{s_{eq}}}$
11	none	0.0	0.000901	1.038	$-29.5\Delta/L + 1.062$	1.035	1.003
50	none	0.0	0.000294	1.055	"	1.053	1.001
1	WB	0.305	0.000901	1.030	$-28.6\Delta/L + 1.056$	1.030	1.000
6	W	0.305	0.000901	1.020	"	1.030	0.990
15	WB	0.305	0.000294	1.046	"	1.047	0.998
18	WB	0.305	0.001000	1.027	"	1.027	1.000
30	WB	0.305	0.000165	1.052	"	1.051	1.001
27	WL	0.405	0.000165	1.035	"	1.031	1.003
33	WL	0.405	0.000294	1.029	"	1.028	1.001
36	WL	0.405	0.001000	1.008	"	1.008	1.000
[illegible]	[illegible]	[illegible]	[illegible]	[illegible]	[illegible]	[illegible]	[illegible]
42	WL	0.385	0.000164	1.028	"	1.039	0.989

Table 4.16. Normalized values of the simulated professional ratio for $\lambda = 0.672$

Test no.	Residual stress code	$\frac{\sigma_{rc}}{\sigma_y}$	Out-of-straightness Δ/L	ρ_s	$\rho_{s_{eq}} = m\Delta/L + b$	$\rho_{s_{eq}}$	$\rho_n = \frac{\rho_s}{\rho_{s_{eq}}}$
12	none	0.0	0.000595	1.164	$-107\Delta/L + 1.227$	1.163	1.001
25	none	0.0	0.000194	1.207	"	1.206	1.000
2	WB	0.305	0.000595	1.031	$-906\Delta/L + 1.088$	1.034	0.997
7	W	0.305	0.000595	0.999	"	1.034	0.966
16	WB	0.305	0.000294	1.064	"	1.034	1.029
19	WB	0.305	0.001000	0.998	"	0.997	1.001
21	WB	0.305	0.000588	1.028	"	1.035	0.993
23	WB	0.305	0.001000	1.001	"	0.997	1.003
46	WB	0.305	0.000500	1.040	"	1.043	0.997
31	WB	0.305	0.000330	1.063	"	1.058	1.005
14	WL	0.405	0.000595	0.970	$-82.1\Delta/L + 1.088$	0.959	1.011
28	WL	0.405	0.000330	0.962	"	0.981	0.981
36	WL	0.405	0.001000	0.907	"	0.926	0.980
38	WL	0.405	0.000588	0.979	"	0.960	1.020
40	WL	0.405	0.001000	0.952	"	0.926	1.028
5	F	0.340	0.000595	1.052	$-87.6\Delta/L + 1.066$	1.014	1.037
45	WNR	0.275	0.000595	1.019	$-83.8\Delta/L + 1.032$	1.005	1.019
47	WB	0.221	0.000595	1.071	$-92.2\Delta/L + 1.105$	1.050	0.971
43	F	0.385	0.000328	1.024	$-95.1\Delta/L + 1.134$	1.077	0.994

Table 4.17. Normalized values of the simulated professional ratio for $\lambda = 1.007$

Test no.	Residual stress code	$\frac{\sigma_{rc}}{\sigma_y}$	Out-of-straightness Δ/L	ρ_s	$\rho_{s_{eq}}=m\Delta/L+b$	ρ_c	$\rho_n = \frac{\rho_s}{\rho_{s_{eq}}}$
13	none	0.0	0.000191	1.397	-315Δ/L+1.446	1.389	1.008
26	none	0.0	0.000585	1.240	"	1.262	0.983
49	none	0.0	0.001000	1.141	"	1.131	1.009
3	WB	0.305	0.000191	1.098	-135Δ/L+1.126	1.100	0.998
8	W	0.305	0.000191	1.096	"	1.100	0.996
17	WB	0.305	0.000294	1.079	"	1.086	0.993
20	WB	0.305	0.001000	0.988	"	0.991	0.997
22	WB	0.305	0.000588	1.042	"	1.047	0.995
24	WB	0.305	0.001000	1.000	"	0.991	1.009
32	WB	0.305	0.0000183	1.137	"	1.124	1.012
29	WL	0.405	0.0000183	1.020	-114Δ/L+1.028	1.026	0.994
34	WL	0.405	0.000294	0.980	"	0.995	0.985
37	WL	0.405	0.001000	0.906	"	0.914	0.991
39	WL	0.405	0.000588	0.972	"	0.961	1.011
41	WL	0.405	0.001000	0.936	"	0.914	1.024
48	WB	0.221	0.000191	1.209	-118.2Δ/L+1.051	1.050	1.024
44	F	0.375	0.0000182	1.076	-184.6Δ/L+1.214	1.178	1.024

different slenderness parameters are given in Table 4.14 as ρ_n and V_n, respectively. The mean values in each case is nearly equal to 1.00 and the coefficients of variation are small.

4.4.5. Experimental factor

In Table 4.18, the results of six computer simulations are compared with the experimental results of McFalls and Tall (1969). All strengths have been non-dimensionalized by dividing by the yield capacity of the column. The mean value of the experimental/computer simulation value is 0.993 with a coefficient of 0.204 when test 3 on the 12H79 at a slenderness ratio of 90 is excluded for not meeting Chauvenet's cri-

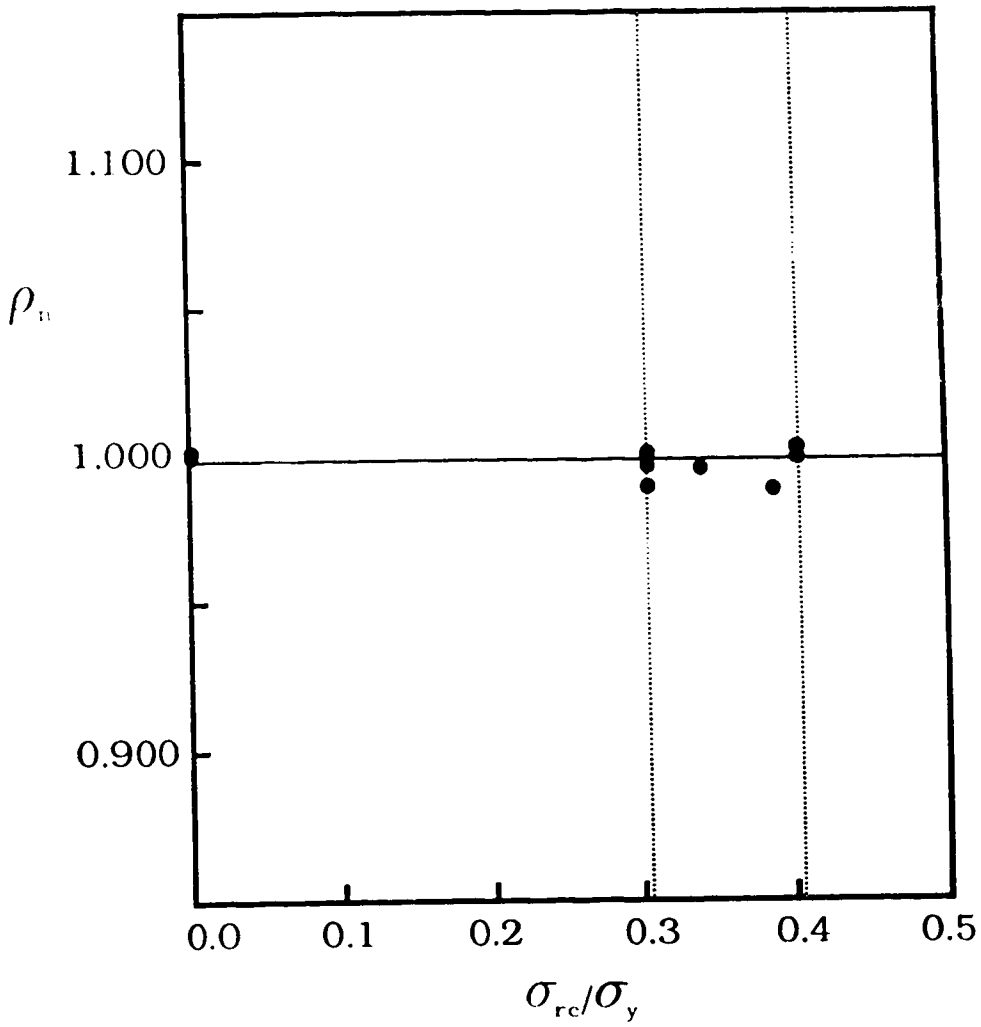

Fig. 4.24 Normalized professional ratio vs. compressive residual stress at $\lambda = 0.336$

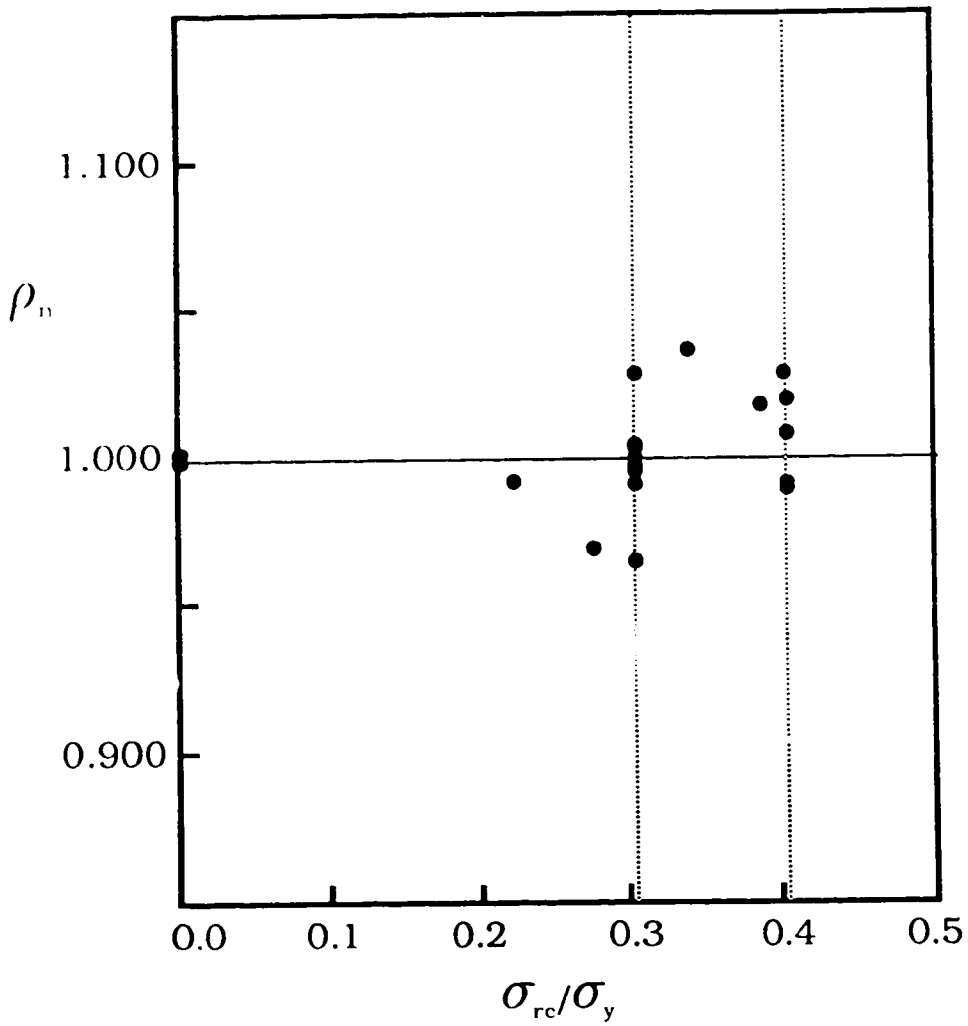

Fig. 4.25 Normalized professional ratio vs. compressive residual stress at $\lambda = 0.672$

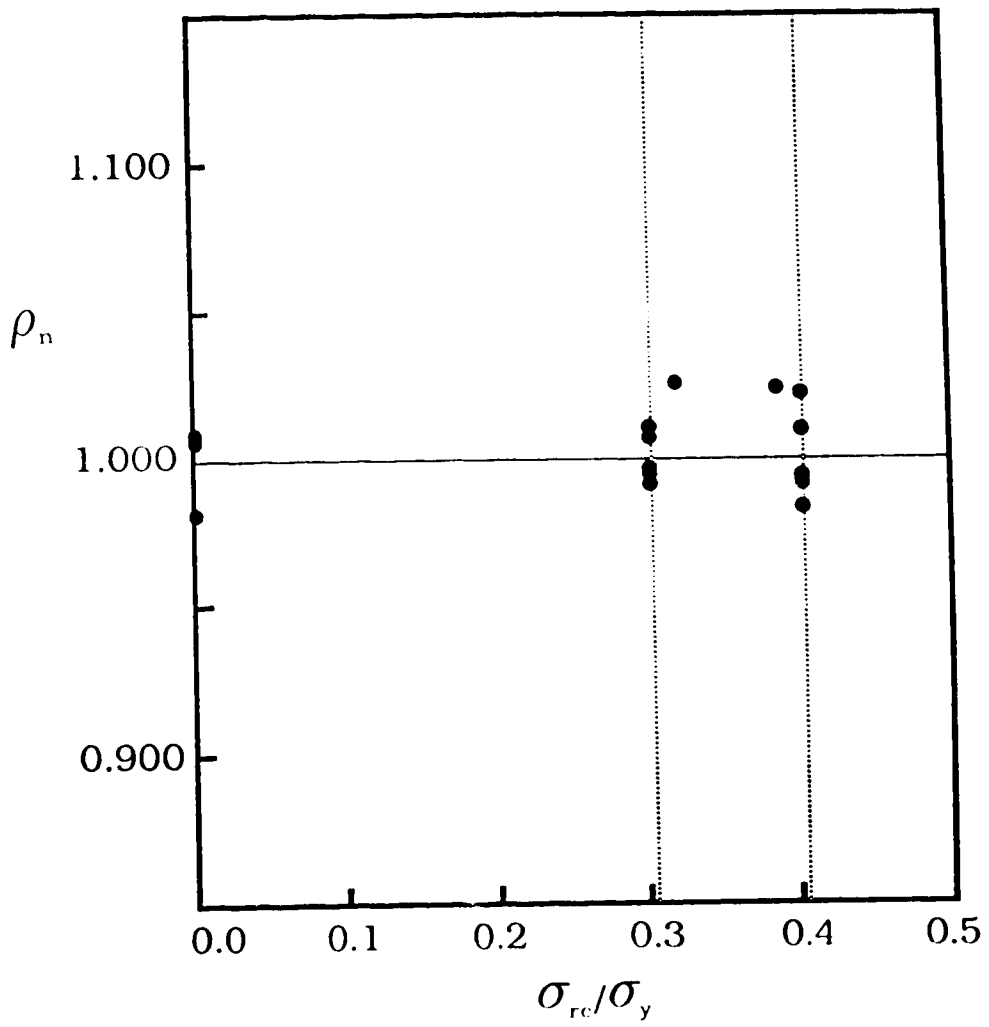

Fig. 4.26 Normalized professional ratio vs. compressive residual stress at $\lambda = 1.007$

Table 4.18. Professional factor relating experimental strengths to strengths predicted by NISA

Section	$\frac{l}{r}$	C_r/C_y		$\rho_e = \frac{EXP}{NISA}$
		NISA	EXP.	
12H79	30	0.976	0.97	0.994
	60	0.769	0.76	0.989
	90	0.619	0.68	1.098
14H202	30	0.970	0.97	1.000
	60	0.824	0.84	1.019
	90	0.665	0.64	0.963

terion for outliers. These values are given in Table 4.14.

This comparison is compromised to some extent because the experimental results were reported to only two significant figures. It is expected that if detailed measurements of pertinent geometric and material properties had been available that the computer simulations would produce results consistently closer to the experimental tests such that ρ_{ex} would be closer to 1.00 with a smaller coefficient of variation than that obtained in the study. It is also expected that no simulation would fail Chauvenet's criterion for outliers. This statement is valid as long as the computer simulations have the capacity to model the behaviour observed in the laboratory. Further testing to confirm the computer simulations is therefore seen as being crucial.

4.4.6. Summary

The professional factors are given in Table 4.14 for the three slenderness parameters studied, for the case when the reference strength taken from the standard is based on clause 13.3.1 of CSA Standard S16.1 and when it is based on clause 13.3.2. The only factors that change in the second case are the values $\rho_{\bar{s}}$ and thus ρ_p. These differ by a factor of the ratio of the predicted strengths of clauses 13.3.1 and 13.3.2 which are 0.9521, 0.8817, and 0.8187 for the three slenderness ratios. The strengths predicted by clause 13.3.1 are lower than those predicted by 13.3.2 for given slenderness ratios and, therefore, the values of $\rho_{\bar{s}}$ when based on clause 13.3.1 are higher than those when based on 13.3.2.

Chapter 5

Evaluation of the Performance of WWF Columns

5.1. Resistance factors

Equation [2.14] is used to calculate resistance factors based on the data assembled in Table 5.1 using a coefficient of separation, α, of 0.55, and a reliability index, β, of 3.0 consistent with limit states design of building in Canada. Resistance factors are evaluated at the three values of the slenderness parameter studied and for use with the column resistance equations given in Clause 13.3.1 and 13.3.2 of CSA Standard S16.1.

The high (and relatively uniform) values of the resistance factor obtained with equation 13.3.1 indicates that this equation is conservative for use with WWF columns and that within the range studied the predicted strengths could be increased by 1.074/0.90 = 1.19 times and still maintain a resistance factor of 0.90.

Clause 13.3.2, on the other hand, gives resistance factors that vary from 1.14 to 0.99 times the current value of ϕ, within the range of λ values studied. Although a value of ϕ of 0.90 could be used for λ =

Table 5.1. Resistance factors for WWF columns.

Clause from S16.1	λ	Mean/Nominal Ratio			Coef. of variation			ρ_{Cr}	V_{Cr}	ϕ
		$\rho_G = \rho_A$	ρ_F	ρ_P	V_G	V_F	V_P	$\rho_G \cdot \rho_F \cdot \rho_P$	$[V_G^2+V_F^2+V_P^2]^{1/2}$	$\rho_{Cr} \cdot e^{-\alpha\beta V_{Cr}}$
13.3.1	0.336	1.008	1.127	1.041	0.00690	0.0543	0.0213	1.183	0.0587	1.074
	0.672	1.008	1.111	1.083	0.00690	0.0452	0.0470	1.213	0.0656	1.089
	1.007	1.008	1.067	1.130	0.00690	0.0265	0.0688	1.215	0.0740	1.076
13.3.2	0.336	1.008	1.131	0.991	0.00690	0.0568	0.0213	1.130	0.0611	1.022
	0.672	1.008	1.118	0.955	0.00690	0.0493	0.0470	1.076	0.0685	0.961
	1.007	1.008	1.088	0.925	0.00690	0.0328	0.0688	1.014	0.0765	0.894

1.007, as is currently used in CSA standard S16.1, it is too conservative for the lower slenderness parameters and does not fit the data well. Clause 13.3.2 is inappropriate for use with a constant value of the resistance factor, as is deemed, without being unduly conservative at lower values of λ.

5.2. Proposed column curves for WWF's

5.2.1. Use existing clause 13.3.1

The existing column curve given in clause 13.3.1 can be used with a resistance factor of 1.07 within the range of slenderness studied to maintain a reliability index of 3.0.

5.2.2. Use a resistance factor of 0.90

5.2.2.1. A second degree curve

Having established factored resistances for three values of λ equal to the resistance factors given in Table 5.1 for use with Clause 13.3.1, a second degree curve can be fitted to this data, thus

[5.1a] $Cr = \phi AF_y[A+0.336B+0.336^2C] = 1.074AF_yf(\lambda)$

[5.1b] $Cr = \phi AF_y[A+0.672B+0.672^2C] = 1.087AF_yf(\lambda)$

[5.1c] $Cr = \phi AF_y[A+1.007B+1.007^2C] = 1.075AF_yf(\lambda)$

where $f(\lambda)$ is the appropriate equation from clause 13.3.1, evaluated at the respective values of λ, as used as the basis of comparison with the current value of ϕ of 0.90. Solving these equations gives

[5.2] $Cr = \phi AF_y[1.201-0.106\lambda-0.365\lambda^2]$

This is valid over the range of λ's studied only and of course must not exceed $0.90AF_y$. This latter limitation restricts its use to values of λ greater than 0.611, or stated in a more positive sense, no reduction in column strength with slenderness is necessary for values of λ less than 0.611 to maintain a safety index of 3.0

It has been tacitly assumed that it is valid to use all the statistical parameters used in developing the resistance factors. These include the coefficient of variation V_F and the measured/nominal ratio ρ_F both of which depend on Clause 13.3.1. They actually should be modified in accordance with the proposed equation but the effect is not considered to be large.

5.2.2.2. Modification of existing clause 13.3.1

The current Clause 13.3.1, valid over the range $0.15 \leq \lambda \leq 1.000$, is

[5.3] $Cr = \phi AF_y(1.035-0.202\lambda-0.222\lambda^2)$

results in resistance factors of about 1.07 or 1.19 times the current value of 0.90. The above equation could therefore be modified using ϕ=0.90 by multiplying $f(\lambda)$ by 1.19 thus,

[5.4] $Cr = \phi AF_y(1.232-0.240\lambda-0.264\lambda^{2)}$

This is virtually indistinguishable from [5.2] when plotted and is valid for $\lambda \geq 0.587$. This confirms that it was valid to use the coefficient of variation V_F and measured/nominal ratio ρ_F in the previous derivation in 5.2.2.1.

Chapter 6

Concluding Notes

6.1. Summary and conclusions

1. Data on the magnitude, variation and typical residual stress patterns for welded H shapes were developed from the literature. The mean values of the average compressive residual stress and its coefficient of variation were established.
2. Fifty computer simulations of compression tests on initially out-of-straight welded wide flange sections with a variety of residual stress patterns characteristic of WWF sections and bent either about the strong or weak axis, were performed using the finite element program NISA. The load-deflection response of two column sections, a 12H79 (WWF 305x312) and a 14H202 (WWF 356x300) was obtained at values of the slenderness parameter of λ of 0.366, 0.672, and 1.007 The out-of-straightness investigated ranged from near zero to the tolerance limit of 1/1000.
3. Statistical data on yield strengths, geometric properties and out-of-straightness were collected during a site visit to

Algoma Steel in Sault Ste Marie, Ontario. The data on yield strengths were supplemented by a limited number of tests conducted at the University of Alberta. The modulus of elasticity was also evaluated statistically from these tests. All data were used to establish measured/nominal ratios and coefficients of variation of the geometric and material properties and out-of-straightness.

4. The professional factor, relating the test or experimental strength to that predicted by a design equation (Clause 13.3.1 of CSA Standard S16.1-M84), was evaluated sequentially for each value of the slenderness parameter λ by:
   (i) determining the mean value of the professional ratio corresponding to the mean values of out-of-straightness and average compressive residual stress,
   (ii) multiplying this value by a ratio, normalized to exclude the effect of out-of-straightness and residual stresses and thus account for other factors such as variations in residual stress patterns, axes of bending, and the use of heavy or light sections, and
   (iii) multiplying by the mean ratio of experimental strengths to those determined by computer simulation.
5. The coefficient of variation of the professional factor was evaluated sequentially in four steps:
   (i) that due to the variation in out-of-straightness,

(ii) that due to the variation in the average value of compressive residual stress,

(iii) that due to variation in residual stress patterns and the like, and,

(iv) that due to the variation in the experimental strength/computer simulation strength ratio.

6. The statistical evaluation shows that the factored resistance of WWF's within the slenderness ratio studied (λ = 0.336, 0.672, and 1.007) is 1.19 times that given by Clause 13.3.1 of CSA Standard S16.1-M84. Comparisons with Clause 13.3.2 give varied results.

7. Three proposals are given for determining the factored compressive resistance of WWF's. These are:

(i) Use of existing Clause 13.3.1 with a resistance factor of 1.07

(ii) A new second degree curve used with a resistance factor of 0.90

(iii) Modification of Clause 13.3.1 used with a resistance factor of 0.90

6.2. Further research

In some sense this study can be considered to be preliminary in nature in that the entire spectrum of work that could have been covered was far too extensive. In some cases data gleaned from the literature were limited. This work has, however, established an effective method of assessing out-of-straightness, residual stresses, and residual stress patterns. It has shown that current design equations are conservative for WWF's in the range investigated by a factor of 1.19 times. Areas of further research touch on many of the facets of this work. These are:

(1) More extensive analysis of both sweep and camber based data collected at the mill and confirmation of sizes of samples.

(2) More extensive analysis of mill yield strengths correlated with static tests that also provide data on the modulus of elasticity. This study should include variations in yield strengths across the width and over the length of the plate.

(3) Sampling of Algoma's production to determine variations in the level of residual stresses and residual stress patterns for shapes of different weights.

(4) Extending the computer simulations over a broader range of slenderness parameters to include columns with values of λ up to 3.6

(5) Physical tests of Algoma production, once all properties are established, to verify the ratio of test strength to the computer simulation developed here.

(6) Computer analysis in which warping of the section is allowed and compared to test results in columns having significant out-of-straightness about both axes would be valuable.

References

ADAMS, P. F., KRENTZ, H. A., and KULAK, G. L., 1981. Limit states design in structural steel - SI units. Canadian Institute of Steel Construction, Willowdale, Ontario.

ALLEN, D. E. 1975. Limit states design - a probabilistic study. Canadian Journal of Civil Engineering. **2**(1). pp. 36-49.

ALPSTEN, G. A., 1972a. Prediction of thermal residual stresses in hot-rolled plates and shapes of structural steel. 9th IABSE Congress, Final Report, Amsterdam. May 1972. pp. 1-13.

ALPSTEN, G. A., 1972b. Residual stresses, yield strength and column strength of hot-rolled and roller-straightened steel shapes. Coll. Column Strength, Paris. November 1972. pp. 39-59.

ALPSTEN, G. A., and TALL, L., 1970. Residual stresses in heavy welded shapes. Welding Journal, Research Supplement, **49**(3), March 1970. pp. 93s-105s.

AMERICAN IRON AND STEEL INSTITUTE, 1974. The variation of product analysis and tensile properties of carbon steel plates and wide flange shapes. AISI. Washington, D.C.

BEEDLE, L. S., and TALL, L., 1960. Basic column strength. Journal of the Structural Division, American Society of Civil Engineers. **86**(ST7). pp. 139-173.

BEEDLE, L. S., and TALL, L., 1962. Basic column strength. Transactions American Society of Civil Engineers, **127**, part II. pp. 138-179.

BJORHOVDE, R., 1972. Deterministic and probabilistic approaches to the strength of steel columns. Ph.D. Dissertation, Lehigh University, May 1972.

BJORHOVDE, R., BROZZETTI, J., ALPTEN, G. A., and TALL, L., 1972. Residual stresses in thick welded plates. Welding Journal, Research Supplement. **51**(8), August 1972. pp. 392s-405s.

BLEICH, F., 1952. Buckling strength of metal structures. McGraw-Hill Book Co. New York.

BOULTON, N. S., and LANCE MARTIN, H. E., 1936. Residual stresses in arc-welded plates. Proceedings of Institute of Mechanical Engineers. **133**. pp. 295-347.

BROZZETTI, J., ALPSTEN, G. A., and TALL, L., 1971. Welding parameters, thick plates, and column strength. Welding Journal, **50**(8), August 1971.

CANADIAN INSTITUTE OF STEEL CONSTRUCTION, 1984. Handbook of steel construction. Canadian Institute of Steel Construction Willowdale Ontario.

CANADIAN STANDARDS ASSOCIATION, 1974. Steel structures for buildings - limit states design. CSA Standard CAN3-S16.1-1974. Canadian Standards Association. Rexdale Ontario.

CANADIAN STANDARDS ASSOCIATION, 1977. General requirements for rolled and welded structural quality steel. CSA Standard G40.20-M1977. Canadian Standards Association. Rexdale Ontario.

CANADIAN STANDARDS ASSOCIATION, 1977. Structural quality steels. CSA Standard G40.21-M1977. Canadian Standards Association. Rexdale Ontario.

CANADIAN STANDARDS ASSOCIATION, 1978. Steel structures for buildings - limit states design. CSA Standard CAN3-S16.1-M1978. Canadian Standards Association. Rexdale Ontario.

CANADIAN STANDARDS ASSOCIATION, 1984. Steel structures for buildings - limit states design. CSA Standard CAN3-S16.1-M1984. Canadian Standards Association. Rexdale Ontario.

CHEN, W., and ATSUTA, T., 1977. Theory of beam columns. McGraw-Hill Inc. New York.

CHERNENKO, D. E., and KENNEDY, D. J. L., 1988. Factored resistance of welded wide flange columns. Proceedings of Canadian Society for Civil Engineering 1988 Annual Conference. Calgary. May 1988. pp. 214-233.

CONSIDÈRE, A., 1889. Resistance des pièces comprimées (The Strength of Compressed Members). Congrés international des procédes de construction, **3**, 1889. Paris. p. 371.

ELLINGWOOD, B., GALAMBOS, T. V., MacGREGOR, J. G., and CORNELL, C. A., 1980. Development of a probability based load criterion for American Nation Standard A58 - building code requirements for minimum design loads in building and other structures. National Bureau of Standards Special Publication 577. U.S. Government Printing Office. Washington.

ENGESSER, F., 1889. Uber die knickfestigkeit gerader stabe (On the buckling strength of straight struts). Zeitschrift fur Architektur und Ingenieurwesen, **35**, 1889.

ENGESSER, F., 1895. Knickfragen (Buckling problems). Schweizerische Bauzeitung, **25**(13), 1895.

ESTUAR, F. R., 1965. Welding residual stresses and the strength of heavy columns. Ph.D. Dissertation, Lehigh University. August 1965.

ESTUAR, F. R., and TALL, L., 1963. Experimental investigation of welded built-up columns. Welding Journal, Research Supplement, **42**(4), April 1963. pp. 164s-176s.

EULER, L., 1759. Sur la force des colonnes (On the strength of columns). Académie

Royale des Sciences et Belles Lettres de Berlin, Mem., **13**, 1759. English translation by J. A. Van den Broek, Am. Journal of Physics, **15**, 1947.

FUJITA, Y., 1956. Built-up column strength. Ph.D. Dissertation, Lehigh University. August 1956.

FUGITA, Y., and DRISCOLL, G. C., 1962. Strength of round columns. Journal of the Structural Division, American Society of Civil Engineers. **88**(ST2). pp. 43-59.

GAD ALY, M., 1978. Performance factors for steel building beams and columns. M.Sc. Dissertation, University of Windsor.

GALAMBOS, T. V., 1965. Strength of round steel columns. Journal of the Structural Division, American Society of Civil Engineers. **91**(ST1). pp. 71-99.

GALAMBOS, T. V., and RAVINDRA, M. K., 1973a. Load factor design for combinations of load. National Structural Engineer Meeting, American Society of Civil Engineers, San Francisco, California.

GALAMBOS, T. V., and RAVINDRA, M. K., 1973b. Tentative load and resistance factor design criteria for steel buildings. Research Report 18, Civil Engineering Department, Washington University, Saint Louis, Missouri.

GALAMBOS, T. V., and RAVINDRA, M. K., 1977. The basis for load and resistance factor design criteria of steel building structures. Canadian Journal of Civil Engineers, **4**. pp. 178-189.

GHALI, A., and NEVILLE, A. M., 1978. Structural analysis. Chapman and Hill. London.

HUBER, A. W., 1956. The influence of residual stresses on the instability of columns. Ph.D. Dissertation, Lehigh University. May 1956.

HUBER, A. W., and BEEDLE, L. S., 1954. Residual stress and the compressive strength of steel. Welding Journal, Research Supplement, December 1954.

HUBER, A. W., and KETTER, T. W., 1958. The influence of residual stress on the carrying capacity of eccentrically loaded columns. IABSE Publications, Zurich. pp. 37-61.

JASINSKY, F., 1895. Noch ein wort zu den knickfragen (Another word on the buckling problems). Schweizerische Bauzeitung, **25**, 1985.

JOHNSTON, B. G., 1961. Buckling behaviour above the tangent modulus load. Journal of the Engineering Mechanics Division, American Society of Civil Engineers **87**(EM6), December 1961 pp. 79-99.

von KÁRMAN, T. V., 1910. Untersuchungen über die knickfestigkeit (Investigations on the buckling strength). Forschungshefte V. D. I., **81**, 1910.

KENNEDY, D. J. L., and BAKER, K. A., 1984. Resistance factors for steel highway bridges. Canadian Journal of Civil Engineering. **11**(2). pp. 324-334.

KENNEDY, D. J. L., and GAD ALY, M., 1980. Limit states design of steel structures - performance factors. Canadian Journal of Civil Engineering, **7**(1). pp. 45-77.

KENNEDY, J. B., and NEVILLE, A. M., 1976. Basic statistical methods. Harper and Row Publishers Inc.. New York.

KETTER, R. L., KAMINSKI, E. L., and BEEDLE, L. S., 1955. Plastic deformation of wide-flange beam-columns. Proceedings, American Society of Civil Engineers, **120**. pp. 1028-1061.

LAY, M. G., 1982. Structural steel fundamentals - an engineering and metallurgical primer. Australian Road Research Board, Vermont South, Victoria, Australia.

LIABLE, J. P., 1985. Structural Analysis. CBS College Publishing. New York.

LIN, T. H., 1950. Inelastic column buckling. Journal of Aeronautical Science, **17**(3).

LIND, 1971. Consistant partial safety factors. Journal of the Structural Division, American Society of Civil Engineers **97**(ST6). pp. 1651-1670.

McFALLS, R. K., and TALL, L., 1969. A study of welded columns manufactured from flame-cut plates. Welding Journal, Research Supplement, **43**(4), April 1969. pp. 141S-153S.

MIRZA, S. A., and MacGREGOR, J. G., 1982. Probabilistic study of strength of reinforced concrete members. Canadian Journal of Civil Engineering, **9**(3). pp. 431-448.

NAGARAJA RAO, N. R., ESTUAR, F. R., and TALL L., 1964. Residual stresses in welded shapes. Welding Journal, Research Supplement, **43**(7), July 1964. pp. 294s-306s.

NAGARAJA RAO, N. R., and TALL, L., 1961. Residual stresses in welded plates. Welding Journal, Research Supplement, **40**(10), October, 1961. pp. 468s-480s.

NARAYANAN, R., 1982. "Centrally compressed members". Axially compressed structures: stability and strength. Applied Science Publishers Ltd., London and New York. pp. 1-40.

NITTA, A. 1960. Ultimate strength of high strength steel circular columns, Ph.D. Dissertation, Lehigh University.

OSGOOD, W. R., 1951. The effect of residual stresses on column strength. Proceedings of the First U.S. NATO Congress on Applied Mechanics. pp. 415-418.

OSTERRIEDER, P., 1983. Traglastberechnung von räumlichen stabtragwerken bei gron Verformungen mit Finiten Elementen. Istitut Für Baustatik der Universität

Stuttgart. Bericht. Nr. 1.

RAJASEKARAN, S., and MURRAY, D. W , 1973. Finite element solution of inelastic beam equations. Journal of the Structural Division, American Society of Civil Engineers. **99**(ST6). June 1973. pp. 1025-1041.

RAMM, E., 1980. Strategies for tracing nonlinear response near limit points. Europe-U.S. Workshop: Nonlinear Finite Element Analysis in Structural Mechanics. Bochum. July 28-31 1980.

RIKS, E., 1972. The application of newton's method to the problem of elastic stability. Journal of applied mechanics. **39**. pp. 1060-1066.

RIKS, E., 1979. An incremental approach to the solution of snapping and buckling problems. International Journal of Solids Structures. **15**. pp. 529-551.

SALMON, E. H., 1921. Columns, a treatise on the strength and design of compression members. Oxford Technical Publications. London.

SHANLEY, F. R., 1949. Applied column theory. Transactions, American Society of Civil Engineers, June 1949. pp. 698-727.

STEGMULLER, H., HAFNER, L., RAMM, E., and STATTELE, J. M., 1983. Theoretische grundlagen zur F. E. - programmsystem NISA80. Institut fur Baustatik der Universitat Stuttgart. Mitteiking Nr. 1, 1983.

STRUCTURAL STABILITY RESEARCH COUNCIL., 1976. Guide to stability design criteria for metal structures, (3rd ed.). John Wiley & Sons, Inc., New York.

TALL, L., 1961. Welded built-up columns. Ph.D. Dissertation, Lehigh University. May, 1961.

TALL, L., 1964a. "Compression members". Structural Steel Design. The Ronald Press Co.. New York. pp. 269-322.

TALL, L., 1964b. Residual stresses in welded plates. Welding Journal, Research Supplement, **42**(1), January 1964. pp. 10s-23s.

TALL, L., and ALPSTEN, G. A., 1969. On the scatter in yield strength and residual stress in steel members. IABSE Symposium on Concepts of Safety of Structures and Methods of Design. London.

WEMPNER, G. A., 1971. Discrete approximations related to nonlinear theories of solids. International Journal of Solids Structures. **7**. pp. 1581-1599.

WILDER, T. W., BROOKS, W. A., and MATHAUSER, E. E., 1953. The effect of initial curvature on the strength of an inelastic column. NACA Technical Note No. 2872. January 1953.

WILLEMS, N., and LUCAS, W. M., 1978. Structural analysis for engineers. McGraw-Hill. New York.

WILSON, W. M., and BROWN, R. L., 1935. The effect of residual longitudinal stresses upon the load-carrying capacity of steel columns. University of Illinois Engineering Experiment Station bulletin no. 280. University of Illinois, Urbana.

YANG, C. H., BEEDLE, L. S., and JOHNSTON, B. G., 1952. Residual stress and the yield strength of steel beams. Welding Journal, Research Supplement, **31**. pp. 2053-2293.